DTIC FILE COPY

Applied Research Laboratory

AD-A197 775

(4)

Technical Report

EXPERIMENTAL STUDY OF TURBULENT MIXING AND SELECTIVITY OF COMPETING REACTIONS

by

Rajendrakumar V. Mehta

DTIC ELECTE JUL 19 1988 S D

DISTRIBUTION STATEMENT A
Approved for public release;
Distribution Unlimited

PENNSTATE

1855

88 7 18 189

The Pennsylvania State University
APPLIED RESEARCH LABORATORY
P. O. Box 30
State College, PA 16804

EXPERIMENTAL STUDY OF TURBULENT MIXING AND SELECTIVITY OF COMPETING REACTIONS

by

Rajendrakumar V. Mehta

DTIC
ELECTE
JUL 19 1988
S D

Technical Report No. TR 88-006

July 1988

Supported by:
Naval Sea Systems Command

L. R. Hettche, Director
Applied Research Laboratory

Approved for public release; distribution unlimited

Unclassified

SECURITY CLASSIFICATION OF THIS PAGE

REPORT DOCUMENTATION PAGE

1a. REPORT SECURITY CLASSIFICATION Unclassified	1b. RESTRICTIVE MARKINGS
2a. SECURITY CLASSIFICATION AUTHORITY	3. DISTRIBUTION / AVAILABILITY OF REPORT Unlimited
2b. DECLASSIFICATION / DOWNGRADING SCHEDULE	
4. PERFORMING ORGANIZATION REPORT NUMBER(S)	5. MONITORING ORGANIZATION REPORT NUMBER(S)
6a. NAME OF PERFORMING ORGANIZATION Applied Research Laboratory The Pennsylvania State University	6b. OFFICE SYMBOL (*If applicable*) ARL
7a. NAME OF MONITORING ORGANIZATION Naval Sea Systems Command Department of the Navy	
6c. ADDRESS (*City, State, and ZIP Code*) P. O. Box 30 State College, PA 16804	7b. ADDRESS (*City, State, and ZIP Code*) Washington, DC 20362
8a. NAME OF FUNDING / SPONSORING ORGANIZATION Naval Sea Systems Command	8b. OFFICE SYMBOL (*If applicable*) NAVSEA
9. PROCUREMENT INSTRUMENT IDENTIFICATION NUMBER	
8c. ADDRESS (*City, State, and ZIP Code*) Department of the Navy Washington, DC 20362	10. SOURCE OF FUNDING NUMBERS PROGRAM ELEMENT NO. / PROJECT NO. / TASK NO. / WORK UNIT ACCESSION NO.

11. TITLE (*Include Security Classification*)
Experimental Study of Turbulent Mixing and Selectivity of Competing Reactions

12. PERSONAL AUTHOR(S)
Rajendrakumar V. Mehta

13a. TYPE OF REPORT	13b. TIME COVERED	14. DATE OF REPORT (*Year, Month, Day*)	15. PAGE COUNT
M.S. Thesis	FROM _____ TO _____	July 1988	203

16. SUPPLEMENTARY NOTATION

17 COSATI CODES			18. SUBJECT TERMS (*Continue on reverse if necessary and identify by block number*)
FIELD	GROUP	SUB-GROUP	fluid flow modeling, multiphase fluid flow, turbulent flow fields, turbulent mixing theory

19. ABSTRACT (*Continue on reverse if necessary and identify by block number*)

Many industrial reactors are inherently limited by imperfect mixing. The flow fields of such reactors are so complex that traditional turbulence models based on the Navier-Stokes and component continuity equations are impractical, particularly when complex reactions are involved. Mechanistic models are much better suited for such applications. In this work, five mechanistic models of mixing and chemical reaction ~~were evaluated~~ in terms of their ability to

20. DISTRIBUTION / AVAILABILITY OF ABSTRACT ☒ UNCLASSIFIED/UNLIMITED ☐ SAME AS RPT. ☐ DTIC USERS	21. ABSTRACT SECURITY CLASSIFICATION Unclassified
22a. NAME OF RESPONSIBLE INDIVIDUAL	22b. TELEPHONE (*Include Area Code*) / 22c. OFFICE SYMBOL

DD FORM 1473, 84 MAR — 83 APR edition may be used until exhausted. All other editions are obsolete.

SECURITY CLASSIFICATION OF THIS PAGE

Unclassified

SECURITY CLASSIFICATION OF THIS PAGE

predict the selectivity of competing reactions. Although all five models were found to be interrelated through an analogy to the isotropic turbulence mixing theories of Corrsin (1964) and Rosensweig (1964), and they successfully correlated single, second-order reaction data published in the literature (Vassilatos and Toor, 1965), it was demonstrated via numerical simulation of two competing reactions in a plug flow reactor that they may predict grossly different selectivities.

Experiments were conducted in a highly segregated but well characterized turbulent plug flow reactor to obtain data for competing reactions. The azo-coupling of 1-naphthol with diazotised sulfanilic acid (Bourne reactions) was used as the reaction system. Concentration of reaction products was measured by absorption spectrophotometry with a fiber-optic probe. Turbulence measurements in the reactor were obtained with a pulsed Doppler Ultrasound Velocimeter. These measurements indicated that the mean velocity profile was nearly flat and the turbulence nearly homogeneous. Thirty-seven mixing-reaction experiments were performed, covering three feed stoichiometries (0.4, 1.0, 1.5) under constant mixing conditions and three different mixing conditions at a fixed feed stoichiometry (1.5). The difference among model predictions was much larger than the experimental errors. The four-environment model of Mehta and Tarbell (1983) was found to successfully correlate the experimental data and is recommended as a general chemical reactor model for homogeneous systems. The other four mechanistic models either were unable to predict experimental selectivity or required prohibitive amount of computational time for such a prediction.

Unclassified
SECURITY CLASSIFICATION OF THIS PAGE

ABSTRACT

Many industrial reactors are inherently limited by imperfect mixing. The flow fields of such reactors are so complex that traditional turbulence models based on the Navier-Stokes and component continuity equations are impractical, particularly when complex reactions are involved. Mechanistic models are much better suited for such applications. In this work, five mechanistic models of mixing and chemical reaction were evaluated in terms of their ability to predict the selectivity of competing reactions. Although all five models were found to be interrelated through an analogy to the isotropic turbulence mixing theories of Corrsin (1964) and Rosensweig (1964), and they successfully correlated single, second-order reaction data published in the literature (Vassilatos and Toor, 1965), it was demonstrated via numerical simulation of two competing reactions in a plug flow reactor that they may predict grossly different selectivities.

Experiments were conducted in a highly segregated but well characterized turbulent plug flow reactor to obtain data for competing reactions. The azo-coupling of 1-naphthol with diazotised sulfanilic acid (Bourne reactions) was used as the reaction system. Concentration of reaction products was measured by absorption spectrophotometry with a fiber-optic probe. Turbulence measurements in the reactor were obtained with a pulsed Doppler Ultrasound Velocimeter. These measurements indicated that the mean velocity profile was nearly flat and the turbulence nearly homogeneous. Thirty-seven mixing-reaction experiments were performed, covering three feed stoichiometries (0.4, 1.0, 1.5) under constant mixing conditions and three different mixing conditions

at a fixed feed stoichiometry (1.5). The difference among model predictions was much larger than the experimental errors. The four-environment model of Mehta and Tarbell (1983) was found to successfully correlate the experimental data and is recommended as a general chemical reactor model for homogeneous systems. The other four mechanistic models either were unable to predict experimental selectivity or required prohibitive amount of computational time for such a prediction.

DTIC
COPY
INSPECTED
6

Accession For
NTIS GRA&I
DTIC TAB
Unannounced
Justification
By
Distribution/
Availability Codes
Dist Avail and/or Special
A-1

TABLE OF CONTENTS

TABLE OF CONTENTS (Continued)

TABLE OF CONTENTS (Continued)

LIST OF TABLES

LIST OF FIGURES

LIST OF FIGURES (Continued)

LIST OF SYMBOLS

A,B,P,R,S	Chemical species
A	Dimensionless constant in Equation (22)
A	Absorbance
A	1-Naphthol
B	Diazotised sulfanilic acid
C_j	Concentration of species j
CRD	Coalescence-redispersion model
CPU	Central processing unit
D	Molecular diffusivity
D	Diameter
E_θ	One-dimensional turbulence spectrum
E.E.	Entering environment
f	Frequency
G	Turbulence spectral density
h	Micromixing parameter
I	Micromixing parameter
I	Intensity of light beam
I_S	Intensity of segregation
IEM	Interaction by exchange with mean model
I.D.	Inner diameter
k, k_1, k_2	Rate constants
k_j^λ	Fiber-optic probe's calibration constant for the specie j at wavelength λ
k_p	Proportionality constant
L	Length

ℓ	Optical path length
ℓ_e	Integral length scale of the turbulence field
L.E.	Leaving environment
L_S	Scalar macroscale
M	Concentration in mol/m^3
MM	Maximum mixedness model
M_1, M_2, M_3	Screens
N_{Sc}	Schmidt number = ν/D
PFR	Plug flow reactor
PRF	Pulse repetition frequency
PUDV	Pulsed Ultrasound Doppler Velocimeter
Q	Flowrate
r	Reaction rate
R	Monoazo dye
Re	Reynolds number
R_s	Micromixing parameter
RTD	Residence time distribution
r.m.s.	Root-mean-square value
SD	Slab diffusion model
S	Diazo dye
S	Solidity
S_D	Spectral density based on ultrasound measurements
T	Temperature
u	Fluctuating velocity
u	Velocity of the moving object, for Equation (8)
u_s	Speed of sound
U	Mean velocity

V	Voltage output
x,x'	Axial distance
X_S	Selectivity of S

Greek Letters

β	Feed stoichiometric ratio
δ	Double slab thickness
Δ	Difference
ε	Turbulent energy dissipation rate per unit mass
θ	Angle
λ	Wavelength
σ^2	Variance of concentration distribution
ν	Kinematic viscosity
τ	Mean residence time
τ_m	Micromixing time
ω	Angular frequency

Subscripts

A,B,R,S	Chemical species
Cr	Critical
d	Wire diameter based
d	Doppler shift
M	Mesh size based

Superscripts

λ	Wavelength

Specific Symbols

Overbar	Time averaged value
Prime	Fluctuating part
3E	Three-environment model
4E	Four-environment model

This work was supported by the Naval Sea Systems Command and the Applied Research Laboratory Exploratory and Foundational Research Program of The Pennsylvania State University. Their support is gratefully acknowledged.

ACKNOWLEDGEMENTS

I wish to express my deep sense of gratitude to many people who have contributed generously towards completion of this work:

- to Professor John M. Tarbell, not only for his advice and encouragement as well as help in much of the data collection, but also a great deal more besides;

- to Mr. Frederick Mensch and Mr. Randall Miller for their affection and invaluable help in construction of the experimental system as well as in solving numerous experimental problems;

- to Mr. A. Murphy of the glass blowing shop, for his timely help in fabrication of the contraction nozzle;

- to Mr. Nevin Engle of ARL electronics services, for his assistance in taming the electrical noise problem;

- to Mr. John Balogh of EE technical services, for his efforts in modifying the colorimeter circuit;

- to my friends, Marty Klanchar, Liang-Jyh Chang and Dishwajit Sen, for lending their helping hands in the data collection and their unflinching moral support throughout this study;

- to Mr. Eric Hills, for his help in the first half of the experimental program;

- to many of my fellow graduate students, for their help in many aspects of this work;

- to Dr. Amitabha Kumar, for his enthusiasm in meticulously drawing most of the figures in this thesis; and

- to the entire faculty and staff of the Chemical Engineering Department, for their kindness and friendship which have meant to much to me.

I. INTRODUCTION

A proper understanding of mixing in chemical reactors is of vital importance in many industrial applications. Liquid phase mixing plays a critical role in precipitation processes where the shape and size of relatively insoluble precipitate can be significantly altered by changing the local mixing environment near the feed port (Garside, 1985). Similarly, the degree of mixing in the reactor strongly influences the initiator consumption in some commercial polymerization reactors (Van der Molen et al., 1982). Mixing is also recognized as a key factor affecting overall performance of a combustor--both in terms of fuel efficiency and formation of pollutants (Pratt, 1982).

The classical perfectly mixed reactor model is one of the most useful models in chemical reactor design. However, the model is based on the assumption that immediately after entering the reactor, the feed-stream is distributed uniformly at the molecular level throughout the reactor volume, and there are no spatial gradients of concentration or temperature. Furthermore, whether the reactants are fed premixed or separately is of no consequence. Thus, the model completely ignores the details of the mixing process which precedes the chemical reaction. For fast reactions, where the mixing rate is comparable or slower than the reaction rate, the perfectly mixed reactor model is clearly inadequate. The problem of modeling mixing and fast reactions is an old one and has spurred publication of several plausible models in the past. However, it is difficult for a practicing engineer to choose among these diverse models with any degree of certainty as very few have been validated against a well-defined set

of experimental data. The principal aim of this work is to obtain data to discriminate among several rival models by experimentally studying the effect of mixing on the selectivity of two fast competing reactions.

The thesis is organized as follows. In Chapter II, several popular approaches to chemical reactor modeling are reviewed. A particular class of models called "mechanistic models" is given special emphasis. Five mechanistic models having a turbulence analogy with known statistical turbulence theories are briefly described.

Chapter III is devoted to the theoretical foundations of the present work. The turbulence analogy of five mechanistic models is evaluated by using published single second-order reaction data. This is followed by numerical simulation of two competing reactions in a highly segregated plug flow reactor. The results of these simulations provide a background for the experimental design.

The details of the experimental design are considered in Chapter IV while Chapter V is devoted to measurement techniques, methods of analysis and details of the operating procedures.

Experimental results are presented in Chapter VI along with a comparison of model predictions with the data and a discussion of the results. The major conclusions of the work are highlighted in Chapter VII. Finally, possible avenues of further research are suggested in Chapter VIII.

II. LITERATURE REVIEW

A. General Review

A great deal of work has been done on mixing from a chemical engineering viewpoint, starting in 1953 with Danckwerts' pioneering papers. In his first paper, Danckwerts (1953a) introduced the concept of residence time distribution (RTD). RTD is a useful characterization of large-scale fluid motion which has come to be known as macromixing. In another paper (Danckwerts, 1953b), he considered the characterization of "local texture," subsequently known as micromixing, of a nonuniform mixture. He defined two characterizing quantities, namely, the scale and intensity of segregation. The scale of segregation is related to underlying fluid mechanics and is analogous to the scale of turbulence used in the statistical theory of turbulence. On the other hand, the intensity of segregation depends upon the interaction of diffusion fluxes with the chemical kinetics in the context of chemical reactors. Although Danckwerts showed how to use a diffusion controlled reaction (e.g., acid-base neutralization) to determine the intensity of segregation (Danckwerts, 1958), his method of characterizing micromixing did not find much practical use because of inherent experimental and conceptual limitations. For example, it was not possible to predict intensity of segregation for a slower reaction from the acid-base measurements. Yet, the concepts of scale and intensity of segregation have provided the framework for nearly all the subsequent work in this area. Most of the mechanistic modeling has proceeded along two distinct directions. In one, much emphasis is laid on the size of the segregation scale which, in turn,

influences the intensity of segregation (e.g., slab-diffusion type models to be described later on). In the other, no attention whatsoever is paid to the scale of segregation and yet, based on a proposed physical picture of turbulent mixing, all levels of segregation intensity are accounted for (e.g., environment and coalescence-redispersion models to be described later on). Bourne (1983) has chronicled part of these developments from a historical perspective.

Substantial progress is also being made in modeling turbulent reacting flows based directly on the Navier-Stokes and component continuity equations. However, the flow in most systems of practical interest is sufficiently complex that accurate modeling is a formidable task (Patterson, 1981). Since mechanistic models can accommodate many of the complexities of practically relevant chemical reactors, our discussion is limited only to the mechanistic models.

Villermaux (1983) provides an extensive review of mechanistic models. All of the mechanistic models contain at least one "micromixing parameter" whose magnitude determines the level of turbulent micromixing in the reactor. The micromixing parameter has generally been treated as an empirical parameter available for correlating experimental data. Because of the supposed empirical nature of the micromixing parameter, most of the mechanistic models have been viewed as lacking a physical basis and have thus been regarded with skepticism --particularly in the context of such important applications as reactor scaleup. The overwhelming variety of models have also led some to believe that given a little imagination, any number of equally plausible models can be conjured up (Villermaux, 1983).

In a recent work, Tarbell and Mehta (1985) have shown that five

mechanistic models (the coalescence-redispersion (CRD) model of Curl (1963), the slab-diffusion (SD) model of Mao and Toor (1970), the interaction-by-exchange with the mean (IEM) model of Villermaux and Devillon (1972), the three-environment (3E) model of Ritchie and Tobgy (1979), and the four-environment (4E) model of Mehta and Tarbell (1983a)) are analogous to theories of isotropic turbulent micromixing as expressed by Corrsin (1957, 1964) and Rosensweig (1964, 1966). The analogy is based on the analytical demonstration that the decay law for the variance of concentration of a nonreactive tracer as derived from the mechanistic models has the same form as that derived from direct turbulence theory. For a batch (plug flow) mixer the variance decay takes the form (Tarbell and Mehta, 1985)

$$I_s \equiv \frac{\sigma^2}{\sigma_o^2} = \exp(-\tau/\tau_m) \ , \tag{1}$$

where I_s is the intensity of segregation, τ_m is a time scale for turbulent micromixing which is characteristic of the fine structure of the turbulence, and τ is the time (residence time). The following estimates of τ_m have been provided:

$$\tau_m \simeq 0.5[4(L_s^2/\varepsilon)^{1/3} + (\nu/\varepsilon)^{1/2} \ln N_{Sc}] \ ; \ N_{Sc} >> 1 \ \text{(liquids)} \tag{2}$$

$$\tau_m \simeq \frac{2}{(3-N_{Sc}^2)} (5/\tau)^{2/3} (L_s/\varepsilon)^{1/3} \ ; \ N_{Sc} < 1 \ \text{(gases)} \tag{3}$$

where L_s is the integral length scale of the concentration field, ε is the turbulent kinetic energy dissipation rate per unit mass, ν is the fluid kinematic viscosity, and N_{Sc} is the Schmidt number. All of these quantities are directly measurable or readily estimated.

The relationships of the micromixing parameters of the mechanistic models to the time scale of isotropic turbulent mixing (τ_m) as required by the turbulence analogies are summarized in Table 1. Figure 1 summarizes the physical picture underlying each model for the case of a plug flow mixer fed with two separate streams carrying A (dark) and B (light), respectively. The left-hand panel in Figure 1 represents the initial inhomogeneity while movement to the right shows the decay of inhomogeneity at successive residence times. Each model is briefly described below.

B. Mechanistic Models with a Turbulence Analogy

1. Coalescence-Redispersion (CRD) Model

The CRD model was originally proposed by Curl (1963) to describe dispersed phase droplet mixing and concurrent chemical reaction. In Curl's view, a chemical reactor population consists of a large number of equal size droplets each having uniform concentration and behaving as an ideal batch reactor. Mixing takes place by random and instantaneous pairwise coalescence, concentration homogenization, and redispersion into an identical pair of droplets. In the turbulence analog for a homogeneous fluid, we might view Curl's droplets as (isotropic) turbulent eddies and the coalescence rate as a measure of the rate of turbulent micromixing. CRD is basically a deterministic population balance model and the governing equation is an integro-differential equation for the probability density function (Curl, 1963; Evangelista et al., 1969; Kattan and Adler, 1972). The micromixing parameter of the model, I, is the average number of collisions experienced by an eddy during its passage through the mixer.

Table 1

Summary of Turbulence Analogies

Model	Micromixing Parameter	Analogy	Comments
CRD	I	$I = \frac{2\tau}{\tau_m}$	Valid at all flow rate ratios
SD	δ	$\delta = \sqrt{2\pi^2 D\tau_m}$	Approximately valid at equal flow rates, invalid otherwise
IEM	h	$h = \frac{1}{2\tau_m}$	Valid at all flow rate ratios
3E	R_s	$R_s = \frac{1}{\tau_m}$	Valid at all flow rate ratios
4E	R_s	$R_s - \frac{1}{\tau_m}$	Approximately valid at equal flow rates, more accurate at unequal flow ratios

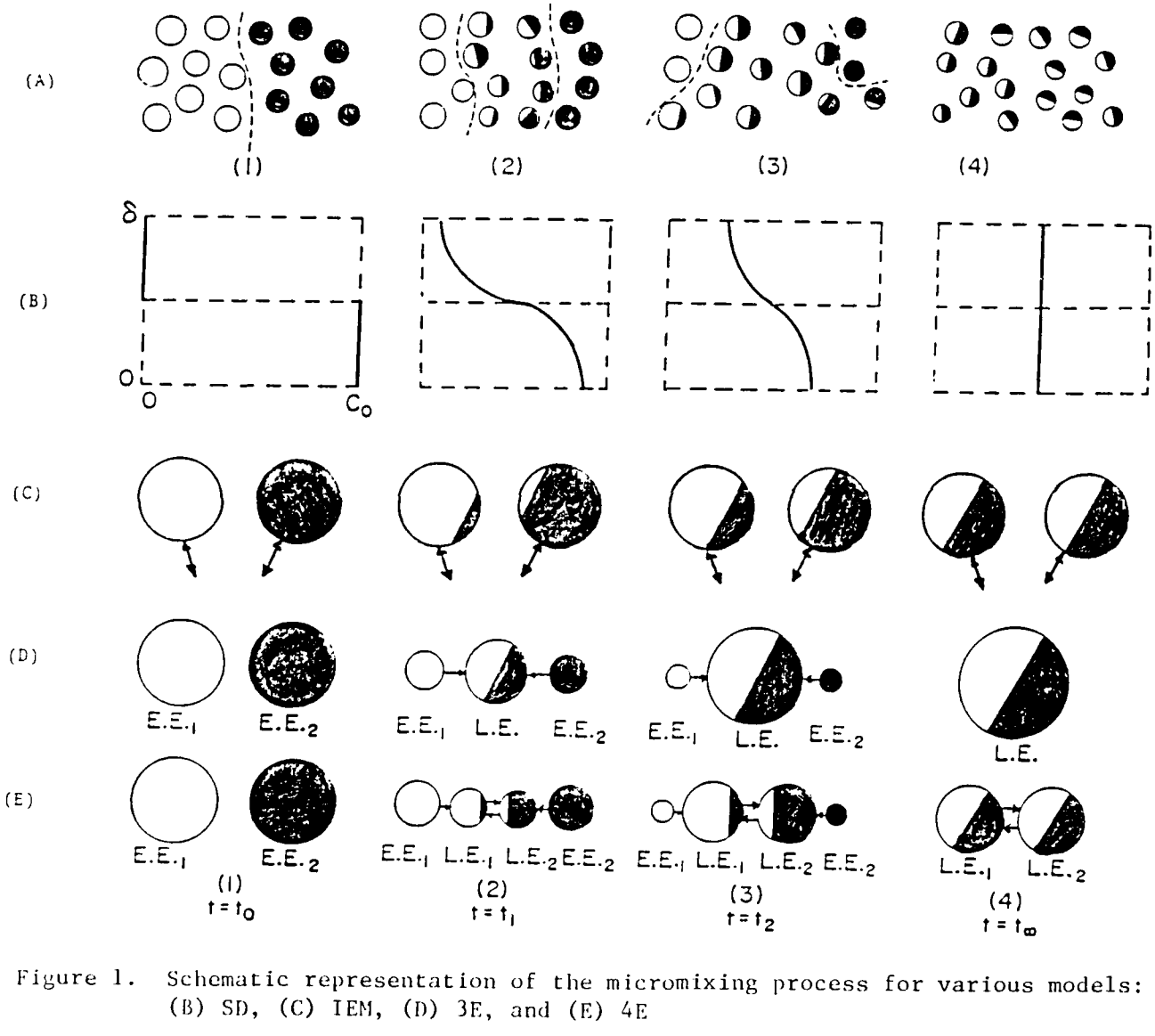

Figure 1. Schematic representation of the micromixing process for various models: (A) CRD, (B) SD, (C) IEM, (D) 3E, and (E) 4E

2. Slab Diffusion (SD) and Related Models

The SD model of Mao and Toor (1970) was developed to describe a chemical reactor with a plug flow RTD and separate feedstreams of reactants (A and B). In the Mao and Toor picture, the reactor fluid is made up of two planar slabs with a common interface open to diffusion and impermeable outer surfaces. The slabs enter the reactor completely segregated (pure A in one and pure B in the other) and they proceed to intermix by molecular diffusion and undergo chemical reaction as they move through the reactor at the mean fluid velocity. The mixing parameter of the model is the double slab thickness, δ. In its original formulation the SD model applies only to reactors with equal flow rate reactant streams, and the turbulence analogy (Table 1) only applies to that case.

For unequal flow rates, if flow inequality is reflected through unequal slab thicknesses, the analogy does not hold. On the other hand, if slab size is assumed to be solely determined by local fluid mechanics, one could argue, as Baldyga and Bourne (1984) have done, that slab thicknesses should be independent of flow rate ratio for dilute, isothermal systems. However, in that case it is not clear how the model can account for the effect of feed flow rate variation on reactor performance. It is simply concluded that the SD model, in its original formulation, does not possess a turbulence analogy when feed flow rates are unequal.

The original SD model is limited to reactors with a plug flow RTD although Guerden and Thoenes (1972) have extended the model to include an arbitrary RTD (with the restriction that the RTD for each feedstream be the same). In the past few years, Ottino et al. (1979) have

developed a "lamellar" mixing model which provides a generalization of the SD model through incorporation of local fluid deformations (shear, extension, etc.) as well as micromixing. However, these models are limited by the fact that flow elements are segregated from their surroundings, and thus "age" mixing is prohibited. The "stretching lamina" model of Angst et al. (1982) is essentially a much simpler (vis-à-vis Ottino et al.) version of an SD model with local fluid deformation. However, it suffers from the physically unrealistic assumption of a diffusion barrier to one of the reactants. The model of Angst et al. (1982) does not possess a turbulence analogy in the same sense as referred to earlier.

3. Interaction by Exchange with the Mean (IEM) Model

As pointed out by Villermaux (1984), the basic idea of the IEM model was suggested by Burgers as early as 1951 (Burgers, 1951). However, the model was independently developed in its present form by Villermaux and co-workers (1972, 1975) as an outgrowth of the work of Harada et al. (1962) and was originally conceived for application to stirred reactors only. For a two-feedstream perfectly stirred reactor, the IEM model consists of two eddies--one associated with each feedstream--which act as well-mixed batch reactors having mass exchange with a mean environment whose concentration is assumed to be constant and to coincide with the mean concentration leaving the reactor. Micromixing is described by a first order exchange process between the mean environment and each eddy (the eddies do not interact directly) with concentration difference as the driving force. The exchange rate is characterized by a mass transfer coefficient, h, which is the

micromixing parameter of the model. The turbulence analogy for the IEM model was apparently first recognized by Costa and Trevissoi (1972) in the context of perfectly stirred reactors. In this work the IEM model is applied to plug flow reactors. It is easy to show that the same turbulence analogy applies to plug flow reactors by inserting a plug flow residence time distribution function into the analysis of Tarbell and Mehta (1985; Equations (18)-(23)).

4. The Three-Environment (3E) Model

The 3E model was developed by Ritchie and Tobgy (1979) to describe chemical reactors with two feedstreams. It is an extension of "two-environment model" of Ng and Rippin (1965) for premixed feed reactors to separate feedstream reactors. In the 3E model, two entering environments (E.E.'s), one for each reactant feedstream in a two-reactant system, are assumed to supply a single leaving environment (L.E.) at rates proportional to their respective masses. While each E.E. acts as a totally segregated reactor (no age or species mixing), the L.E. behaves as a maximum mixedness reactor (complete age and species mixing). As pointed out by Mehta and Tarbell (1983a), the E.E.'s should be viewed as lumped representations of turbulent eddies of pure reactant which have only interacted with other pure reactant eddies and as such, they model the extremes of the turbulent concentration spectrum. The L.E. is a lumped representation of eddies in the intermediate region of the turbulent concentration spectrum. Micromixing is modeled by the first order transfer of material from the E.E.'s to the L.E. with a transfer coefficient R_s which is the model's micromixing parameter.

The 3E model has a very general structure which can accommodate an arbitrary RTD for each feedstream all within the computationally efficient format of ordinary differential equations. Since there are only three effective eddies in the model, the computations should be modest by comparison to those required for Monte Carlo simulations with the CRD model (300 eddies).

In spite of many positive attributes, the 3E model is lacking in an important structural feature which the CRD, SD, and IEM models possess--the presence of reacting regions which are rich in each of the reactants in a two-reactant (A and B) feedstream reactor. The 3E model has only one reacting environment with reactant concentrations at the mean of the concentration spectrum. This structural feature of A rich and B rich regions becomes very important in competing reaction systems where the stoichiometric ratio of the reactants may have a profound effect on the selectivity. This point is discussed further in a later chapter.

5. The Four-Environment (4E) Model

To overcome the limitation of only a single reacting environment in the 3E model, Mehta and Tarbell (1983a) developed the 4E model by introducing a separate L.E. for each feedstream and allowing mutual interaction between the L.E.'s. The reactant stoichiometry of each L.E. may now be rich in the reactant fed through its respective E.E.

The 4E model retains the basic features of the 3E model. The E.E.'s are segregated flow reactors; the L.E.'s are maximum mixedness reactors; and the transfer of material from E.E. to L.E. is first order in the mass of the E.E. with a transfer coefficient R_s. It is further

assumed that the reversible transfer between L.E.'s is first order in the mass of each L.E., also with a transfer coefficient R_s. The two L.E.'s of the 4E model are a somewhat finer lumped representation of the intermediate region of the turbulent concentration spectrum than the single L.E. of the 3E model. But more importantly, they provide the structural feature of multiple reacting regions.

The mathematical structure of the 4E model is similar to that of the 3E model with an additional set of material balances required for the second L.E. (see Mehta and Tarbell (1983a) for complete details). Thus, the computational requirements of the two models are similar.

III. BACKGROUND FOR THE PRESENT WORK

The existence of a turbulence analogy for the models described earlier blunts the criticism that all such models are useful only for data correlation. A priori estimation of the micromixing parameter is possible now. Tarbell and Mehta (1985) and more recently, Chang et al. (1985) have shown that all five mechanistic models which have a turbulence analogy are well supported by single second-order reaction data in various reactors, and that the micromixing parameters required to fit single reaction data are in accord with Corrsin's expression of τ_m. However, these models are not all equivalent. Chang et al. (1985) have demonstrated this through numerical simulations of competing reactions in a PFR. These results emphasize the importance of certain structural features of the mixing models which are independent of the existence of a turbulence analogy. They also point towards the importance of obtaining experimental data for competing reactions in a highly segregated PFR to discriminate among rival mixing models. The remainder of this chapter is based on the study by Chang et al. (1985).

A. Experimental Evaluation of the Turbulence Analogies for Single Reactions

First, the simulation of representative experiments of Vassilatos and Toor (1965) are considered using the five models possessing a turbulence analogy. In these often quoted experiments, single, irreversible, second-order reactions ($A+B \rightarrow P$; $r_A = -kC_AC_B$) were studied in an isothermal, turbulent flow, tubular reactor. The hydrodynamics were maintained constant while the reaction rate was varied

over nine orders of magnitude. For brevity, simulation of only three experiments are considered, although they span the entire range of reaction rates (see Table 2). In these experiments, the two aqueous reactant solutions were separately introduced through 100 alternate jets, and the reaction proceeded in the resulting microscale inhomogeneous mixture. Since no RTD measurements were reported, it has generally been assumed in models of this reactor that an ideal plug flow RTD is appropriate. Since the flow rate of each stream was maintained constant, the feed stoichiometry was varied by changing the concentration in one of the feed streams.

In a previous work, Mehta and Tarbell (1983b) simulated Vassilatos and Toor's data with both the 3E and 4E models assuming a plug flow RTD. For each model they determined the value of the parameter R_s which provided the best fit (mean square error minimization) to the entire data set. That resulted in a value of $\tau_m = 0.0082$ sec through use of the turbulence analogy (Table 1). This value of τ_m is used to calculate the micromixing parameter for each model based on the turbulence analogy (Table 1), to simulate the three cases listed in Table 2. The results are displayed in Figure 2. Numerical methods are discussed in the next section.

For the "slow" reactions (Figure 2a), the data and all of the models follow the maximum mixedness prediction closely. Both the "moderately fast" and "very fast" reactions are fairly well described by all of the models although IEM provides the best and 3E the worst fit to the data. Overall, the comparisons are quite favorable for all models, and this lends significant support to the turbulence analogies since each model employs the same value of τ_m.

Table 2

Parameters for Simulated Experiments of Vassilatos and Toor (1965)[a]

Case	Reaction Type	Reaction	Rate Constant k $m^3/mol'sec$	Stoichiometric[b] Ratio β	Concentration of Limiting Reactant
I	Slow	$CH_3COOH + NaOH$	4.7×10^2	1.56	0.01
II	Moderately fast	$CO_2 + 2NaOH$	1.24×10^1	1.26	0.007
III	Very Fast	$HCl + NaOH$	1.0×10^8	1.0	0.002

[a] Average axial flow velocity was 0.405 m/s.

[b] $\beta = (Q_B C_{Bo} / Q_A C_{Ao})$.

Figure 2. Comparison of model predictions with data of Vassilatos and Toor (1965): (A) slow reactions; (B) moderately fast reactions; (C) very fast reactions

0 CRD

X SD

▲ IEM

Δ 3E

□ 4E

+ (and dotted line) - max. mix.

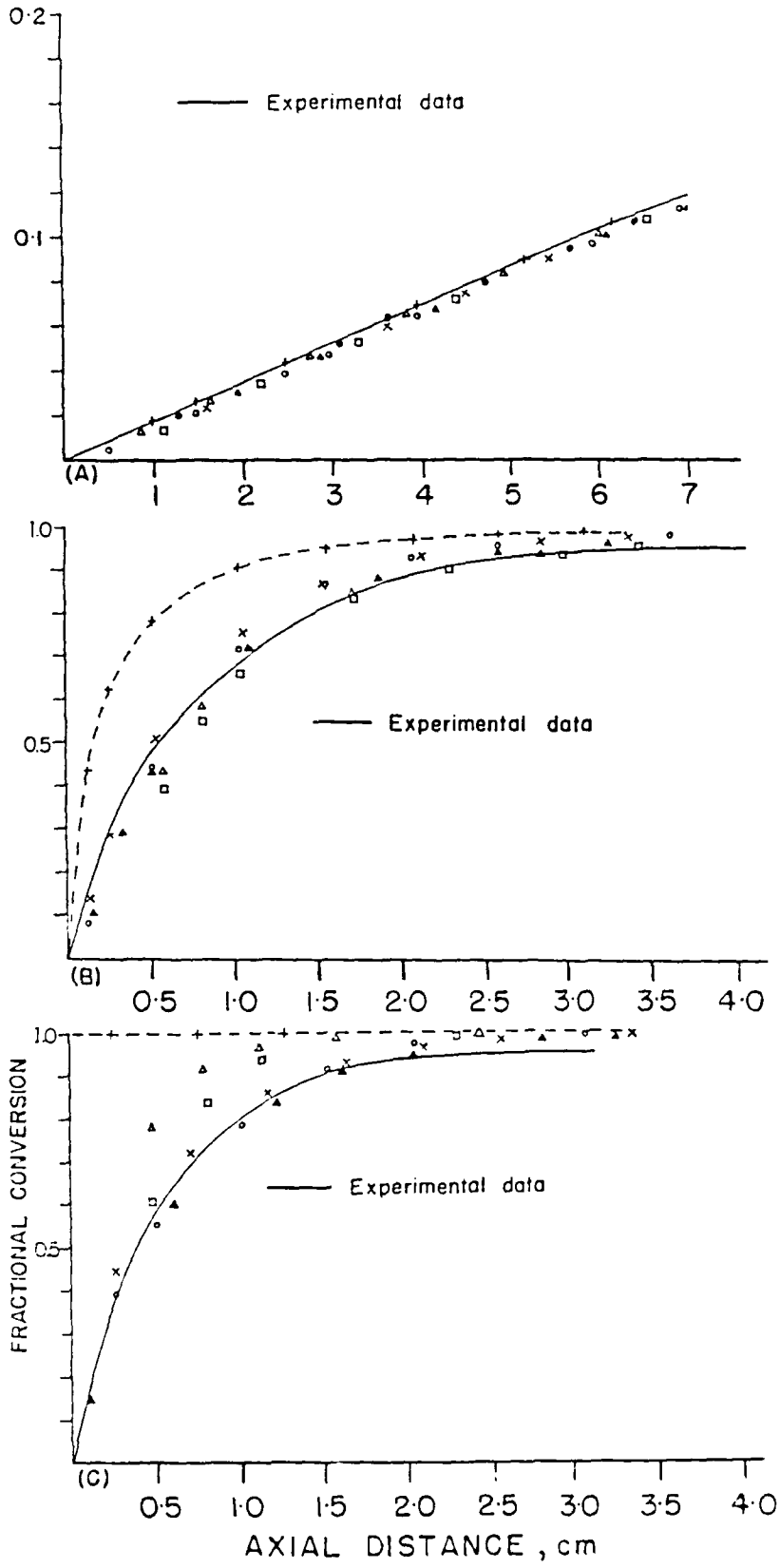
0·2
0·1
Experimental data
(A)
1
2
3
4
5
6
7
1·0
0·5
Experimental data
(B)
0·5
1·0
1·5
2·0
2·5
3·0
3·5
4·0
1·0
FRACTIONAL CONVERSION
0·5
Experimental data
(C)
0·5
1·0
1·5
2·0
2·5
3·0
3·5
4·0
AXIAL DISTANCE, cm

Experimental evaluation of the turbulence analogy is pursued further by noting that McKelvey et al. (1975) have determined τ_m in a duplicate of Vassilatos and Toor's reactor by measuring the decay of concentration fluctuations with distance downstream of the injector in a nonreactive system. τ_m (as defined by Equation (1)) was observed to be a function of axial position: its value was 0.0042 sec at 1.1 cm, and 0.015 sec at 3.02 cm. No significant reaction took place beyond this entrance region of the reactor for the "moderately fast" and "very fast" reactions (Figure 2). Thus, the average value of τ_m measured in the reaction zone was 0.0096 sec, which is within 17 percent of the value determined independently by fitting the mean axial concentration profiles (τ_m = 0.0082 sec was employed in the simulations of Figure 2). This lends support to the interpretation of micromixing parameters in terms of turbulence properties.

Treleaven and Tobgy (1973) studied single, second order, liquid phase chemical reactions in a tubular reactor with one reactant entering through a single central jet and the second reactant through the annulus surrounding the jet. Individual feedstream RTD data had been obtained previously (Treleaven and Tobgy, 1972a). A range of feed stoichiometric ratios (0.1 - 15.0) and flow rate ratios (1.0 - 3.0) were considered with reactions which could be described as "moderately fast" in the sense of Vassilatos and Toor's experiments.

Treleaven and Tobgy (1972b) used experimental RTD information and a CRD model to simulate the experiments, while Ritchie and Tobgy (1979) used the same data in 3E model simulations, and also reported results of simulations with the SD model (Ritchie and Tobgy, 1978). For the cases which were simulated by all three models, the best fit

values of τ_m determined by the turbulence analogies (Table 1) are nearly identical--differing by at most 8 percent. These observations provide additional support for the turbulence analogies.

It should also be pointed out that Mehta and Tarbell (1983b) accurately modeled the extensive set of perfectly stirred reactor data reported by Plasari (1976) with the 3E and 4E models and found values of τ_m which were within 10 percent of estimates based on Equation (2).

The comparisons in this section indicate that the five mechanistic models and their turbulence analogies are quite strongly supported by experimental data involving a single chemical reaction. This raises an important question: Is it possible to clearly discriminate among the models?

It has been generally recognized that rapid competing reactions of the type

$$A + B \xrightarrow{k_1} R$$

$$R + B \xrightarrow{k_2} S$$

are particularly sensitive to mixing as reflected in the selectivity ($2C_S/[C_R + 2C_S]$). However, Ritchie and Tobgy (1974) have shown via numerical simulations that the CRD and IEM models yield nearly the same selectivity predictions for such competing reactions in a perfectly stirred reactor when the micromixing parameters of the two models are related by: $4\tau/I = 1/h$, as prescribed by the turbulence analogies (Table 1) and $I > 4$ (we will return to this point in a later section). Prompted by this and other model comparisons, Villermaux (1983) suggested that all such mechanistic models are approximately equivalent.

Indeed, from analysis of single reaction data, one would tend to concur. However, in the next section it will be demonstrated that the models are not equivalent through simulations of a plug flow reactor with competing reactions. Unmixed feedstream plug flow reactors are intrinsically more sensitive to micromixing than stirred tanks because both reactant concentration and reactant segregation are elevated in the entrance region of the reactor. Backmixing in stirred tanks tends to reduce both of these effects.

B. Numerical Simulations for Competing Reactions

For simulations, a tubular reactor with two separate feedstreams, each characterized by the same plug flow RTD, by individual flow rates Q_A and Q_B, and by unmixed reactant concentrations C_{A0} and C_{B0} is considered. For the competing reaction scheme the kinetics of the diazo-coupling reactions reported by Bourne and co-workers (1981) is employed. The kinetic rate constants are: $k_1 = 7.3 \times 10^3$ $m^3/mol/s$; $k_1/k_2 = 2086$. Through several preliminary simulations it was found that a clear discrimination of the mixing models is apparent when the micromixing time constant is set at $\tau_m = 0.315$ s, and thus all of the results to be presented are based on this value. This τ_m is some 38 times larger than that describing Vassilatos and Toor's reactor, and is thus characteristic of a highly segregated reactor.

1. Numerical Techniques

All of the simulations were carried out on an IBM 3033 computer. The CRD model was solved by Monte Carlo methods (Spielman and Levenspiel, 1965; Treleaven and Tobgy, 1972) using a random number generator to select pairs of eddies for instantaneous mixing and

redispersion. Each eddy in the ensemble was treated as a batch reactor with appropriate material balances accounting for the reaction kinetics. Between collisions the eddy material balances were integrated by simple first order explicit predictor-corrector methods. Three hundred eddies were maintained in the ensemble and no significant changes in predictions were observed when the number of eddies was increased to 500. Typical computation times for CRD simulations varied between 500 and 5000 CPU seconds while all of the remaining models required no more than 15 seconds. The 3E, 4E, and IEM models required numerical integration of systems of nonlinear ordinary differential equations which was carried out with standard IMSL routine, DVOGER based on Gear's method. The partial differential equations of the SD model were solved by a fully implicit finite difference method with 100 uniformly spaced grid points to cover the double slabs. The 3F and 4E model equations were available in Mehta and Tarbell (1983a). The IEM and SD equations were simple extensions of equations available in Tarbell and Mehta (1985), incorporating appropriate reaction rate terms and separate material balances for each species.

The computer codes were extensively checked for accuracy and convergence (see Appendix A.1-A.5 for computer codes). In particular, the predictions of all five models were compared with available analytical expressions for two asymptotic cases: (1) diffusion of an inert tracer ($k_1 = k_2 = 0$; $C_{Bo} = 0$), (2) competing reactions under maximum mixedness conditions ($\tau_m \to 0$). In the first case, the predicted value of the tracer concentration variance was compared with the exact analytical expression presented in Tarbell and Mehta (1985), and the agreement was always found within 0.1 percent on a relative basis. For

the maximum mixed condition, very low values of τ_m were employed (τ_m = 0.0001 sec, 0.0003 sec) and the predictions were observed to be independent of τ_m. Next, for a sequence of values of C_A (average concentration) predicted by each model, the associated values of C_R and C_B were compared with values of C_R and C_B calculated from analytical expressions available in a standard text (Levenspiel, 1962):

$$C_R = \frac{C_A}{1-k_2/k_1}\left[\left(\frac{C_A}{C_{AO}}\right)^{k_2/k_1} - \frac{C_A}{C_{AO}}\right] \tag{4}$$

and

$$C_B = C_{BO} - 2(C_{AO} - C_A) + C_R \tag{5}$$

Once again, all the comparisons were within 0.1 percent on a relative basis.

2. Simulation Results and Discussion

Five different cases were simulated to provide a basis for comparison. The input parameters and predicted selectivities (X_S) are summarized in Table 3. X_S represents the fraction of B consumed to produce S when B is completely depleted. Representative concentration profiles of products R and S along the reactor length are plotted in Figures 3 to 5. Figure 3 is the base case in which flow rates and concentrations of each reactant feedstream are equal. Figure 4 shows the effects of a large variation in the flow rate ratio (Q_A/Q_B = 100), and Figure 5 shows the consequence of varying the feed concentration ratio (C_{AO}/C_{BO} = 2).

The S concentration profiles (Figures 3-5) and selectivities (X_S, Table 3) very clearly reveal large differences in the predictions of

Table 3

Selectivity of Competing Reactions in a Plug Flow Reactor as Predicted by Five Models[a]

Case	τ_m (S)	C_{Ao} (M)	C_{Bo} (M)	Q_A/Q_B	$X_s = 2\bar{C}_s/(\bar{C}_R + 2\bar{C}_s)$					(CRD-4E)/CRD %	(IEM-SD)/IEM %
					CRD	4E	3E	IEM	SD		
1	0.315	0.6×10^{-3}	0.6×10^{-3}	1	0.144	0.140	0.026	0.297	0.261	2.8	12.1
2	0.315	0.33×10^{-3}	0.33×10^{-2}	10	0.192	0.174	0.026	0.221	--[b]	10.4	--
3	0.315	0.303×10^{3}	0.303×10^{-1}	100	0.222[c]	0.186	0.026	0.058	--[b]	16.2	--
4	0.63	0.2×10^{-3}	0.2×10^{-3}	1	0.117	0.1071	0.022	0.237	0.205	8.5	13.5
5	0.315	0.6×10^{-3}	0.3×10^{-3}	1	0.0408	0.029	--	0.125	0.089	28.9	28.8

[a] Average axial flow velocity was 6.3 cm/s.

[b] No turbulence analogy, hence no valid way to choose δ.

[c] Concentration profile was sensitive to number of eddies due to high inequality in flow rate, but X_s always remained the same.

Figure 3. Axial concentration profiles for competing reactions in a PFR predicted by five models--Case 1: (A) profile of intermediate products; (B) profile of final product

0 CRD

X SD

▲ IEM

Δ 3E

□ 4E

\+ (and dotted line) - max. mix.

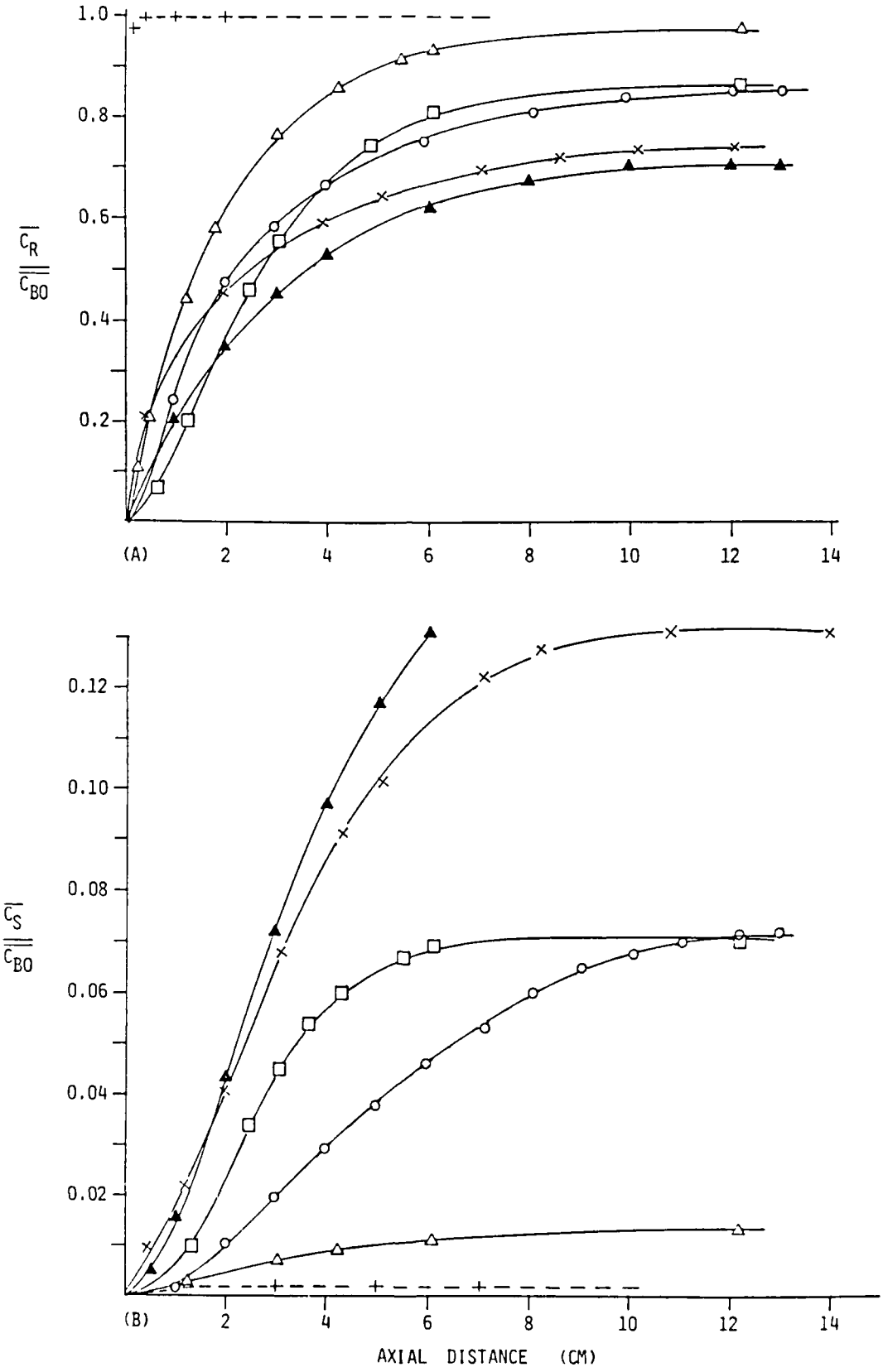
1.0
0.8
0.6
0.4
0.2
$\frac{C_R}{C_{BO}}$
(A)
2
4
6
8
10
12
14
0.12
0.10
0.08
0.06
0.04
0.02
$\frac{C_S}{C_{BO}}$
(B)
AXIAL DISTANCE (CM)

Figure 4. Axial concentration profiles for competing reactions in a PFR predicted by five models--Case 3: (A) profile of intermediate products; (B) profile of final product

▲ IEM

Δ 3E

□ 4E

\+ (and dotted line) - max. mix.

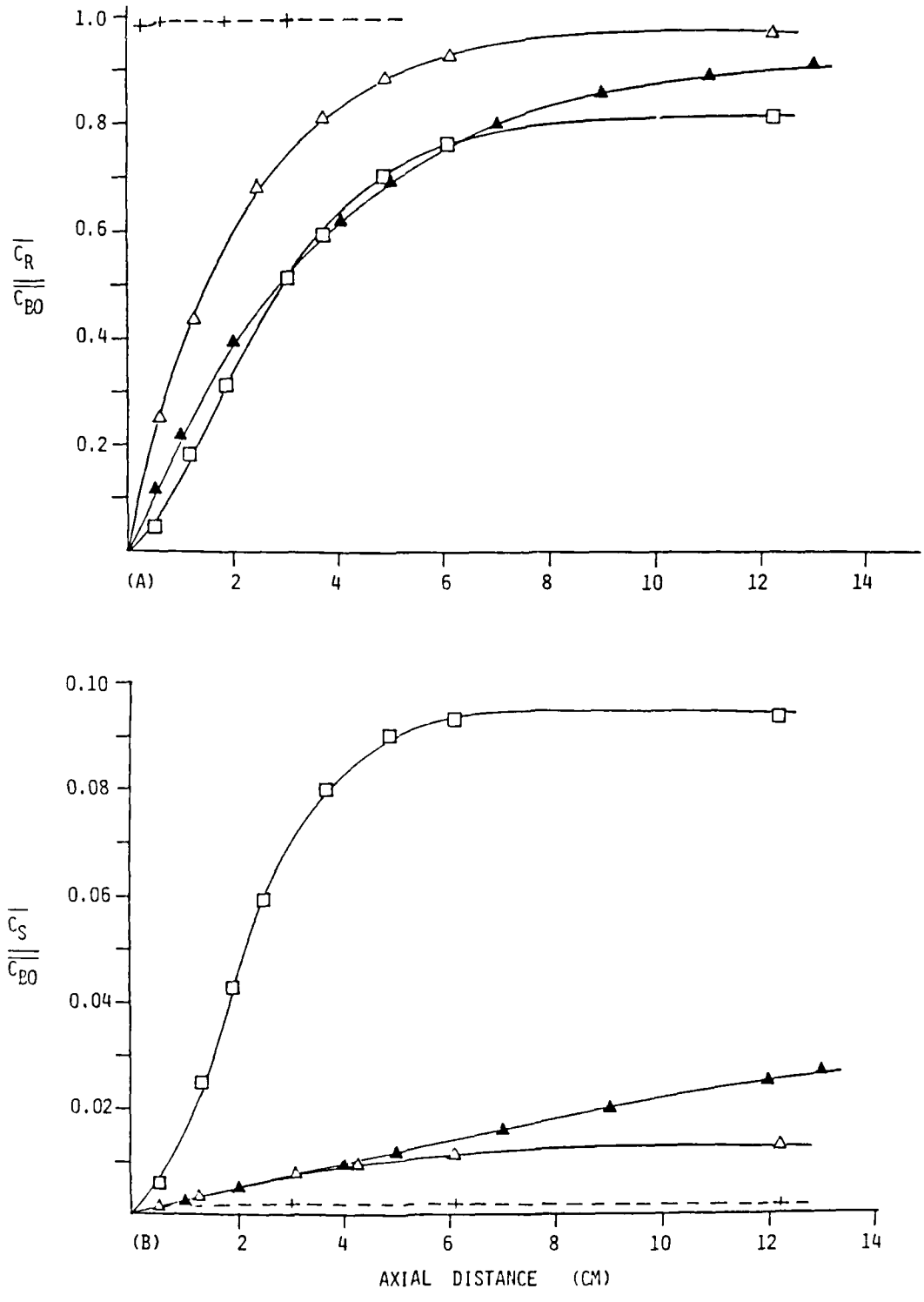
1.0
0.8
0.6
0.4
0.2
$\frac{\bar{C}_R}{\bar{C}_{BO}}$
(A)
2
4
6
8
10
12
14
0.10
0.08
0.06
0.04
0.02
$\frac{\bar{C}_S}{\bar{C}_{BO}}$
(B)
AXIAL DISTANCE (CM)

Figure 5. Axial concentration profiles for competing reactions in a PFR predicted by five models--Case 5: (A) profile of intermediate products; (B) profile of final product

O CRD

X SD

▲ IEM

Δ 3E

□ 4E

\+ (and dotted line) - max. mix.

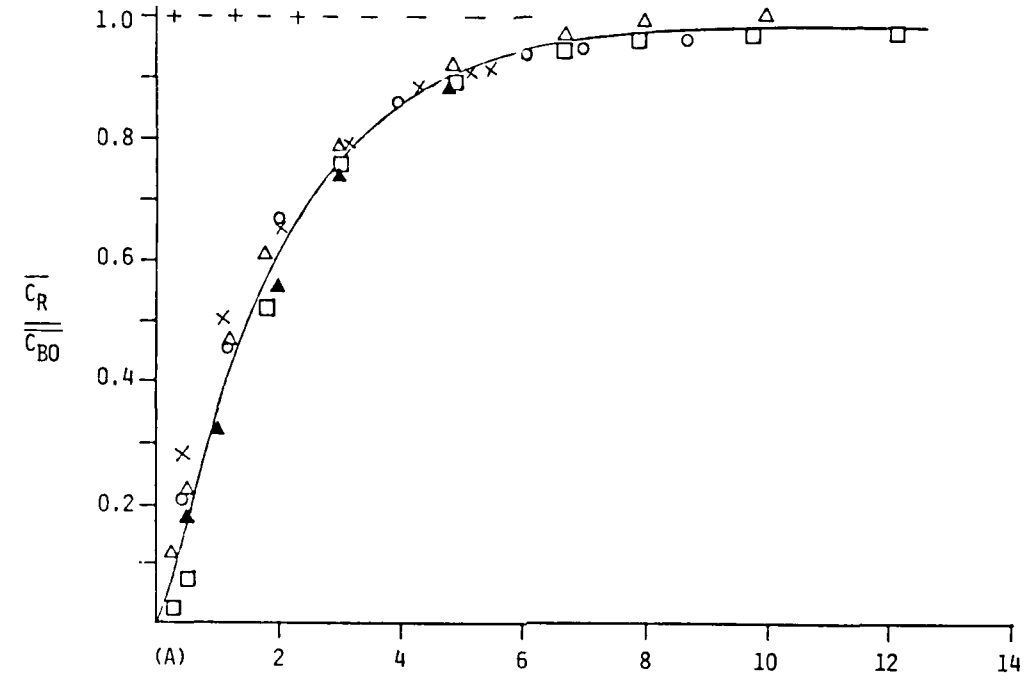
1.0
0.8
0.6
0.4
0.2
$\frac{\overline{C_R}}{\overline{C_{BO}}}$
(A)
2
4
6
8
10
12
14

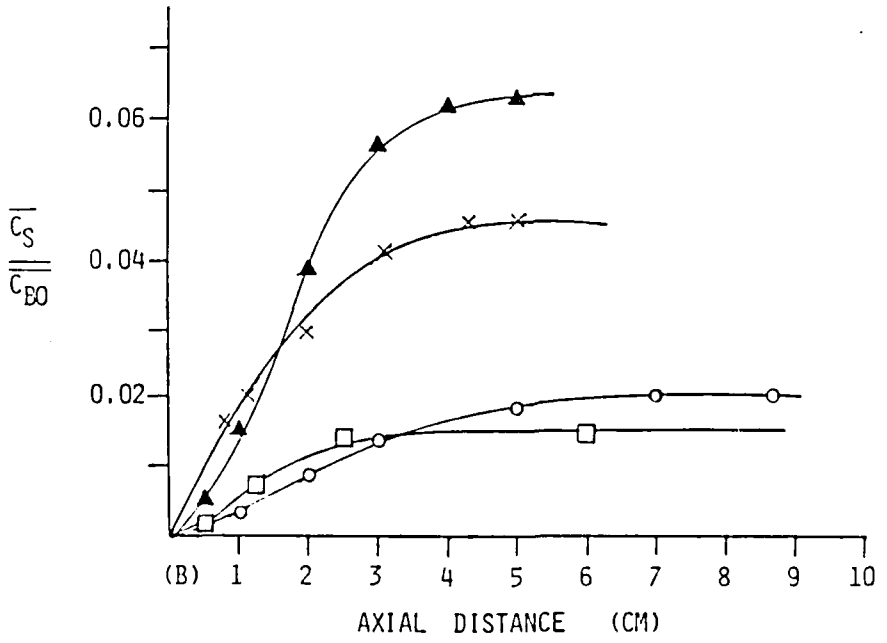
0.06
0.04
0.02
$\frac{\overline{C_S}}{\overline{C_{BO}}}$
(B)
1
2
3
4
5
6
7
8
9
10
AXIAL DISTANCE (CM)

the models. For example, there is nearly a tenfold difference in predicted S production between the CRD and 3E models for case 3, and a fourfold difference for the same case when the CRD and IEM models are compared. On the other hand, the CRD and 4E models give quantitatively similar predictions, and the same may be said of the IEM and SD models (see the last two columns of Table 3). Although not shown in Figure 5, it should be noted for case 5 (excess of A) that both the maximum mixedness and 3E models predict no production of S over the entire reactor length.

Of course, it is not possible to decide from hypothetical simulations which model, if any, is correct. This most important question must ultimately be decided by comparisons with well designed experiments. However, these simulations do seem to indicate that the 3E model is inadequate for selectivity estimation as its predictions are very insensitive to the parameter variations we have considered and are always close to maximum mixedness values. This finding is consistent with the conclusions of Mehta and Tarbell (1983b) who simulated a methane combustor with the 3E and 4E models. The failure of the 3E model is apparently a consequence of reactions taking place in a single concentration environment (L.E.) which is at the mean concentration. All of the other models contain at least one rich reacting region for each of the reactants. This all points to the importance of structural features of mixing models.

Because of the observation that the CRD and 4E models give similar predictions which are significantly different from those of the IEM and SD models, we naturally wonder if there are prominent structural differences between these pairs of models which may be responsible for

the observations. As mentioned previously, all four models possess the structural feature of "rich reacting regions" for each reactant. However, only the CRD and 4E models contain unmixed (unreacted) regions, while the IEM and SD models do not (see Figure 1). The presence or absence of "unmixed regions" in the reaction mixture may be important in selectivity predictions, particularly in highly segregated reactors. In fact, in simulations of the parallel-consecutive reaction scheme in a CSTR by both the IEM and CRD models, Ritchie and Tobgy (1974) found that in highly segregated reactors ($I < 4$), the predictions of the models differed substantially, whereas the comparisons were quite favorable in less segregated reactors ($I > 4$). The simulated plug flow reactor above is characterized by a maximum value of $I \simeq 6$ at the end of the reaction zone, and this value of course decreases to zero at the reactor entrance. Thus the simulated reactor is highly segregated over most of its length.

The present experimental study derives its motivation from these results. The details of the experiments are considered next.

IV. EXPERIMENTAL DESIGN

A. General Discussion

The goal of this experimental study is to obtain reliable data from a highly segregated turbulent flow reactor such that the observed mixing effects are significantly larger than the errors in the measurements. Furthermore, we want to discriminate among rival models by comparison of model predictions with the experimental data. Thus, proper choice of reactor and reaction system is very critical.

Turbulence is a complex flow phenomenon and its interaction with chemistry of competing reactions makes it even more complex. In this context it is desirable to use as simple a flow field as possible in our reactor. Conceptually, the simplest turbulent flow is a completely isotropic one in which all turbulence properties are invarian to axis rotation, reflection, and translation. Such a fluid implies spatial homogeneity, but it would be decaying with time because its definition excludes existence of any turbulence generation within the field. A field which is nearly isotropic can be produced downstream from a periodic grid placed perpendicular to the mean flow in a pipe. A similar one-dimensional isotropic field can also be produced downstream from a multitube mixing head placed in a pipe. The resultant turbulence field is homogeneous in any plane parallel to the grid or the mixing head, except in the wall boundary layers, but decays in the downstream direction. Thus, the turbulence field would be statistically stationary in space but inhomogeneous in the streamwise direction. This is essentially a plug flow with fairly well defined turbulence characteristics. It is important to note that a PFR with separate

feedstreams is intrinsically more sensitive to mixing than a perfectly stirred reactor as the absence of any backmixing in a PFR allows much higher reactant concentration and segregation in the entrance region. Thus, a turbulent PFR appears to be an appropriate choice for our purpose.

Both screens (Keeler et al., 1965) and multitube mixing heads (Vassilatos and Toor, 1965; Mao and Toor, 1972; Torrest and Ranz, 1970; Fisher, 1974) have been employed in the past to generate a characteristic turbulent field in a uniform mean flow field. Both of them provide similar flow conditions downstream from their backfaces. The flow emerges as jets which coalesce some distance downstream of the turbulence generator. The region up to the coalescence plane is somewhat ill-defined. Previous studies of very fast reactions in multitube mixing head reactors have shown that the conversion of limiting reactant is 60 percent or higher at the jet coalescence plane (Vassilatos and Toor, 1965; Mao and Toor, 1972; Fisher, 1974). This is a significant shortcoming of a multitube mixing head. A more satisfactory arrangement, with screens, is found in the flow reactor of Keeler et al. (1965). It consists of a specially designed "hair-brush" injector and an ordinary wire mesh at the reactor entrance (see Figure 6). Reactant A enters the reactor through the main flow and B enters isokinetically through the "hairbrush" injector. The isokinetic injection implies a large difference of flow rates between two streams. As a result, the low flow rate stream (i.e., B) is proportionately more concentrated to render the two streams stoichiometric. The injector provides a uniform coarse scale distribution of reactants over the cross-section with only a little micromixing

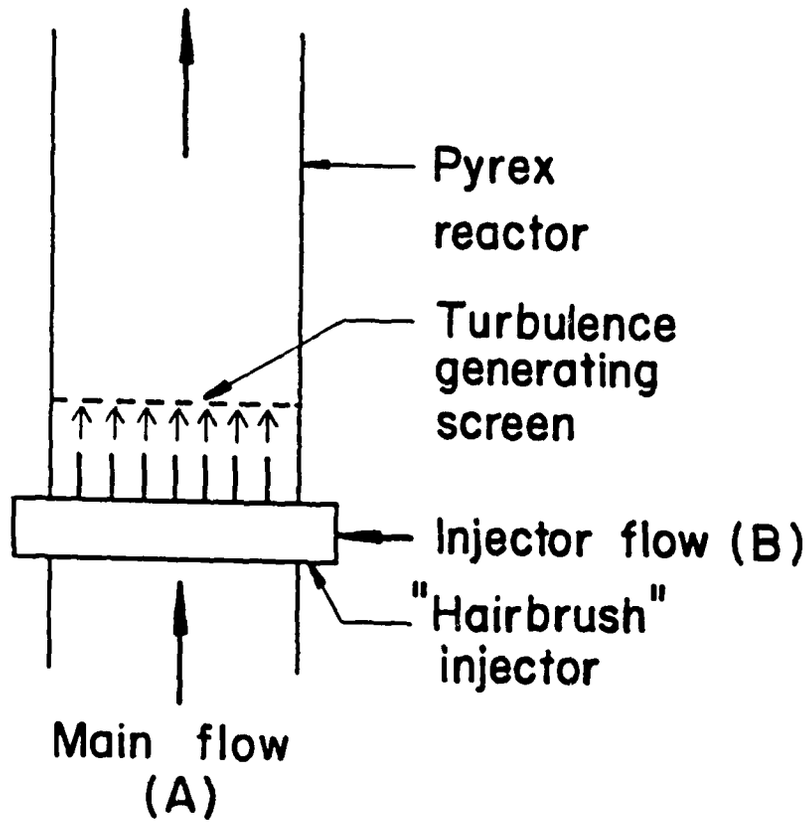

Figure 6. Schematic diagram of Keeler's reactor (Keeler et al., 1965)

(hence, little reaction). The screen downstream of the injector trips the turbulence and thereby induces micromixing and reaction. Keeler's experiments showed that the extent of conversion at the jet coalescence plane was merely 2 to 5 percent (Keeler et al., 1965). A similar arrangement of "hairbrush" injector and screen is employed in the present work.

Many single phase competing reactions of the type

$$A + B \rightarrow R \tag{6}$$

$$R + B \rightarrow S \tag{7}$$

have been reportedly found to be sensitive to micromixing. Bourne (1982) has compiled a list of such reactions. All the reactions occur in a single liquid phase. Among these, the azo-coupling of 1-naphthol (A) with diazotised sulfanilic acid (B) in dilute aqueous solution at room temperature is considered the most suitable. In this scheme (Bourne et al., 1981), the first coupling leads to formation of 4-(4-sulfophenylazo)-1-naphthol (R), briefly described as monoazo dye, and the subsequent coupling of R with B produces 2,4-bis(4-sulfophenylazo) -1-naphthol (S), briefly, diazo dye. Both R and S absorb light in the visible part of the spectrum (400 nm-600 nm) and their concentrations can be measured spectrophotometrically. The reaction system has several attractive features:

(1) The reactions are irreversible and the kinetics are relatively well understood.

(2) Among the candidate competing reactions, these two reactions have the fastest kinetics at room temperature. The

characteristic reaction time scale for the first coupling is 0.5 msec and for the second one is 1 sec. Computer simulations have shown that for a given mixing time, this system of reactions yields the largest difference among the predictions of rival models as compared to other reported reaction schemes. This fact makes these reactions particularly suitable for our purpose.

(3) The reactions are conducted in an aqueous medium (pH = 10.00). This is convenient, safe and inexpensive.

(4) The low reagent concentrations (0.1-0.3 mol m^{-3}) are economically attractive.

B. General Description

A schematic diagram of the flow system used in this study is shown in Figure 7. A 0.21 m^3 polyethylene tank serves as the feed tank for the reactant A. The solution is pumped by a 746 W sealless, magnetic drive centrifugal pump (Model TE-7R-MD, March Mfg., Inc., IL) through a rotameter (Fischer & Porter Co., PA, precision bore flowrator tube No. B6-35-10/77) to a flow distributor. The passage of the flow through this distributor leads to the development of a nearly flat velocity profile and the subsequent passage through a contraction nozzle further reduces the existing turbulence. The flow then passes through the "hairbrush" injector, the turbulence producing screen, and enters the reactor. The reactor is simply a 0.45 m section of 5.08 cm I.D. Pyrex pipe which terminates in a stainless steel overflow chamber.

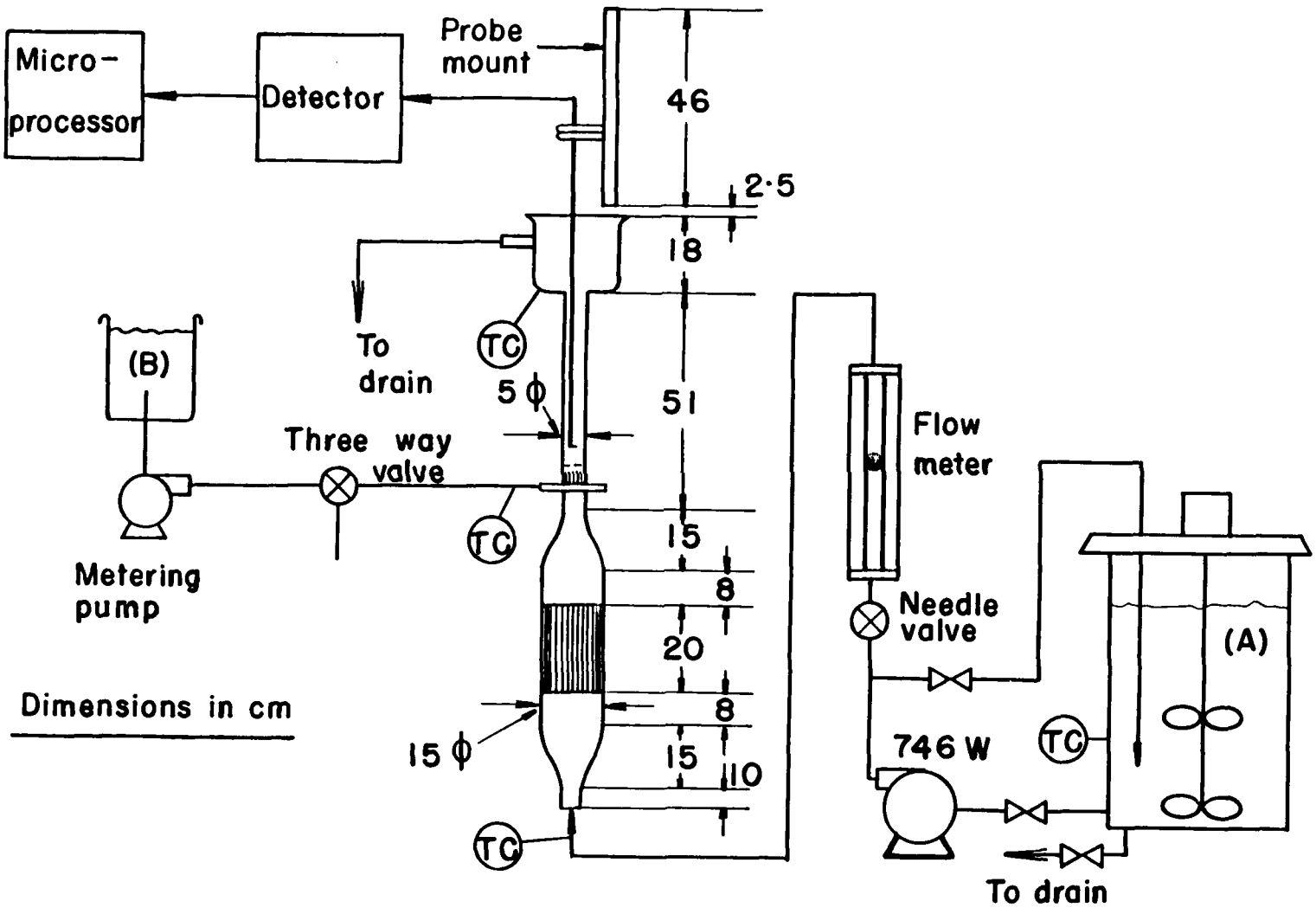

Figure 7. Schematic diagram of experimental system

The reactant B solution is pumped from a $2x10^{-3}$ m^3 laboratory glass beaker by a $5.4x10^{-5}$ W laboratory metering pump with a micrometer flow adjuster (Fluid Metering, Inc., NY, Model RP-D) into the plenum chamber of the "hairbrush" injector. The solution then enters the main flow through the "hairbrush" (hypodermic) needles in the form of axial jets. The flowrate of B is usually 1/100th of the flow rate of A but feed B is proportionately more concentrated than feed A.

The needle valve controlling the naphthol flow rate and the three-way valve before the injector, are both made from stainless steel. All other auxiliary parts such as piping, bends, tees, and unions are made from PVC. The piping for the naphthol stream is 2.54 cm I.D. PVC and that for the diazotised sulfanilic acid is 0.64 cm I.D. PVC. The mechanical vibrations from the pumps are reduced by putting styrofoam paddings underneath the pumps and by connecting the pump outlet to the remaining flow loop by a Tygon tubing of the same diameter. Flexible Tygon tubing further damps the vibrations.

Copper-Constantan thermocouples are placed at appropriate locations and temperatures of the two feedstreams are monitored with a digital thermometer (Omega Engineering, Inc., CT, Model 2176A).

C. Flow Distributor and Contraction Section

A honeycomb type flow distributor is used in this work where the cells have a large length-to-diameter ratio (L/D = 33). Such honeycombs have been used successfully in water tunnels to reduce turbulence to acceptable levels (Lumley and McMohan, 1967). The honeycomb has two effects: it reduces the level of the existing turbulence, and it creates additional turbulence of its own. By evenly distributing the

flow, the honeycomb also yields a nearly flat mean velocity profile. For economy and convenience, the packing of plastic drinking straws (6 mm I.D.) into a honeycomb-like matrix is used. Such a "poor man's honeycomb" has been successfully employed in low-speed wind tunnel research (Loerhke and Nagib, 1972). The straws are packed into a 15 cm I.D. Pyrex pipe and held in place by adhesive on the straw-wall. The estimated solidity (fraction of pipe area which is not open to the flow) of this honeycomb is 0.33. For any turbulence manipulator, such as this honeycomb, it is important that the solidity be maintained below a critical value (usually 0.43), otherwise jets emanating from the manipulator coalesce to form a central jet which is highly undesirable (Tan-Atichat et al., 1982). A settling chamber about 0.5 diameter long follows the honeycomb. This allows the mean profiles emanating from individual straws to merge and settle to a more uniform overall profile. This section is known to improve the flow at the entrance to the test section (Pope, 1947).

Next, the flow enters the contraction section. It has been shown that the fluctuating component of velocity varies inversely as the square of the contraction ratio (Pope, 1947). The contraction ratio of nine used in this research conforms to standard water tunnel practice. The shape of the contraction zone is not critical. In general, any smooth curve is satisfactory (Pope, 1947; Steele, 1951). The section is about one upstream diameter long and tapered very gradually at the downstream end so that the flow has space to even out.

D. Injector Head and Turbulence Producing Screens

The "hairbrush" injector is a duplicate of the one used by Keeler (1965). It consists primarily of a matrix of 18 gauge stainless steel hypodermic needles (total of 37 needles) arranged on a 9/32 in. square lattice as shown in Figure 8. Diazotised sulfanilic acid enters the circumscribing plenum chamber (10 cm O.D., 5 cm I.D.) which distributes it among its seven 3.18 mm I.D. tubes. These tubes, in turn, further distribute the flow among the needles they support. For easy fabrication, the plenum chamber is constructed from brass. However, brass reacts with diazotised sulfanilic acid at experimental concentration. Consequently, the interior of the plenum chamber is coated with protective varnish ordinarily available at a local art supply store (Univar, F. Weber Co., PA). The thin protective coating prevents any measurable reaction between the B stream and the plenum chamber wall (see Figure 9 for a photographic view of the injector).

Keeler (1965) has reported that the variation in injection rates from needle to needle is less than 0.5 percent. Cairns and Prausnitz (1960) have shown by calculations that at a distance of about 13 mm downstream from the injector there is only 9 percent "ripple" in the radial concentration profile if an inert dye is injected through the needles. Thus, this system is an attractive device to establish a nearly plane concentration front. The feed tubes and the needles do generate turbulence but it is modified by the turbulence generator screen downstream of the needles. In the present work, a screen is placed either upstream or downstream of the injector, producing different mixing conditions depending on the screen placement.

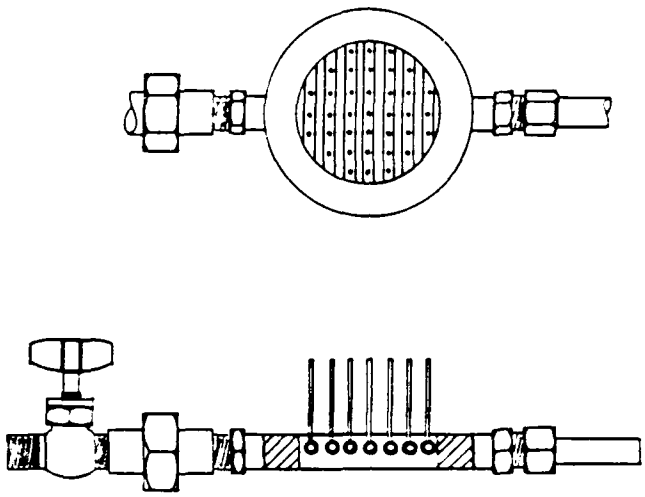

Figure 8. Sectional view of "hairbrush" injector

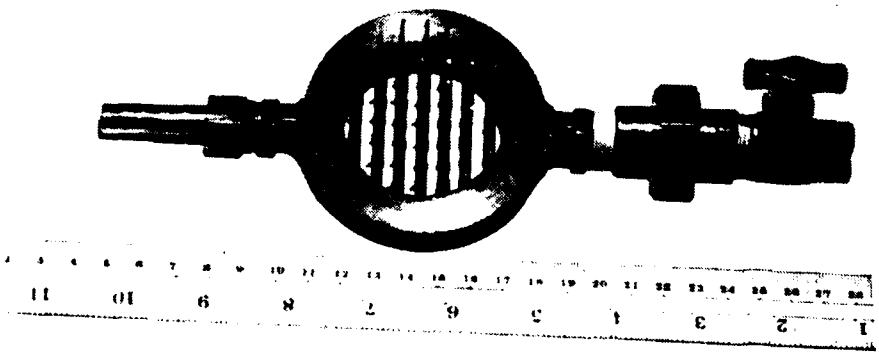

Figure 9. "Hairbrush" injector

The screens are ordinary wire mesh screens (Newark Wire Cloth Co., NJ). They are chosen to generate different turbulence scales in the flow. The screens are placed about 7 mm downstream or upstream of the needle tips. A Lucite piece with a 6.4 mm recess provides the seat for the screen (see Figure 10). The screen is actually sandwiched between two carefully cut rubber gaskets. The Lucite piece and the gaskets have the same I.D. as the reactor and the assembly rests on another rubber gasket placed on the downstream face of the injector. The relevant screen dimensions are listed in Table 4.

Table 4

Screen Characteristics

Screen	M_1	M_2	M_3
Solidity, (S)*	0.43	0.39	0.60
Wire diameter (d) mm	1.01	0.46	0.31
Mesh length (M) mm	4.24	2.12	0.85
Mesh ratio (M/d)	4.22	4.63	2.73

*Solidity, $S = 1 - (M-d)^2/M^2$.

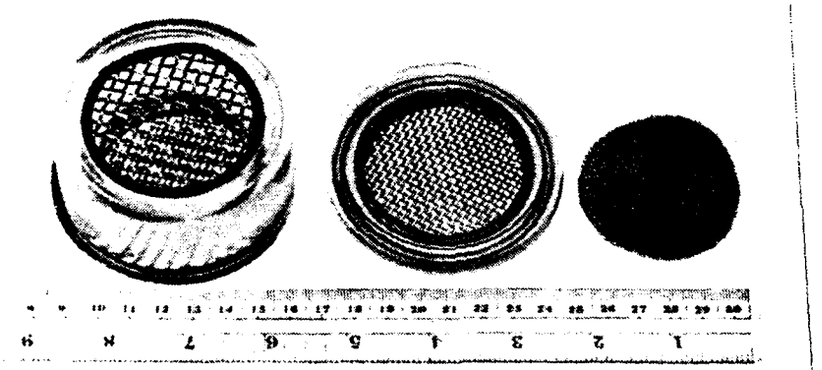

Figure 10. Turbulence producing screens

E. Probe Mount

The probe mount is a 50 cm long vernier slide which is attached to a steel base plate (see Figure 11). The groove in the base plate permits movement of the slide in a horizontal plane. Since the groove can be rotated around the center, the probe mount essentially allows three-dimensional movement, with an axial positioning accuracy of 0.25 mm.

F. Pulsed Ultrasonic Doppler Velocimeter

In this study a well characterized turbulent flow field is desired in the reactor. Measurements of local mean and fluctuating velocity at several locations are necessary for such a characterization. A pulsed ultrasonic Doppler velocimeter (PUDV) is used for these measurements.

The PUDV operates on the Doppler principle. When sound waves are reflected off a moving object, there is a shift in their frequency. This Doppler shift is related to the velocity of the object in the following manner:

$$\Delta f_d = \frac{2uf_o\cos\theta}{u_s} \tag{8}$$

where u is the velocity of the object, Δf_d is the Doppler shift in frequency, u_s is the speed of sound in the medium, θ is the acute angle between the sound beam and the velocity vector and f_o is the source frequency.

The acoustic transducer consists of a single unfocused piezoelectric crystal (3 mm diameter) which covers the tip of a tungsten-epoxy stem (Etalon Corp., IN). The crystal transmits 10 MHz ultrasound

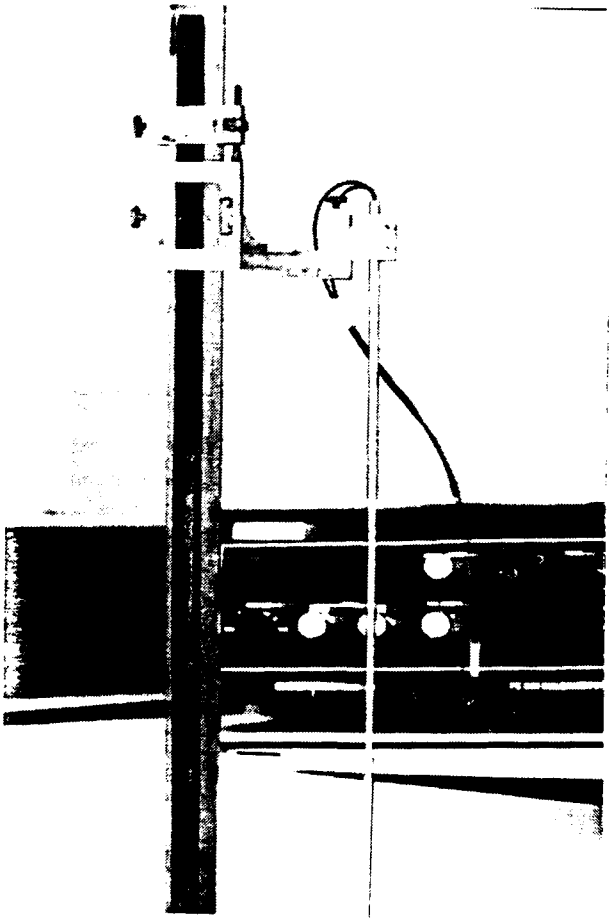

Figure 11. Probe-mount

in 0.4 μsec pulses with a pulse repetition frequency of 20 kHz. The echoes returning from scattering particles in the fluid are quadrature phase detected and sampled by 0.3 μsec pulses with variable delay between 3 and 51 μsec. This delay provides range-gating between 2 and 39 mm. The sample volume is located 3.5 diameter way from the transducer face. Thus, the sample flow field is expected to be free from transducer induced disturbances. The quadrature audio signal is filtered at the pulse repetition frequency, and low frequency components below about 200 Hz are removed prior to processing by a directional zero crossing counter which converts Doppler frequency shift into voltage. This voltage proportional to velocity signal is ultimately smoothed by a one-pole filter at 120 Hz. The maximum velocity which can be resolved by the PUDV without aliasing error is 75 cm/sec. The system was designed and built by Dr. C. J. Hartley of Baylor Medical College, TX.

The sample volume is approximately cylindrical, 0.45 mm in the direction of transmission and 3 mm in the transverse direction with the equivalent volume of a sphere having 1.8 mm diameter. It is important to consider how the turbulence scales might compare with these dimensions. One would expect the energy containing eddies, which make the predominant contribution to the root-mean-square velocity fluctuations (u_{rms}), to have a length scale (ℓ_e) of order of the size of the dominant turbulence generator (6.5 mm) which is discussed later on. Thus, the sample volume of the velocimeter would appear to be sufficiently small in the direction of transmission to resolve the most important scales of the turbulence. The frequency of fluctuations in the energy containing eddies (ω_e) should have an order of magnitude

given by (u_{rms}/ℓ_e). For the maximum u_{rms} measured within the reactor (~0.8 cm/sec), ω_e is of order of 2 Hz. Thus, the frequency response of the velocimeter output (120 Hz) should be more than adequate for the large scales.

The smallest scales in the flow may be characterized by the Kolmogorov microscales of length (η) and frequency (ω) as follows:

$$\eta = (\nu^3/\varepsilon)^{1/4}, \quad \omega = (\varepsilon/\nu)^{1/2}, \quad . \quad . \quad . \tag{9}$$

where ν is the fluid kinematic viscosity and ε is the kinetic energy dissipation rate per unit mass ($\varepsilon = u_{rms}^3/\ell_e$). Taking ℓ_e and u_{rms} as before and noting $\nu = .008$ cm^2/sec, we find $\eta \sim 0.3$ mm and $\omega \sim 10$ Hz. Thus, the frequency response of the velocimeter output (120 Hz) is also adequate for these scales, but the sample volume is an order of magnitude too large.

Scattering of ultrasound is provided by fine air-bubble mist found in the ordinary tap water (mean bubble diameter $\approx$ 60 μ). The mean rise velocity of the bubbles is 3 percent of mean flow velocity in the reactor. Therefore, the bubbles are expected to easily follow the fluctuating velocities in the reactor. Jorgensen et al. (1973) describe the PUDV and Garbini et al. (1982) discuss the use of this ultrasonic technique in measurement of fluid turbulence. The velocimeter yields an output signal of 0.25 volts/KHz shift in frequency. This analog signal is passed through a low pass filter (Model 3750, Krohn-Hite Corp., MA) to an integrated data acquisition and data processing microcomputer system (Model DATA 6000, Data Precision, MA). The microcomputer provides mean and r.m.s. values of the detected

signal from which the mean and r.m.s. velocities are calculated (see Appendix B for a sample calculation). The results are reproducible within 5 percent for the mean and 15 percent for the r.m.s. voltages, with $\pm$ mV accuracy.

G. Spectrophotometer System

The primary goal in this work is to measure local concentrations of R (monoazo dye) and S (diazo dye) at several locations in the reactor. Since both R and S absorb visible light, absorption spectrophotometry (colorimetry) is employed to measure these concentrations. This technique is based on the Beer-Lambert law. According to this law, when a monochromatic light beam of constant intensity I_o^λ passes through a small volume containing an absorbing specie i with concentration C_i and over a length ℓ, the resultant attenuated light intensity I^λ is given by

$$I^\lambda = I_o^\lambda \exp(-\varepsilon_i^\lambda C_i \ell) \tag{10}$$

ε_i^λ is the molar absorptivity of the specie i at the wavelength λ.

For our purposes, the Beer-Lambart law is assumed to hold for a stochastic concentration C_i as well, where

$$C_i = \bar{C}_i + C_i' \tag{11}$$

The overbar denotes the time-mean value while prime denotes the fluctuating part. Then, the attenuated light intensity, I^λ, is also stochastic in nature. Now, if only R and S absorb in the visible range, and do so independently at the prevailing concentration levels

(of order 10^{-2} to 10^{-1} mol/m^3), one can write

$$I^{\lambda} = I_o^{\lambda} \exp(-\varepsilon_R^{\lambda} C_R \ell - \varepsilon_S^{\lambda} C_S \ell) \tag{12}$$

Alternatively,

$$\ell n \left(\frac{I_o^{\lambda}}{I^{\lambda}}\right) = \varepsilon_R^{\lambda} \ell C_R + \varepsilon_S^{\lambda} \ell C_S \tag{13}$$

Taking time-mean values of all the stochastic variables, one arrives at

$$\overline{A^{\lambda}} = \overline{\ell n \left(\frac{I_o^{\lambda}}{I^{\lambda}}\right)} = \varepsilon_R^{\lambda} \ell \overline{C_R} + \varepsilon_S^{\lambda} \ell \overline{C_S} \tag{14}$$

where $\overline{A^{\lambda}}$ is the mean absorbence of the medium. In general,

$$\overline{A^{\lambda}} = \overline{\ell n \left(I_{ref}^{\lambda}/I^{\lambda}\right)} = \varepsilon_R^{\lambda} \ell \overline{C_R} + \varepsilon_S^{\lambda} \ell \overline{C_S} \tag{15}$$

where I_{ref}^{λ} is the intensity of light in a reference medium. This linear relationship of $\overline{A^{\lambda}}$ with $\overline{C_R}$ and $\overline{C_S}$ is very critical to measurements. A standard linear regression can be used on $\overline{A^{\lambda}}$ values at several wavelengths (but at the same spatial location) to determine $\overline{C_R}$ and $\overline{C_S}$, provided $\varepsilon_R^{\lambda} \ell$ and $\varepsilon_S^{\lambda} \ell$ are known. The latter quantities can be determined separately by calibration of a sample of known concentration.

It turns out that R and S are highly absorbing in the range 400-600 nm (i.e., ε_R^{λ} and ε_S^{λ} have relatively large magnitudes). This indicates that the path length ℓ must be about 1 mm if Equation (14) is to be used to measure concentration levels of 10^{-2} to 10^{-1} mol/m^3 without saturating the detector ($\overline{A^{\lambda}}$ should lie between 0.1 and 1.0). Thus, an intrusive fiber-optic probe is needed to measure absorbance locally.

In the past, fiber-optic probes have been successfully used to measure concentration fluctuations in chemically nonreacting (Lee and Brodkey, 1963; Nye and Brodkey, 1967) and reacting (Mahalingam and Chevray, 1983) flows. For greater precision, all these studies have employed their own designs of optical and electronic measurement system. Since measurement of mean concentrations is of primary interest, which is considerably less demanding than measuring fluctuating concentrations, an off-the-shelf colorimeter (Brinkman, Model PC-801) is used in conjunction with a specially designed fiber-optic probe for the absorbance measurements. The design of the probe is based on the requirements that the probe introduce only a minimum of flow disturbance in the measurement volume and that it provide an acceptable spatial resolution. These and other fabrication requirements have led us to the fiber-optic probe shown schematically in Figure 12. The probe was fabricated according to our specifications by Fiberoptics Fabrications, Inc., MA.

The transmitter fiber bundle has a 1 mm O.D. and is illuminated by the colorimeter light source at one end. The receiver fiber bundle, which also has a 1 mm O.D., is separated by 1 mm from the end of the transmitter bundle (see bottom of Figure 12) and carries the attenuated signal back to the colorimeter. The signal passes through an interference filter mounted on a filter wheel before impinging on the silicon photodetector. The filter wheel has six different filters mounted on it which allows selection of six different wavelengths (450, 470, 490, 520, 545, and 570 nm), with a 20 nm half-peak bandwidth for each filter. The photodetector generates a current directly proportional to the light

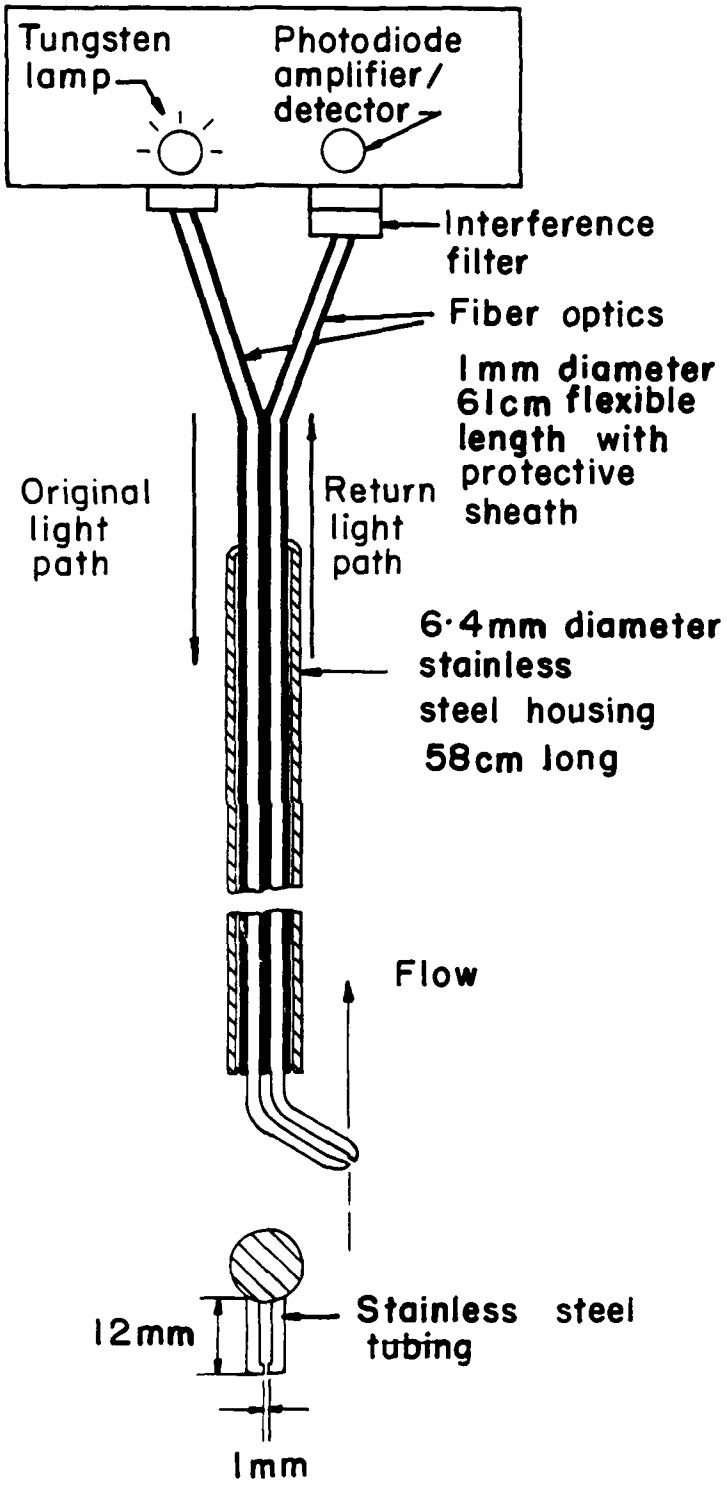

Figure 12. Schematic diagram of fiber-optic probe

intensity, which is, after passage through a variety of electronic circuits (somewhat modified by us), available as an output voltage.

The output voltage is directly proportional to $\overline{\ell n(I_o^{\lambda}/I^{\lambda})}$, which is different from $\overline{A^{\lambda}} = \overline{[\ell n(I_o^{\lambda}/I^{\lambda})]}$. The former involves first taking the time average of a signal and then taking the natural logarithm of it while it is exactly the other way around for the latter. Fortunately, even very conservative estimates show that the error introduced by equating these two quantities, i.e.,

$$\overline{\ell n(I_o^{\lambda}/I^{\lambda})} \approx \overline{A^{\lambda}} \tag{16}$$

is less than 1 percent in the experimental range (see Appendix C). Thus, we are able to get an output signal $(\overline{V^{\lambda}})$ which is directly proportional to the absorbance $(\overline{A^{\lambda}})$.

The Brinkman colorimeter is chosen because it has several attractive operating characteristics:

(1) It supplies phase shifted, AC modulated light to the probe tip. At the detector end, it uses an amplifier with an electronic chopper that is synchronized with the light source, but phase-shifted by 90°; as a result, ambient light does not affect the instrument reading.

(2) It has electronic circuitry that ensures excellent line stability. Other laboratory appliances such as stirring motors and pumps, plugged into the same circuit, do not affect the stability of the colorimeter output.

(3) It exhibits good linearity in the sense of Beer-Lambart law under the experimental conditions.

It is important to note that the Brinkman colorimeter is a single beam spectrophotometer. Since the electronic chopper at the detector end is electrically synchronized with the light source, I_o^λ is an arbitrary internal reference which is always a constant. For an absorbance value with respect to another reference medium (I_{ref}^λ), two separate measurements are required. The basic method of analysis is as follows. For a given solution containing R and S,

$$\overline{V^\lambda} = k_p \ell n(\frac{\overline{I^\lambda}}{I_o^\lambda}) \tag{17}$$

where k_p is the proportionality constant. Similarly, for a reference solution,

$$\overline{V_{ref}^\lambda} = k_p \ell n(\frac{\overline{I_o^\lambda}}{I_{ref}^\lambda}) \tag{18}$$

Subtracting (17) from (16), we get

$$\begin{aligned}
\Delta\overline{V^\lambda} &= \overline{V^\lambda} - \overline{V_{ref}^\lambda} \\
&= k_p \ell n(\frac{\overline{I_o^\lambda}}{I^\lambda}) - k_p \ell n(\frac{\overline{I_o^\lambda}}{I_{ref}^\lambda}) \\
&= k_p \ell n(\frac{\overline{I_{ref}^\lambda}}{I^\lambda}) \\
&\simeq (k_p \varepsilon_R^\lambda \ell)\ \overline{C_R} + (k_p \varepsilon_S^\lambda \ell)\ \overline{C_S} \quad (\because \text{Equation (15)}) \\
&= k_R^\lambda\ \overline{C_R} + k_S^\lambda\ \overline{C_S}
\end{aligned} \tag{19}$$

where $k_R = k_p \varepsilon_R^{\lambda} \ell$ and $k_S = k_p \varepsilon_S^{\lambda} \ell$. Both k_R^{λ} and k_S^{λ} are constants and are independently determined by calibration of the probe with known solutions of R and S. Thus, $\overline{\Delta V^{\lambda}}$ values are needed, each of which involve two measurements ($\overline{V^{\lambda}}$ and $\overline{V_{ref}^{\lambda}}$) at each location, to determine $\overline{C_R}$ and $\overline{C_S}$. A standard linear regression routine is used to determine the values of $\bar{C}_R$ and $\bar{C}_S$ which will minimize the square of the difference between the measured $\overline{\Delta V^{\lambda}}$ at five wavelengths and the calculated values of $\overline{\Delta V^{\lambda}}$ (based on $\bar{C}_R$ and $\bar{C}_S$). These values of $\bar{C}_R$ and $\bar{C}_S$ are termed the "experimental values." In general, the standard deviations of these regressed values are 10 and 17 percent for $\bar{C}_R$ and $\bar{C}_S$, respectively.

The gap size of the fiber-optic probe is small (1 mm) and it would seem that the boundary layer along the exposed fiber-faces may affect the local flow field in the gap. Based on the fact that Lee and Brodkey (1963) did not find any such effects in concentration fluctuation measurements with a similar probe (1 mm tip diameter, 1 mm gap), it is expected that the boundary layer growth has negligible effect on the mean concentration measurements of this study.

V. MEASUREMENTS

The experimental work was divided into two parts: Flow Field Characterization, and Mixing-Reaction Studies.

A. Flow Field Characterization

1. Comments

The flow field characterization involved measurement of the mean and r.m.s. velocities at several locations in the reactor. These experiments were conducted separately from the mixing-reaction studies but retained the same hydrodynamic conditions (i.e., the same pipe Reynolds number).

Two points deserve comments here.

(1) It is generally necessary to seed the flow with scattering particles when a PUDV is used. Polystyrene microspheres at 0.5 wt% concentration perform satisfactorily in such cases. Nevertheless, it was difficult to maintain a uniform suspension of microspheres in the feed tank. This was mainly due to the large hold-up (0.05 m^3) and the inability of the stirrer to sweep the particles from the floor of the feed tank. It was found, per chance, that the fine mist of air bubbles in ordinary tap water obviated the need for any further seeding of the flow. Therefore, ordinary tap water was used as the working fluid. The validity of the experimental procedure is considered in the next section.

(2) The PUDV and the data acquisition system initially were found to electrically interact with each other resulting in a highly

noisy and nonreproducible signal. A specially designed low pass filter, which filtered both on the "hot" and the ground sides of the connecting cable at 120 Hz, along with a large length of the cable, was found effective in reducing the interaction to an acceptable level. The measured values contained this small amount of electronic noise. Furthermore, the Doppler signal in this technique is always contaminated with a broad-band random noise called the "Doppler ambiguity." This phenomenon is similar to that occurring in laser anemometry, but its effect is very significant for this technique because of a much larger sample volume. The random noise is caused by the random transit of scattering particles through the finite sample volume. There is also noise associated with buoyancy of bubbles and the bubble size distribution. All except the Doppler ambiguity were considered in the subsequent calculation of velocities in the reactor.

2. Validation of the Experimental Method

To establish the validity of our experimental procedure, a test case of fully developed turbulent flow in a pipe was chosen. The principal advantage of this configuration was that a large body of experimental results using hot-film and laser-Doppler anemometry was available in the literature. Comparison of our data with the reported data provided a convenient check on our method. The mean and r.m.s. velocities as well as the turbulence spectra at the centerline of the pipe were compared.

A schematic diagram of the test flow system is shown in Figure 13.

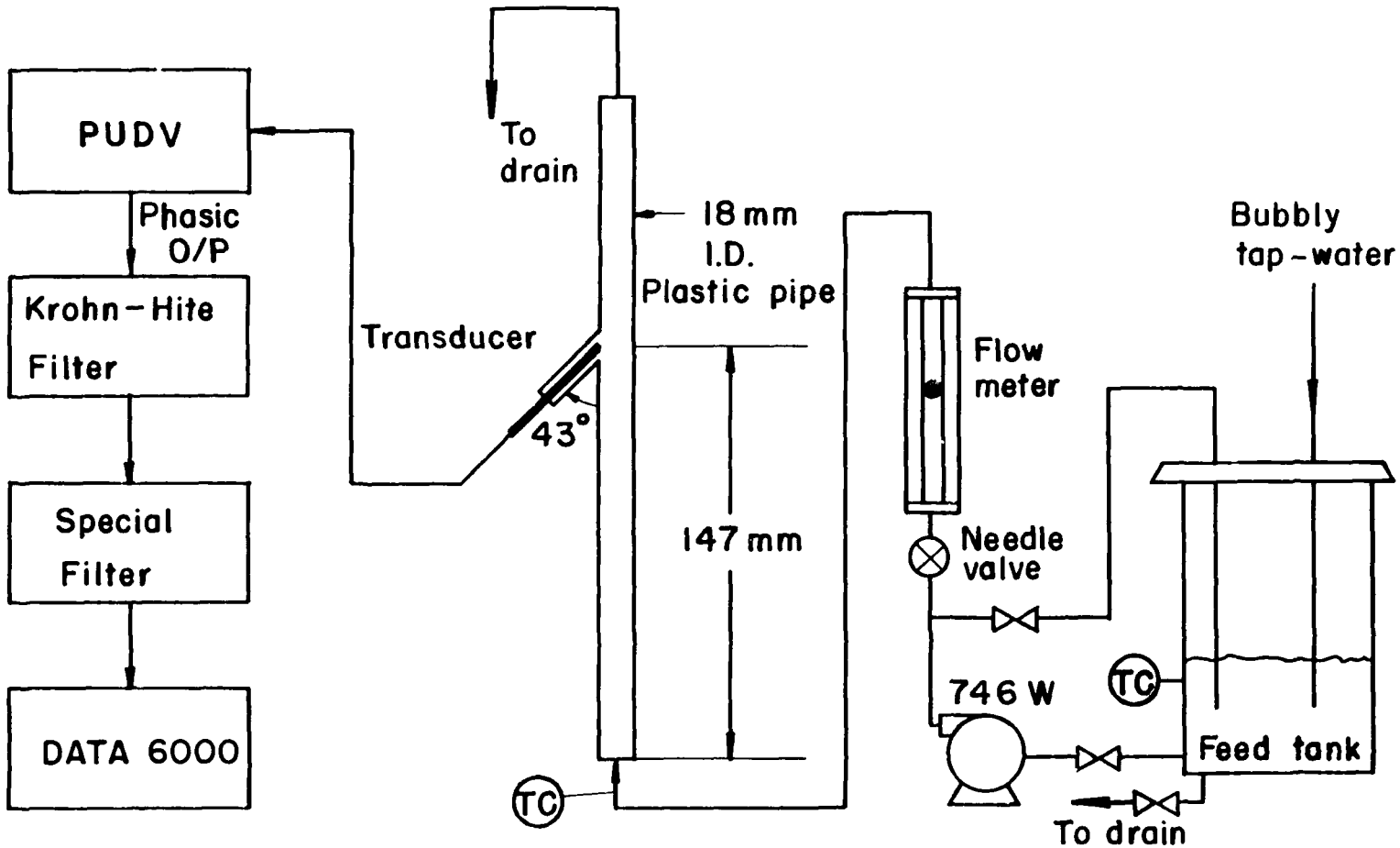

Figure 13. Schematic diagram of fully developed pipe flow system

It utilized all the parts of the original flow system except that a 1.8 cm I.D. pipe was used in place of the reactor assembly. Tap water was added to the $0.21\ m^3$ polyethylene tank continuously. It was then pumped through the rotameter to the base of the vertical pipe, eventually to the drain. The ultrasound transducer was placed at an angle $\theta = 43°$ to the flow direction. The transducer emitted a 3 mm wide unfocused beam at 10 MHz, which had a range of 2 to 35 mm but began diverging after 20 mm. For experimental purposes, the range was adjusted to locate the measurement volume at the centerline. This was achieved by finding the location where the PUDV output was maximum.

The phasic (raw) signal of the PUDV was passed through the Krohn-Hite filter whose cut-off frequency was set at 120 Hz, and also through the special passive filter before it was fed to the microprocessor. The sampling period was 2 ms and the signal was continually recorded and processed. The data-acquisition was stopped when the mean and the r.m.s. values of the entire record became stable. Typically this corresponded to a real time record of about 10 sec. For spectral measurements, 200 records with 512 points per record and frequency smoothing (Hanning) were ensemble averaged to get a stable, reproducible spectrum.

The microprocessor gave mean and r.m.s. values in mV. These were appropriately converted to proper units of velocity by using Equation (B.1) of Appendix B. The power spectrum was given in terms of mV^2/Hz as a function of frequency in Hz. This, too, was appropriately scaled to compare with other published results. Computational details are given in Appendix D.

The raw data are presented in Table 5. The final comparisons are shown in Figures 14 and 15. The turbulence intensity measurements fall in the same range as the reported values as seen in Figure 14. Similarly, spectral measurements at pipe Reynolds number of 5900 follow data of Garbini et al. (1982) very closely. Thus, the comparisons were very favorable. They provided a reasonable basis for the use of the present method in investigating the fluid mechanics of the actual reactor.

3. Experimental Procedure

Unlike in the previous verification test, for characterization of the reactor the ultrasound transducer was inserted vertically into the flow field ($\theta = 0°$) as shown previously in Figure 7. This allowed measurement at any desired location in the flow field but required special precaution in the data collection. In this configuration, the bubble mist impinged directly on to the transducer face. The tiny bubbles had a tendency to cling to the transducer face and after a short time they coalesced to form a much bigger bubble which distorted the signal considerably and caused it to drift. It was observed, however, that a freshly cleaned transducer face gave reproducible results in the period prior to the drift. Furthermore, although the transducer was inserted into the flow, the actual measurement volume was kept about 1 cm in front of the transducer face. Thus, effectively, this technique did not disturb the flow field to any significant extent.

An experiment was conducted in the following sequence:

Table 5

Centerline Turbulence Intensities in a Straight Pipe
(Pulsed Ultrasound Doppler Velocimeter Data)

Re	$\bar{V}$ (mV)	v_{rms} (mV)	$\bar{U}_{exp}$ (cm/s)	$\bar{U}_{theo}$ + (cm/s)	$\frac{u_{rms}}{\bar{U}_{exp}} \times 100$ * %
8029	1315	96	55.1	70.1	5.34
8029	1307	96	54.7	70.1	5.37
7104	1247	78	52.2	62.0	4.57
7104	1205	86	50.5	62.0	5.22
6180	1131	61	47.4	54.0	3.94
6180	1140	66	47.7	54.0	4.23
6180	1127	67	47.2	54.0	4.35
5564	1040	60	43.5	58.6	4.22
5564	1038	61	43.5	48.6	4.30
5564	1016	67	42.5	48.6	4.82
4948	920	58	38.5	43.2	4.61
4948	919	63	38.5	43.2	5.01
4331	815	52	34.1	37.8	4.67
4331	816	55	34.2	37.8	4.93
4331	805	58	33.7	37.8	5.27

* $u_{rms}/\bar{U}_{exp} = (v_{rms}\cos 43°)/\bar{V}$.

+ $\bar{U}_{theo} = \frac{Q}{A(0.8)}$; Q: flow rate; A: cross-sectional area.

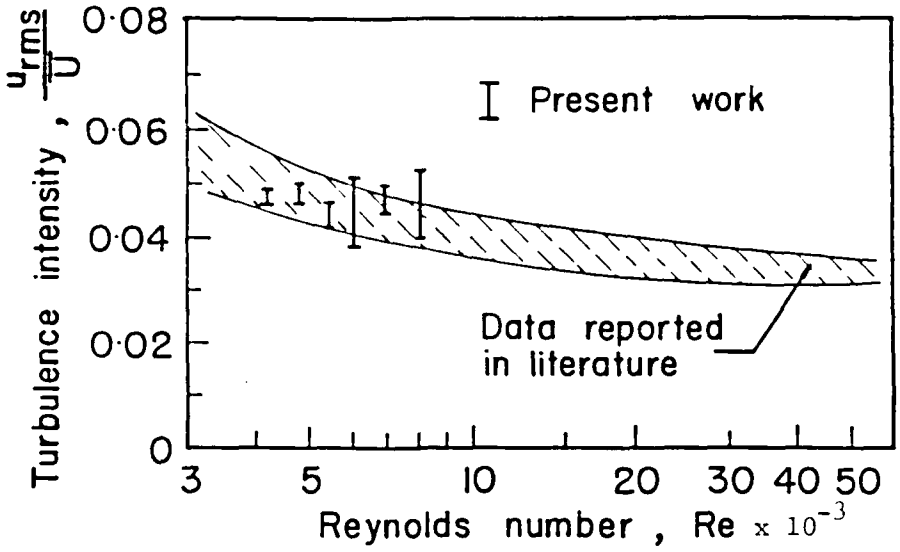

Figure 14. Turbulence intensity measurements [Hatched area--values reported in literature (Garbini et al., 1982)]

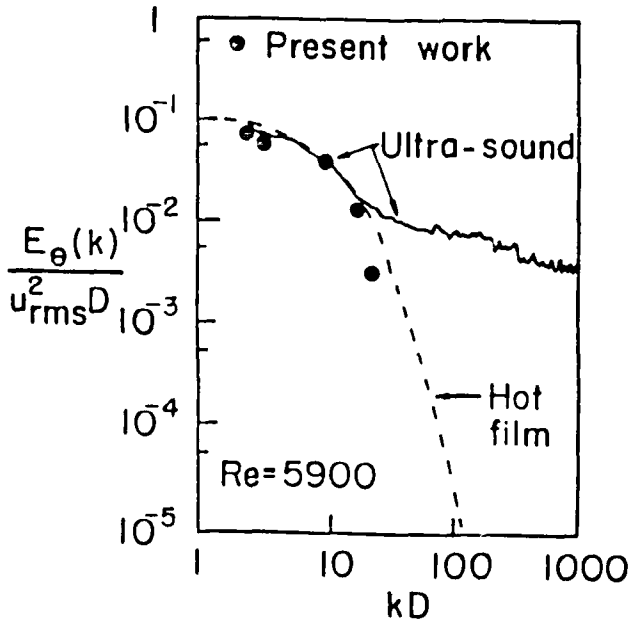

Figure 15. Normalized turbulence spectral densities [(—) ultrasound, and (- - -) hot film data of Garbini et al. (1982)]

(1) The PUDV and the low pass filter were turned on to allow for approximately half an hour warm-up time.

(2) Ordinary tap water and another stream of hot water were continuously added to the 0.21 m^3 tank (A stream). The height and the temperature of the liquid were controlled by manual adjustments. Typically the tank had a 0.04 to 0.05 m^3 hold-up and the temperature was 25-27°C.

(3) The flow rate of the bubbly water through the rotameter was adjusted by the needle valve and the globe valve in the recycle loop. As a precaution, the rotameter was always calibrated prior to each run.

(4) Ordinary distilled water was used as the working fluid for the secondary (B) stream. It did not contain any air bubbles. The flow rate of this stream was adjusted by the micrometer attached to the metering pump. This also was always calibrated prior to each run. The distilled water was periodically replenished throughout the run to ensure a continuous supply to the "hairbrush" injector.

(5) First, the PUDV was internally calibrated. The output voltage from the phasic jack was adjusted to positive and negative 0.610 volts when the polarity switch on the front panel of the instrument was kept at the positive and negative positions, respectively. The transducer was unplugged during the calibration.

(6) Next, the transducer was plugged into the PUDV. Since the pulse-repetition-frequency (PRF) of PUDV was 19.53125 KHz,

the calibration for the range control was 0.3125 volts/cm. The range was adjusted accordingly to adjust the measurement volume at about 1 cm in front of the probe.

(7) The instrument was switched from the calibration (CAL) to the directional (DIR) mode, the polarity switch to the "toward" position--since the flow moved towards the transducer--and the filter was set at the phasic position. The sensitivity control was set approximately midway so that the background audio noise just barely triggered the decoder.

(8) The ultrasound probe was hand-held in air to measure any background electronic noise.

(9) Next, it was mounted on the vernier slide and was lowered to the desired location.

(10) Immediately, the data collection was begun. The sampling period was 2 ms and there were 2048 points per record. The overall mean and r.m.s. values were monitored until they stabilized within ± 1 mV. Generally, this required 10 sec of real time record. By this time, bubble accumulation on the transducer tip began to distort the signal and hence data collection was stopped. The measured mean and r.m.s. voltages were recorded from the microprocessor screen manually.

(11) The transducer face was wiped gently with a tissue paper and again lowered into the flow field for another measurement.

The entire flow loop was purged frequently with a high flow rate pulse to flush out most of the bigger air bubbles which accumulated in the loop. Otherwise, such big bubbles passed through the measurement

volume, making that measurement unacceptable. Nevertheless, with proper care and patience, it was possible to obtain reproducible data.

The pulsed ultrasound technique was further used to characterize the scattering bubble mist in terms of a mean bubble rise velocity. Since the rise velocity is related to bubble diameter, it is also a direct measure of the mean bubble diameter. The random noise associated with bubbles was also obtained from the same measurement.

At the end of each run, the flow was suddenly stopped and a freshly wiped transducer was introduced into the fluid. The mean and the r.m.s. voltages measured in this fashion directly corresponded to the two quantities of interest--bubble rise velocity and the random noise.

4. Experimental Conditions

Mean and r.m.s. velocities were measured in the reactor at several axial locations on the centerline and also a few radial locations. Each measurement was repeated at least twice to check its reproducibility.

Four different experimental conditions were investigated corresponding to four different placements of the turbulence generating screen and the "hairbrush" injector. In Case 1, the honeycomb section was directly connected to the reactor pipe and the injector and the screen were not used at all. This allowed measurement of details of the flow from the downstream section of the honeycomb, all the way to the middle of the reactor pipe. In the second case, only the "hairbrush" injector was introduced and no screens were used. This was to

assess the effect of the injector on the turbulence intensity level. In Case 3, the largest screen (M_1) was placed just 7 mm upstream of the injector, to evaluate the effect of this configuration on the turbulence. Finally, in Case 4, the same screen was placed 7 mm downstream from the injector.

The presence of large bubbles in the system and their tendency to accumulate at the screen in the case of the smaller screens (M_2 and M_3) prevented us from measuring the effect of the smaller screens on the turbulence.

The raw data are listed in Appendix E, along with the data for bubble rise velocity and the random noise. The latter values are used to correct mean and r.m.s. velocities. The corresponding calculated values, although not reported numerically, are plotted and discussed in the next chapter.

B. Mixing-Reaction Studies

1. Materials

Distilled water at room temperature was used as the working fluid in our mixing-reaction experiments. Sodium carbonate and sodium bicarbonate ("Baker analyzed," J. T. Baker and Co., NJ) were used as buffer salts. Recrystallized 1-naphthol ("Certified," Fisher Scientific Co., NJ) and diazotised sulfanilic acid ("purum p.a.," Fluka Chemical Corp., NY)--reactants A and B--were both reagent grade pure. The latter was available as a moist paste from the manufacturer because it is explosive when dry. It was always stored in a refrigerator. The actual diazotised sulfanilic acid content of the paste was supplied by

the manufacturer as actual lot analysis. Typically the paste contained about 30 percent water.

2. Calibration of the Fiber-Optic Probe

Our technique was based on Equation (19) of the previous chapter:

$$\overline{\Delta V^{\lambda}} = k_R^{\lambda}\overline{C_R} + k_S^{\lambda}\overline{C_S}$$

The determination of k_R^{λ} and k_S^{λ} was done through separate calibrations of standard solutions of monoazo dye (R) and diazo dye (S).

Due to its use as an indicator in microscopy, R was commercially available as a very pure powder ("Standard Fluka," Fluka Chemical Corp., NY). Thus, preparing a standard solution of R in alkaline water of pH = 10.00 was a simple matter.

A standard solution of S was prepared by reaction of a standard solution of R with an aqueous solution of diazotized sulfanilic acid. Essentially, the second azo coupling reaction R + B → S was carried out in a beaker under similar conditions of pH and ionic strength as in reactor and was allowed to go to completion. By adding a slight excess of B it was ensured that no unreacted R remained in the solution.

The preparation of primary standards in the above manner was a departure from the procedure followed by Kozicki (1980). Kozicki's method synthesized pure R by dissolving 1-naphthol in ethanol and then reacting it with a concentrated slurry of diazotised sulfanilic acid at room temperature. Since R was available in very high purity commercially, the commercial R was preferred. Regarding synthesis of pure S, it was not possible to separate S in a solid form from the solution when Kozicki's procedure was followed. Similar difficulty was

encountered by other researchers as well (Li, 1984). Thus, we were compelled to use a solution of S for the primary standard. In this context, reacting R with B to form S in a buffer solution was a reasonable way to prepare the standard.

The molar absorption coefficients of these solutions are plotted as a function of wave length in Figures 16 and 17. For comparison, values obtained by Kozicki (1980) and Li (1984) are also displayed on the same plots. In most cases, ε_R^λ values for this study are 20-25 percent lower than Kozicki's values while Li's values are 3-8 percent lower than the latter.

Li (1984) used R synthesized by Kozicki's method but in the present study commercially available high purity R was used. Hence, the difference in values is attributed to relative purity of R and errors involved in making solutions. On the other hand, the ε_s^λ values for this study are 47-56 percent lower than Kozicki's values and Li's values also are 10-18 percent lower. Kozicki (1980) reported that the elemental analysis of R conformed within 0.8 percent of the theoretical values but that of S differed by as much as 17 percent. Thus, Kozicki's S either had significant impurities or even a somewhat different molecular structure. Since the method of making primary standard of S in the present work mimics the reactor conditions, it is considered more reliable.

In each case, five different solutions of varying concentrations in the range of 0.07 to 0.35 mol/m^3 were prepared by suitably diluting the standard solution with an alkaline buffer of $Na_2CO_3/NaHCO_3$ (pH = 10.00). The same buffer was used as the reference solution. The

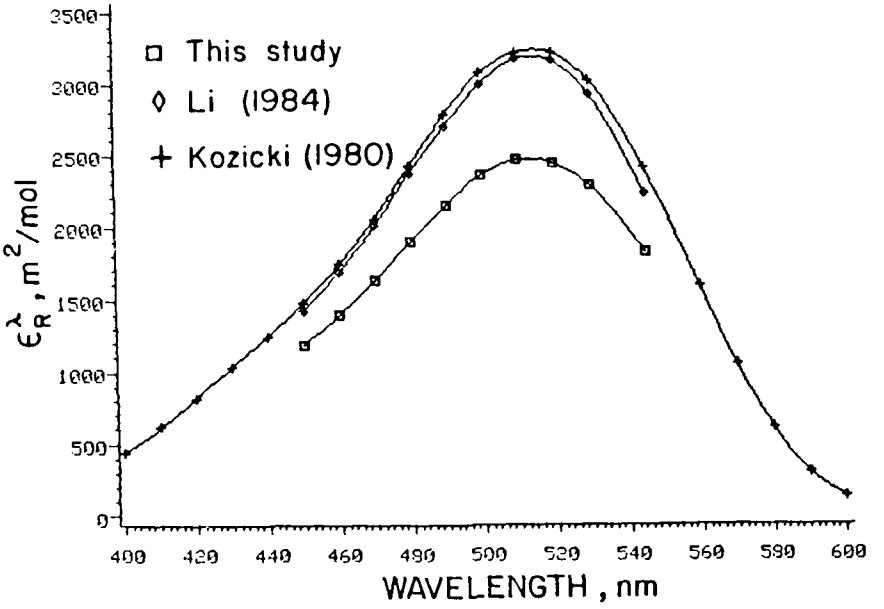

Figure 16. Molar absorption coefficient of monoazo dye at various wavelengths [T = 298 K; pH = 10.0; I = 40 g ion/m^3]

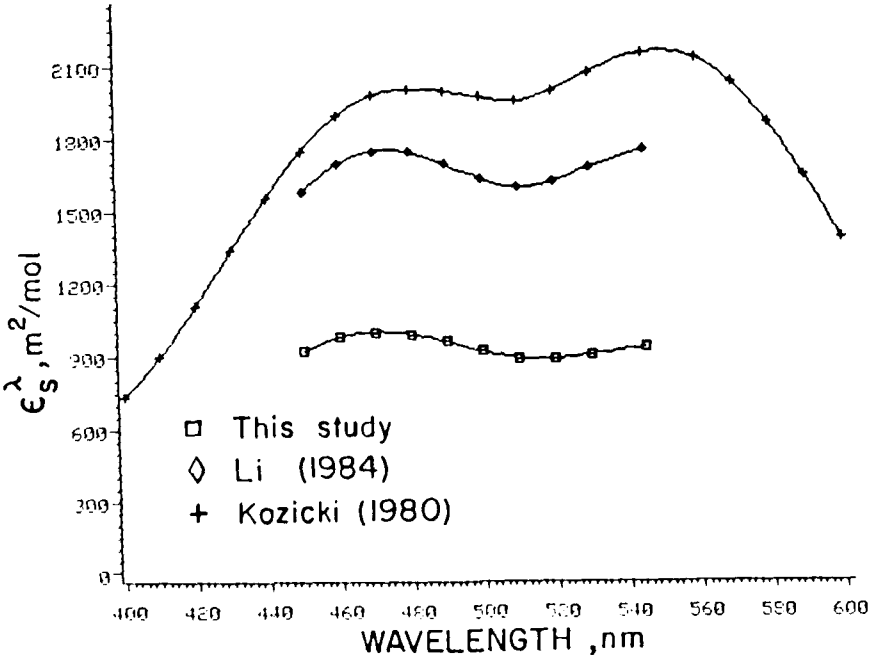

Figure 17. Molar absorption coefficient of diazo dye at various wavelengths [T = 298 K; pH = 10.0; I = 40 g ion/m^3]

colorimeter output was measured first by dipping the fiber-optic probe in the solution and in the reference solution immediately thereafter. All solutions were made in duplicate to improve the accuracy. As such, ten $\overline{\Delta V^{\lambda}}$ values were obtained at each wavelength, two values at each of the five concentrations of R (or S). Standard least square linear regression of these ten values yielded k_R^{λ} (or k_S^{λ}) (see Figures 18 and 19).

3. Method of Analysis

In the mixing-reaction experiments, $\overline{\Delta V^{\lambda}}$ was measured at five different wavelengths at each location in the reactor. When these values were substituted in Equation (19), along with calibration constants k_R^{λ} and k_S^{λ}, a set of five equations involving only two unknowns ($\overline{C_R}$ and $\overline{C_S}$) was obtained.

A standard linear regression package (MINITAB) was used to find the best fit values of $\overline{C_R}$ and $\overline{C_S}$. These best fit values are termed the "experimental values" in this thesis.

This method of calculating concentrations of R and S was tested with sample solutions containing known concentrations of R and S. The concentration range covered was typical of the range expected in most of the mixing-reaction experiments. A comparison of actual and measured values is displayed in Table 6. It is evident that in all but one case, the measured concentrations are within 12 percent of the actual ones. This was considered satisfactory in view of the low level of concentrations.

A similar comparison is presented in Table 7 for a set of solutions where S is present in very low concentration. It is clear that

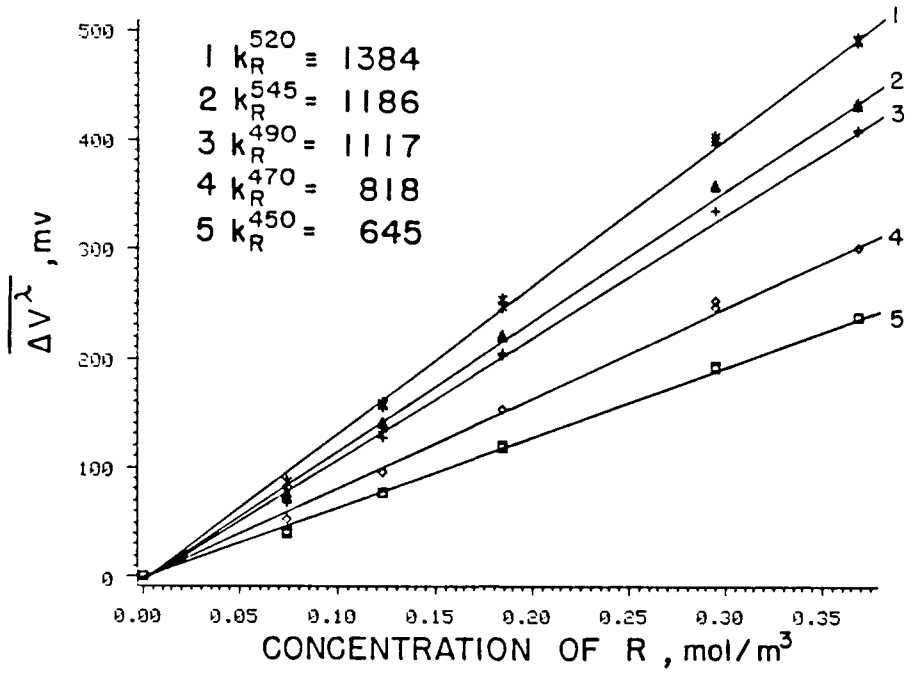

Figure 18. Calibration of fiber-optic probe for monoazo dye (R)

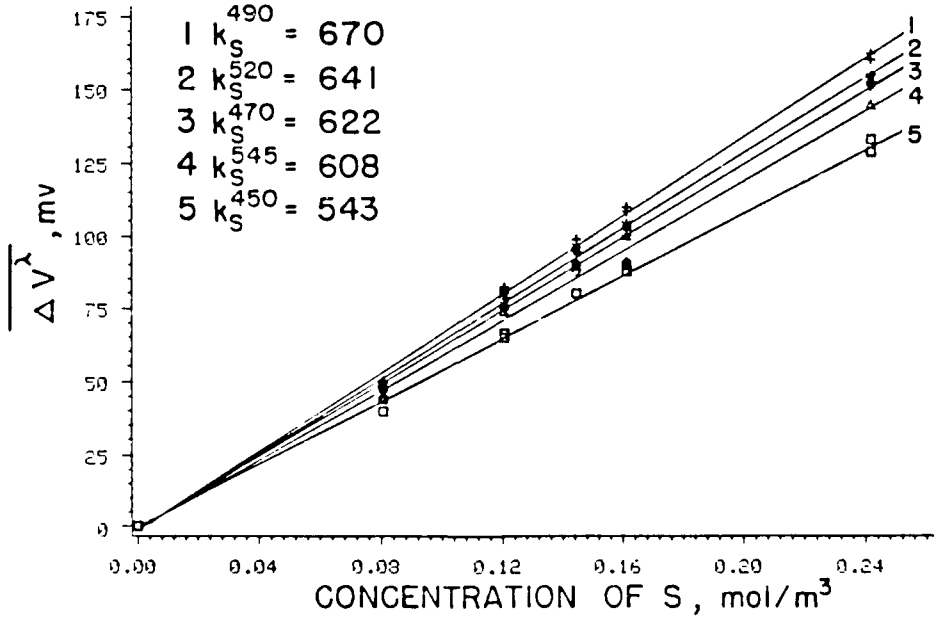

Figure 19. Calibration of fiber-optic probe for diazo dye (S)

Table 6

Data for Evaluation of Method of Analysis

Actual Concentration (mol/m^3)		Measured Concentration (mol/m^3)		Difference (%)[a]	
$\overline{C}_R$	$\overline{C}_S$	$\overline{C}_R$	$\overline{C}_S$	Δ_R	Δ_S
0.140	0.017	0.130	0.017	-7.14	0.00
0.183	0.017	0.167	0.019	-8.74	11.76
0.048	0.018	0.047	0.013	-2.08	-27.77
0.095	0.018	0.087	0.016	-8.42	-11.11
0.286	0.048	0.289	0.045	1.05	- 6.25
0.274	0.091	0.253	0.101	-7.66	10.99

[a] $\Delta_j = \left(\frac{\text{Measured concentration}_j - \text{actual concentration}_j}{\text{Actual concentration}_j}\right) \times 100$ percent.

Table 7

Data for Evaluation of Method of Analysis for Solutions with Low $\bar{C}_S$

Actual Concentration (mol/m^3)		Measured Concentration (mol/m^3)		Difference (%)[2]		Approximate Concentration (mol/m^3)	$\%^a$
$\bar{C}_R$	$\bar{C}_S$	$\bar{C}_R$	$\bar{C}_S$	Δ_R	Δ_S	$\bar{C}_R\|_{\bar{C}_S=0}$	$\Delta_R\|_{\bar{C}_S=0}$
0.049	0.009	0.043	0.012	-12.24	33.33	0.061	24.02
0.063	0.008	0.088	-0.007	39.68	--	0.084	33.33
0.075	0.008	0.091	0.010	21.33	25.00	0.096	28.00
0.083	0.007	0.074	-0.004	-10.84	--	0.072	-13.22
0.091	0.007	0.080	0.007	-12.09	--	0.083	- 8.79
0.095	0.009	0.100	0.007	5.26	-22.22	0.110	15.91
0.140	0.009	0.137	0.011	- 2.14	22.22	0.153	9.11
0.190	0.010	0.194	-0.008	2.11	--	0.189	- 0.53
0.292	0.024	0.275	0.048	- 5.82	100.00	0.305	4.45
0.303	0.006	0.269	0.059	-11.22	89.83	0.305	0.66

[a] $\Delta_j = \left(\frac{\text{Measured concentration}_j - \text{actual concentration}_j}{\text{Actual concentration}_j}\right) \times 100$ percent.

the method may yield negative values of $\overline{C_S}$ in some cases and the relative error in measuring $\overline{C_S}$ is fairly high. This seems unsatisfactory. However, it may be argued that since S is present in very low concentration, it is reasonable to ignore the presence of S in these solutions and use $\overline{\Delta V^{\lambda}}$ values to determine $\overline{C_R}$ only. The regression equation then becomes

$$\overline{\Delta V^{\lambda}} = k_R \overline{C_R}\Big|_{\overline{C}_S=0} \tag{20}$$

The last two columns of Table 7 show that $\overline{C_R}$ values, calculated thus, are within 15 percent of the actual $\overline{C}_R$ values, except when $\overline{C}_R < 0.08$ mol/m^3. Generally, this method gives closer agreement with the actual value of $\overline{C}_R$ when $\overline{C}_R$ is at least 15 times higher than $\overline{C}_S$. As will be discussed later, this approximate method was used to measure the concentration of R in runs with a low ratio of B to A in the feed.

4. Characterization of Feedstreams

The primary feedstream in the mixing-reaction experiments contained 1-naphthol (A) in an aqueous buffer solution of $Na_2CO_3/NaHCO_3$ (pH = 10.00 ± 0.02).

The same amounts of distilled water and 1-naphthol were used for each experiment. Thus, the unmixed feed concentration C_{A0} was always about 0.3 mol/m^3. The exact value was determined by measuring the UV-absorbance of the solution at 245 nm. A standard solution of 1-naphthol in an identical buffer was used to determine UV-absorbance at 245 nm as a function of concentration. This was used as calibration for the feedstream A. A UV-visible spectrophotometer (Model 8450A,

Hewlett-Packard Corp., CA) was used for this purpose. It was important to use micropipettes to prepare solutions of appropriate dilution, usually one part solution in sixteen parts buffer, to get precise results. It was also necessary to use quartz couvettes in all these measurements. Also, the spectrophotometer was allowed to warm up for at least a period of 20 minutes to ensure reproducibility. A sample calculation is shown in Appendix F.

The secondary stream was a relatively concentrated solution (10-30 mol/m^3) of diazotised sulfanilic acid in water. The actual lot analysis supplied by the manufacturer was used to calculate the amount of paste required to prepare a solution of required concentration. Usually it took about 10 minutes of stirring with a stirrer rod to dissolve the entire amount of acid into the water. The resultant solution was yellowish brown in color.

5. Experimental Procedure

The nature of our experimental design was such that at least two, preferably three, persons were required to carry out a mixing-reaction experiment. The actual duration of an experiment was about 20 minutes but altogether the experiment required 24 hours for the preparation. The protocol outlined below had evolved during a series of preliminary experiments conducted primarily to establish an appropriate procedure:

(1) The fiber-optic probe was calibrated first. Standard solutions of R and S were prepared and the calibration was carried out in the manner described earlier.

(2) Next, the flow system was flushed with fresh tap water several times to remove any adhering dust particles from the

system. The system was drained at the end of the flushing.

(3) The $0.21\ m^3$ tank was filled with distilled water. Through a hose pipe connected to an available distilled water supply line. The flow loop had a hold up of about $0.013\ m^3$. By flushing the system once with a little distilled water, most of the remaining tap water was pushed out.

(4) In a small mortar, 1-naphthol was ground with a pestle to a very fine powder. About 9.7 g of that powder was weighed on a weighing paper.

(5) Next, the stirrer in the $0.21\ m^3$ tank was turned on and 1-naphthol powder was slowly added to the swirling content of the tank through a small hole on the tank top. It was important to set a proper stirrer speed by a variac, as a higher speed might only make the swirling faster but not disperse the powder effectively. The stirring was continued overnight, altogether for a period of 12 hours. That much time was sufficient to dissolve the entire amount of 1-naphthol added. Such a long time was necessitated by the low solubility of 1-naphthol in pure water at room temperature. It was possible to speed up the dissolution process by adding the buffer salts beforehand but it also led to slight coloration of the fluid after a few hours. The coloration was attributed to 1-naphthol's sensitivity to light in an alkaline environment, and was deemed undesirable for our purposes.

(5) When the aqueous solution of 1-naphthol was ready, the buffer salts were added to it in appropriate amounts (typically 235 g

of Na_2CO_3 and 190 ± 5 g of $NaHCO_3$). The salts dissolved very rapidly and brought pH to 10.00 ± 0.02. That also corresponded to an approximate ionic strength of 10 g ion/m^3. The pH was measured with a standard pH meter (Orion digital ionalyzer/501, Orion Corp., MA).

(6) Next, the colorimeter and the low pass filter were turned on. The cut-off frequency was set at 0.25 Hz.

(7) The 1 hp pump was turned on and the alkaline naphthal solution was recycled through the loop back to the feed tank. The recycling dislodged any air bubbles in the honeycomb and also removed air pockets at the corners of the flow loop. It also brought the entire loop to a thermal steady state.

(8) The rotameter for the mainstream was then calibrated with a measuring cylinder and a stopwatch.

(9) Next, the mainflow was stopped and the needle valve was closed so that the hydrostatic head at the tip of the needles of the "hairbrush" injector was maintained. Under those conditions the secondary stream metering pump was calibrated by pumping distilled water against the head. Once again a small measuring cylinder and a stopwatch were used in the calibration.

(10) Thirty-five hundred cc of distilled water was added to a separate 5000 cc stainless steel beaker. A precalculated amount of diazotised sulfanilic acid paste was weighed in a small beaker and was completely transferred to the stainless steel beaker by rinsing. A glass rod was used as a stirrer to facilitate rapid dissolution. Usually it took 10 minutes.

That was the feed solution B which was transferred to the 2000 cc beaker connected to the injector. The stage was now set for an experiment.

(11) One person was required to position the fiber-optic probe in the reactor. The same person also monitored the temperatures, maintained the flow rate of the mainstream at a constant level, added the feed solution B to the feed beaker to maintain a continuous supply to the injector and collected effluent samples to check for the stability of the operation.

The other person collected and recorded the experimental data. That involved manipulation of several keys on the microprocessor front panel to begin and end data collection for a certain probe location. The person had to monitor the integrated average of the raw signal to get meaningful values of $\overline{V^{\lambda}}$.

(12) An experiment began when the overflow chamber outlet was connected to the drain and the mainstream was turned on. The flow rate was set at a desired level by adjusting the needle valve.

(13) The secondary stream flow rate was set very high in the beginning to purge any residual air from the feedline and "hairbrush" injector, and then the rate was adjusted to the proper level by turning the micrometer screw.

(14) A small beaker of pure A solution was kept at hand for use as the reference solution. The fiber-optic probe was dipped into it to measure the reference voltage, $\overline{V^{\lambda}}_{ref}$, at each wavelength λ.

(15) The probe was then lowered into the reactor and the data collection begun. When the person monitoring the microprocessor indicated that the signal was statistically stable, the probe was moved to the next location. The sampling time for the microprocessor was 50 μsec. Two thousand forty-eight points per record were used and typically 32 such consecutive records gave a stable value that corresponded to about three seconds of real time. For each λ, six different axial stations were used. After measuring at the sixth location, the probe was again dipped into the reference solution to check for any baseline drift. An arithmetic mean of the two $\overline{V_{ref}^{\lambda}}$ values was used in calculation of $\overline{\Delta V^{\lambda}}$. Thus, for each λ a total of eight voltages were measured. The amount of feed A solution available permitted such measurements at five different wavelengths.

(16) At the end of the run, the metering pump was turned off first and tap water was added to the 0.21 m^3 tank to continually supply fluid to the reactor. That permitted washing out of the colored products.

(17) The feed-beaker of stream B was washed and filled with tap water and the injector was purged with a high flow rate. That removed all the residual B from the injector and prevented its reaction with the injector wall by diffusion through the protective coating.

(18) Three effluent samples were collected during the run and were analyzed at the end of the experiment. The procedure for

analysis of effluent samples was the same as before. The probe was first dipped into the sample and then into the reference solution; the voltage difference provided the needed $\overline{\Delta V^{\lambda}}$ value.

6. Experimental Conditions

Thirty-seven mixing-reaction experiments were carried out over a period of three months. The selected experimental conditions for successful experiments are summarized in Table 8. In one set of runs, the effect of feed stoichiometry β (ratio of B and A) on the product distribution was studied at a fixed mixing intensity. Three different stoichiometries (β = 0.39, 1.00, and 1.54) were used. In another set of runs, at a fixed β of 1.51, the mixing intensity was varied by altering the mesh size and mesh placement.

In general, all the experimental conditions were repeated at least three times to check for the reproducibility. In some cases, more than three runs were made to obtain data from the region very close to the injector to the farthest end of the reactor. A six-inch section of reactor was added to or removed from the reactor length for that purpose. It was connected to the rest of the reactor by a short two-inch section of hose pipe and clamps.

The raw data thus collected are compiled in Appendix G. The analysis of these data and the consequent discussion is considered in the next chapter.

Table 8

Experimental Conditions for Mixing-Reaction Studies

Date	Experiment	Q_A (cm^3/s)	Q_B (cm^3/s)	C_{A0} (mol/m^3)	C_{B0} (mol/m^3)	T_{avg}[a] (°C)	$\beta = \frac{Q_B C_{B0}}{Q_A C_{A0}}$	Screen[b]
3/17/85	8	131±5	1.31±0.06	0.3	30.26	27.3	1.01	M_1^u
3/19/85	9	131	1.31	0.3	30.05	29.6	1.01	
3/31/85	11	131	1.31	0.3	30.03	23.8	1.01	
4/2/85	12	131	1.31	0.3	30.04	28.0	1.01	
4/3/85	13	131	1.31	0.3	30.04	27.8	1.01	
4/16/85	16	135	2.12	0.3	28.76	30.6	1.51	M_1^u
4/23/85	19	138	2.13	0.3	29.97	30.4	1.54	
4/26/85	20	135	2.12	0.3	30.00	25.9	1.57	
5/4/85	22	128	1.99	0.3	30.01	25.2	1.56	M_2^u
5/6/85	23	130	2.00	0.3	30.03	24.4	1.54	M_3^u
5/9/85	25	135	2.02	0.3	30.05	28.0	1.50	M_2^d
5/13/85	26	133	2.00	0.3	30.05	29.8	1.51	
5/14/85	27	135	2.02	0.3	30.05	29.7	1.51	
5/17/85	28	135	2.02	0.3	30.02	27.1	1.50	M_3^d
5/21/85	30	135	2.00	0.3	30.05	27.5	1.50	
5/23/85	31	133	2.01	0.3	30.01	27.0	1.51	M_1^d
5/24/85	32	133	2.01	0.3	30.02	25.8	1.51	
5/26/85	33	133	2.01	0.3	30.03	28.5	1.51	

Table 8 (Continued)

Date	Experiment	Q_A (cm^3/s)	Q_B (cm^3/s)	C_{AO} (mol/m^3)	C_{BO} (mol/m^3)	T_{avg}[a] (°C)	$\beta = \frac{Q_B C_{BO}}{Q_A C_{AO}}$	Screen[b]
6/14/85	34	130	2.01	0.3	30.00	25.8	1.55	M_1^u
6/17/85	35	135	2.13	0.3	7.43	25.6	0.391	
6/18/85	36	135	2.13	0.3	7.45	26.0	0.392	
6/19/85	37	135	2.14	0.3	7.43	27.2	0.393	

[a]Average over the reactor length.

[b]u - upstream of injector; d - downstream of injector.

VI. RESULTS AND DISCUSSION

A. Fluid Mechanics

The turbulent reactive flow considered in this study is a special case where reaction takes place in a dilute liquid medium. The dilute nature of the reactive flow field provides a clear separation between fluid mechanics and chemistry. The flow is isothermal and the viscosity of the fluid also remains unchanged during the reaction. As a result, the velocity field drives the concentration field but the latter does not affect the former. The measurement of velocity is thus useful not only to characterize the flow field but also to infer something about the micromixing.

The turbulence measurements were conducted at a pipe Reynolds number of 3400, which was the same as in the mixing-reaction experiments. The measured axial mean velocity at the reactor centerline is plotted as a function of axial distance in Figure 20(A), and the corresponding turbulence intensity in Figure 20(B). The zero on the abscissa of these figures corresponds to the plane of the injector needles.

The mean velocities plotted in Figure 20(A) incorporate the correction due to the rise velocity of bubbles. Generally, this correction is less than 3 percent. The rise velocity of bubbles corresponds to a mean bubble diameter (based on Stoke's law) of about 60 μm, which is well within the range of particle sizes generally used in PUDV measurements. The axial mean centerline velocity profile shows how dramatically the flow speeds up during its passage through the contraction nozzle. The axial profile becomes relatively flat as

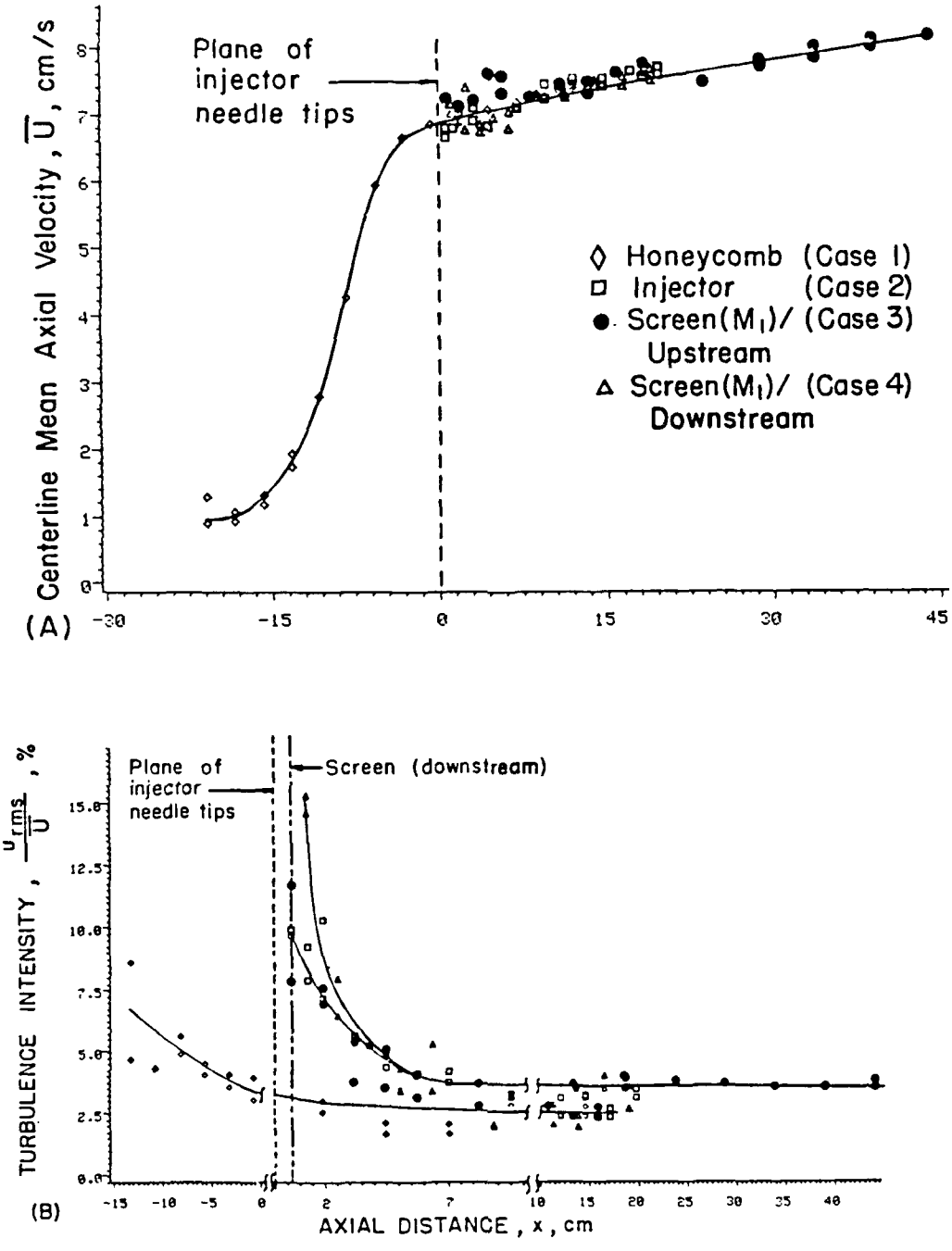

Figure 20. Fluid mechanical measurements: (A) centerline mean axial velocity, and (B) centerline turbulence intensity (Symbols defined in (A). (——) smoothed data)

the flow enters the reactor pipe although the velocity continues to increase gradually over the reactor length.

The mean centerline velocity increases sevenfold in going from the settling chamber to the reactor entrance while the area of cross-section for the flow decreases by a factor of nine. Material balance requires that the cross-sectional average velocity also increase ninefold. However, the measured velocities are centerline velocities and are maximum velocities at a given axial location. Therefore, a ratio of seven implies that the radial profiles of mean axial velocity at the two locations--settling chamber and reactor entrance--are not completely flat. This may have resulted from growth of the wall boundary layer. This growth is further reflected in the gradual increase of the mean axial velocity over the reactor length. The growing boundary layer acts as an invisible contraction section and accelerates the flow in the pipe core. Figure 20(A) reveals a 16 percent increase in the velocity from entrance of the reactor to the exit. This applies to all the cases studied. Consequently, it is important to determine by how much the flow deviates from its desired one-dimensional character.

Velocity measurements were made at the reactor exit at several radial locations (see Appendix E). Owing to the limitations of the probe design, it was possible to access only the central 3 cm core of the reactor. The radial profile of the mean axial velocity was indeed found to be relatively flat. The maximum variation of the velocity was less than 3 percent from the mean axial centerline velocity. These results suggest that the mean velocity field was uniform in the central core over the entire length of the reactor. Since the boundary layer growth, which causes the acceleration of the core, is confined to the

unaccessible annulus between the core and the pipe wall, the boundary layer thickness can only be estimated. Assuming a flat mean velocity profile in the central core and a linear mean velocity profile in the boundary layer with no slip at the wall, it is possible to calculate the boundary layer thickness which will cause a 16 percent rise in the core velocity at the exit. The calculation involves a simple mass balance of the fluid between the reactor entrance and the exit. Such a calculation yields a boundary layer thickness of 0.37 cm. The actual boundary layer would be thinner than this. Since the boundary layer is thin and the measured radial profile of the mean axial velocity is flat, it is concluded that the reactor provides a nearly uniform mean axial velocity field along its length.

The axial turbulence intensity profile depicted in Figure 20(B) can also be used to make inferences about the homogeneity of the turbulent flow field. Note that the plotted turbulence intensities incorporate corrections for the electrical noise as well as the random noise associated with bubbles. The corrections, which involve simply subtracting the noise levels from the measured signals, imply that the noise processes are uncorrelated with the true turbulence. No attempt is made here to justify this assumption since the turbulence intensity values are not used in any critical computations, but mainly as an indication of the homogeneity of the turbulence. The measured and corrected values may serve as upper and lower bounds on the actual turbulence intensity. It should be noted that no such corrections were applied to the fully developed pipe flow data (cf. Section V.A.2), since the bubble sizes were not measured in those experiments. Considering the fact that the signal level was three to six times higher

in those experiments compared to the reactor measurements, the effect of the noise is expected to be reasonably small and should not affect the conclusions of Section V.A.2.

It is evident that the turbulence intensity decays very rapidly to an asymptotic value of about 4 percent (10 percent if uncorrected) within 5 cm downstream of the injector. Nearly the same asymptotic level is reached in all the cases studied and this includes when the screen M_1 is placed upstream or downstream of the injector. It is interesting to note that when the screen is placed upstream of the injector, it does not seem to alter the intensity profile at all as compared to the case where only the injector (compare circles and squares in Figure 20(A)). In terms of micromixing, this indicates that placing a screen in the upstream location may not induce any additional mixing compared to that induced by the injector itself. The highest turbulence level is measured within 2 cm downstream of the screen M_1 when it is in its downstream location (note the elevated positions of triangles in Figure 20(A)). This implies that this configuration may lead to better micromixing than the other cases.

In any case, the first one-eighth of the reactor has varying turbulence level while the last seven-eighths has an almost constant turbulence intensity. Actually, the turbulence intensity may well be decaying over the entire length of the reactor, but with the present measurement technique, the weak decay is not measurable. An estimate of the rate of decay of velocity fluctuations which supports this idea is given below.

Most experimental data on flow behind grids are correlated by the following equation (Hinze, 1959):

$$\left(\frac{\bar{U}}{u_{rms}}\right)^2 = \frac{m}{M}\,[x - x_o] \qquad (21)$$

In this equation, $\bar{U}$ and u_{rms} are the mean and rms velocities, respectively; m is a constant which depends on mesh size, shape and geometry; x is the axial distance downstream of grid, M is the mesh length and x_o is the virtual origin where experimental data intersect the x axis when $(\bar{U}/u_{rms})^2$ is extrapolated to zero. For the square-mesh grids used in the present study, m is estimated to be 86 based on many measurements for square-mesh grids with round bars (Hinze, 1959). The axial distance at which the asymptotic turbulence level is reached (5 cm) is taken as the virtual origin (x_o) and M = 0.42 cm (M_1). It is estimated that the turbulence intensity would vary from 3.1 percent at x = 10 cm to 1.2 percent at x = 40 cm, the exit of the reactor. Clearly, the screen generates a relatively low level of turbulence which decays very slowly over the reactor length.

The radial profile of turbulence intensity at the reactor exit reveals a reasonable uniformity (within 10 percent at 0.8 cm/sec) over the cross-section.

The foregoing discussion indicates that the reactor can be divided into two zones. The first zone corresponds to the initial 5 cm of the reactor which has higher but varying turbulence level and hence better but changing micromixing conditions. The second zone corresponds to the rest of the reactor which is reasonably homogeneous for both the mean and fluctuating velocity fields. This zone has uniform micromixing conditions and is better suited for characterization by a single value of the micromixing parameter τ_m. The first zone covers

only one-eighth of the reactor and is not expected to influence the reactions much except when the screens are placed downstream of the injector.

Finally, it is useful to employ turbulence intensity values in estimating the micromixing time (τ_m). τ_m is given by Equation (2) where ε may be estimated as

$$\varepsilon \approx A\, u_{rms}^3/\ell_e \tag{22}$$

The proportionality constant A is of order unity (Hinze, 1959). ℓ_e in the above equation is the characteristic integral length scale of the velocity field and corresponds to a characteristic transverse dimension of the flow field, that of the dominant turbulence generator. There are three turbulence generators in the present system: honeycomb, injector and screen. Fortunately, all of them have similar characteristic dimensions: straw diameter = 0.6 cm, injector tube spacing = 0.65 cm and the mesh spacing (M_1) = 0.42 cm. Any one of the above dimensions is adequate for the purpose of estimating τ_m. ℓ_e = 0.65 is chosen in the following estimate.

A reasonable estimate of L_s, the integral length scale of the concentration field, is 0.8 cm, which is the spacing of the injector needles. It is based on the fact that the secondary stream jets, which carry the reactant B, expand and fill the reactor cross-section at about 2 cm downstream from the needles. Therefore, the expanded jet diameter, which equals the spacing of the injector needles, is an appropriate characteristic dimension of the concentration field. Similar arguments are used in literature to estimate L_s (McKelvey et al., 1975). Equation (2) then becomes

$$\tau_m \approx 0.5\left[4\left(\frac{L_s^2 \ell_e}{u_{rms}^3}\right)^{1/3} + \left(\frac{\nu \ell_e}{u_{rms}^3}\right)^{1/2} \ln N_{Sc}\right] \quad (23)$$

For the above estimates of ℓ_e and L_s and $\nu = 0.008$ cm^2/s (kinematic viscosity of water at 25°C) and a typical liquid phase Schmidt number (N_{Sc}) of 700, two estimates of τ_m are obtained:

$$\tau_m \approx 2.20 \text{ sec } (u_{rms} = 0.8 \text{ cm/s (uncorrected)})$$

and

$$\tau_m \approx 8.63 \text{ sec } (u_{rms} = 0.23 \text{ cm/s (corrected)}).$$

Thus, fluid mechanical measurements indicate that the micromixing time in the reactor may lie between two and nine seconds. This magnitude is quite striking because if indeed the mixing time is in this range, the reactor would be the most segregated reactor ever to be used in any mixing-reaction experiment. (For comparison, the reactor of Vassilatos and Toor (1965) had a mixing time of 0.0082 sec.)

B. Mixing and Reaction

1. Preliminaries

Before the results of the mixing-reaction experiments are discussed, several preliminary points are considered. An important element of any experimental mixing-reaction study, such as the present one, is to have reliable kinetic information. This refers to reaction rate expressions and the associated rate constants. Generally, a stopped-flow apparatus is required to study the kinetics of such fast reactions as employed in the present study. Unavailability of such an

apparatus has compelled us to use the kinetic information reported in the literature (Kozicki, 1980; Bourne et al., 1981). Both the reactions (6) and (7) are reportedly irreversible and second order in concentration dependence:

$$-r_A = k_1 C_A C_B \tag{24}$$

and

$$r_S = k_2 C_R C_B \tag{25}$$

Bourne et al. (1981) report the following values for the rate constants at pH = 10.00 and 298 K:

$$k_1 = 7.3 \times 10^3 \text{ m}^3/\text{mol/s}$$

and

$$k_2 = 3.5 \text{ m}^3/\text{mol/s}$$

The temperature dependence of k_2 is reported by Kozicki (1980):

$$k_2 = 1.93 \times 10^9 \exp(-5989/T) \text{ m}^3/\text{mol/s} \tag{26}$$

It is instructive to see how the second azo-coupling reaction (Equation (7)) was studied by these workers. Equimolar solutions of R and B were injected into the stopped-flow apparatus and absorbance was measured at λ = 620 nm as a function of time. Absorption due to R was neglected at that wave length and the absorbance-time data was used to calculate k_2 (Kozicki, 1980).

This method has some obvious limitations. Estimated values of ε_R and ε_S at 620 nm are 126 and 850 m^2/mol, respectively. Clearly,

absorption due to R may be small but not negligible. Since absorbance was attributed entirely to S, the reaction rate was overestimated by some unknown amount, resulting in a higher than actual value of k_2. Recently, Baldyga and Bourne (1984) reported another expression for k_2:

$$k_2 = 1.11 \times 10^6 \exp(-3957/T) \ m^3/mol/s \qquad (27)$$

Baldyga and Bourne (1984) gave no details of their experimental method, but since the new value of k_2 is half of the old value of k_2 at 298 K, Equation (27) appears to be an improvement over Equation (26). Nevertheless, there is some ambiguity associated with the value of k_2.

The question of the accuracy of k_2 acquires further significance in light of variations in values of ε_R and ε_S as measured in the present work and reported by others (see Figures 16 and 17). Figure 17 suggests that if indeed Kozicki's values of ε_S were higher than the actual, his measured C_S values were lower than the actual C_S values. Consequently, k_2 given by Equation (26) may be lower than the actual k_2. On the other hand, errors introduced by a higher ε_S value and neglecting the absorption due to R may cancel each other out. In that event, k_2 given by Equation (26) may be more reliable than Equation (27) even though the latter is the most recent value. In the present work, the values of ε_R and ε_S used in the data analysis are different (and lower) than those of Bourne et al. (1981). Therefore, k_2 given by Equation (26) is considered more accurate and is emphasized in fitting models with the data. However, the sensitivity of predictions to variations in k_2 are considered.

The first rate constant, k_1, is three orders of magnitude higher than k_2. Therefore, the reported value of k_1 at 298 K can be used equally well for all experimental runs. The model predictions are insensitive to minor variation in k_1.

Next, it is important to check the internal consistency of the experimental concentration measurements. The values of ε_R^λ and ε_S^λ displayed in Figures 16 and 17 were obtained with the Hewlett-Packard UV-visible spectrophotometer and not the fiber-optic probe used in the reactor experiments. In these experiments, k_R^λ and k_S^λ were obtained through calibration of the fiber-optic probe prior to each set of experiments. Recalling the fact that $k_R^\lambda = k_P \varepsilon_R^\lambda \ell$ and $k_S^\lambda = k_P \varepsilon_S^\lambda \ell$, it follows that a ratio of k_R^λ (or k_S^λ), measured by the probe, and ε_R (or ε_S^λ), measured in a separate spectrophotometer, must be a constant ($k_P \ell$), independent of compounds as well as the wavelength. It is found that the ratio is in the range 0.50-0.53 for R and 0.63-0.71 for S for all five wavelengths. The relative constancy of the ratio for R or S is encouraging. The difference in the values for R and S may stem from the fact that the optical fiber was directly in contact with the solutions. The chemical contact may have affected (e.g., etched) the exposed fiber surface. Nevertheless, the existence of a nearly constant ratio lends further support to the concentration measurement technique.

The final preliminary point concerns models to be used for comparison with experimental results. In Chapter III, where simulation of the present competing reactions was considered, it was shown that of the five mechanistic models with a turbulence analogy, the 3E model

is grossly inadequate for selectivity estimation. The failure of 3E was attributed to the lack of "rich" and "lean" reacting regions in the model structure. The evaluation of the remaining four models can be attempted by comparison of model predictions with the experimental data. Unfortunately, for the present experimental conditions--which involve highly unequal reactant flow rates--the SD model does not possess a turbulence analogy, and the CRD model required a staggering amount of computer time to achieve meaningful results. Owing to the high inequality of flow rates, the concentration profiles predicted by the CRD model were very sensitive to the number of eddies chosen for the simulation, although the exit concentrations were fairly stable. For meaningful predictions of the profiles, either the number of eddies had to be increased by an order of magnitude or the simulation had to be conducted several times, each with a different sequence of random numbers, and the results ensemble averaged. Either of these alternatives was economically prohibitive. However, the previous simulations (Chapter III) did show that the CRD and 4E models give similar predictions and that the IEM and SD models also give similar predictions. In the following, therefore, the 4E and IEM models are used to compare model predictions with the experimental data.

2. Experimental Results

The results of the mixing-reaction experiments are displayed in Figures 21-25. The ordinates of all the figures are concentrations normalized by the (mixed) feed concentration of B, $\bar{C}_{BO}$. $\bar{C}_{BO}$ is calculated by $\bar{C}_{BO} = C_{BO}Q_B/(Q_A + Q_B)$. The ordinates of profiles for S S are magnified compared to R except in Figure 21. The abscissa

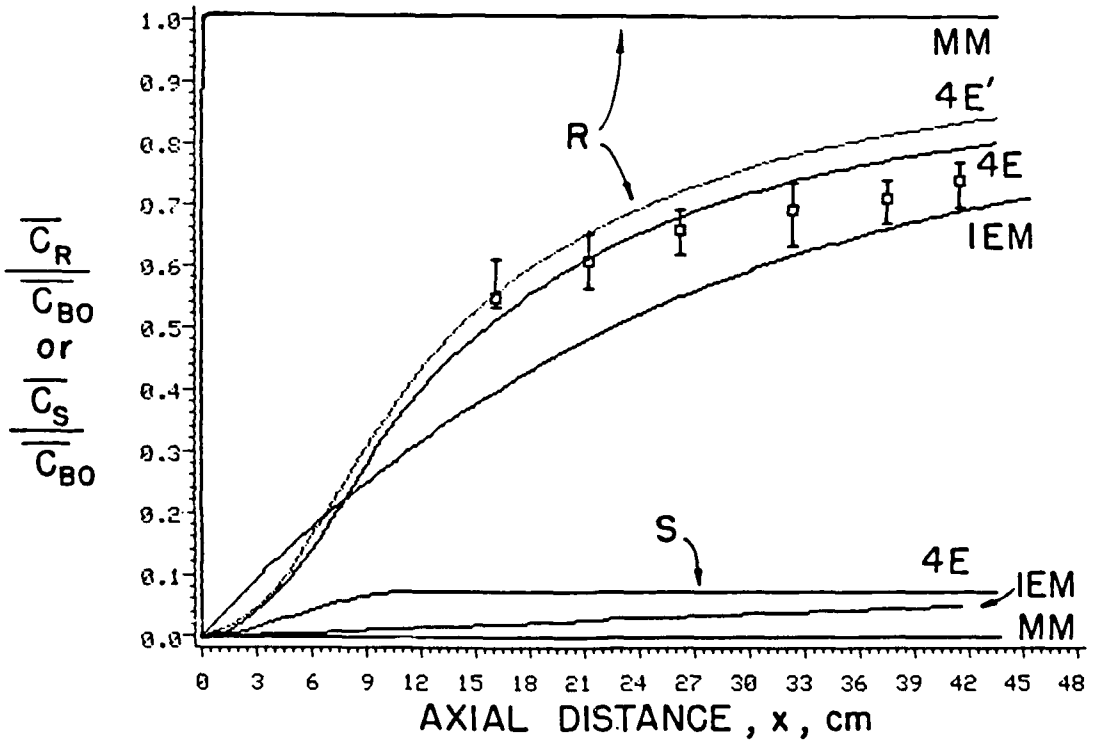

Figure 21. Mean concentration profile of products (β = 0.4; screen (M_1) upstream of injector; τ_m = 2.0 sec) [4E, 4E': 4E model predictions for k_2 given by Equations (26) and (27), respectively; MM: maximum mixedness (PFR) predictions]

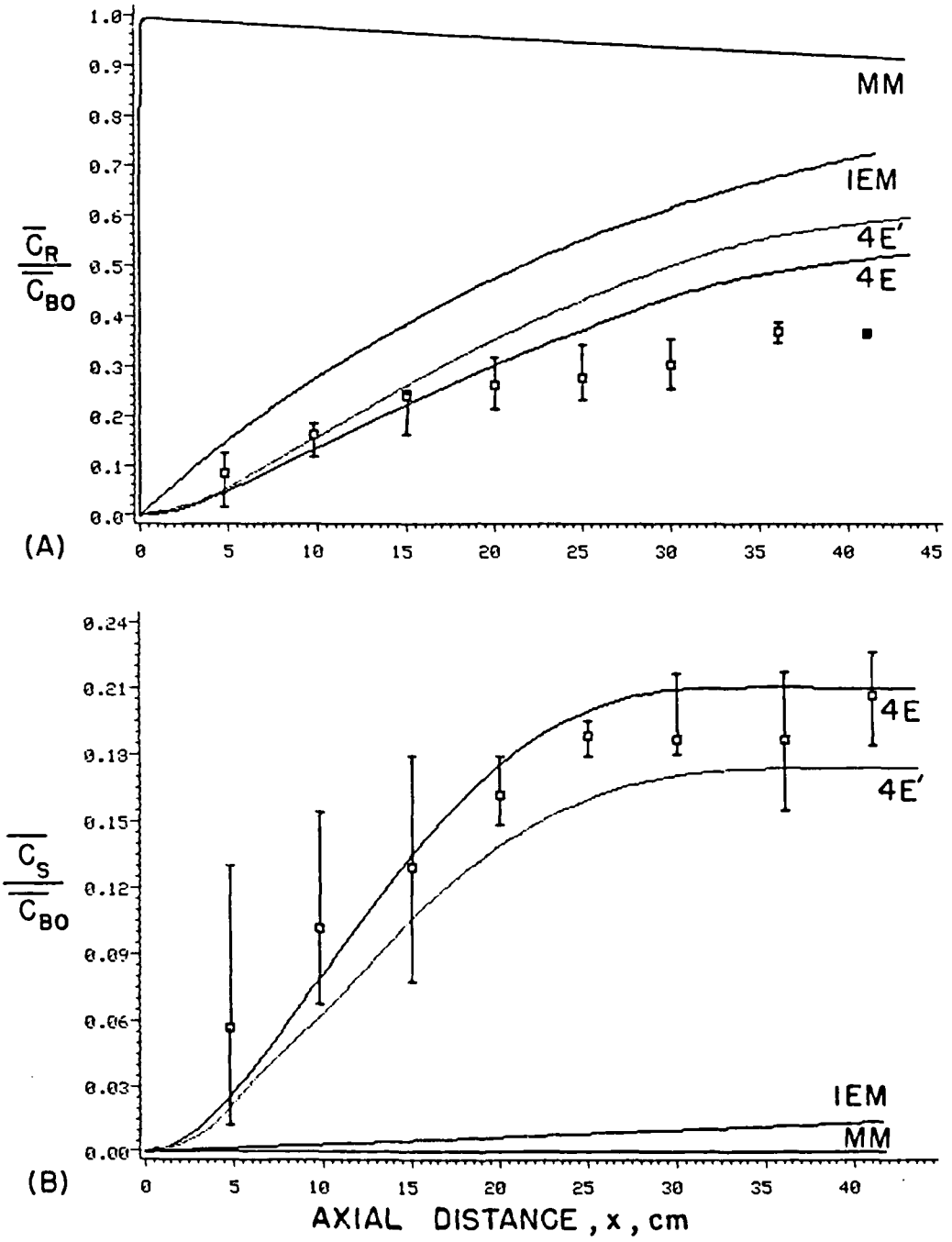

Figure 22. Mean concentration profile of products (β = 1.0; screen (M_1) upstream of injector; τ_m = 2.0 sec): (A) profile of monoazo dye, and (B) profile of diazo dye

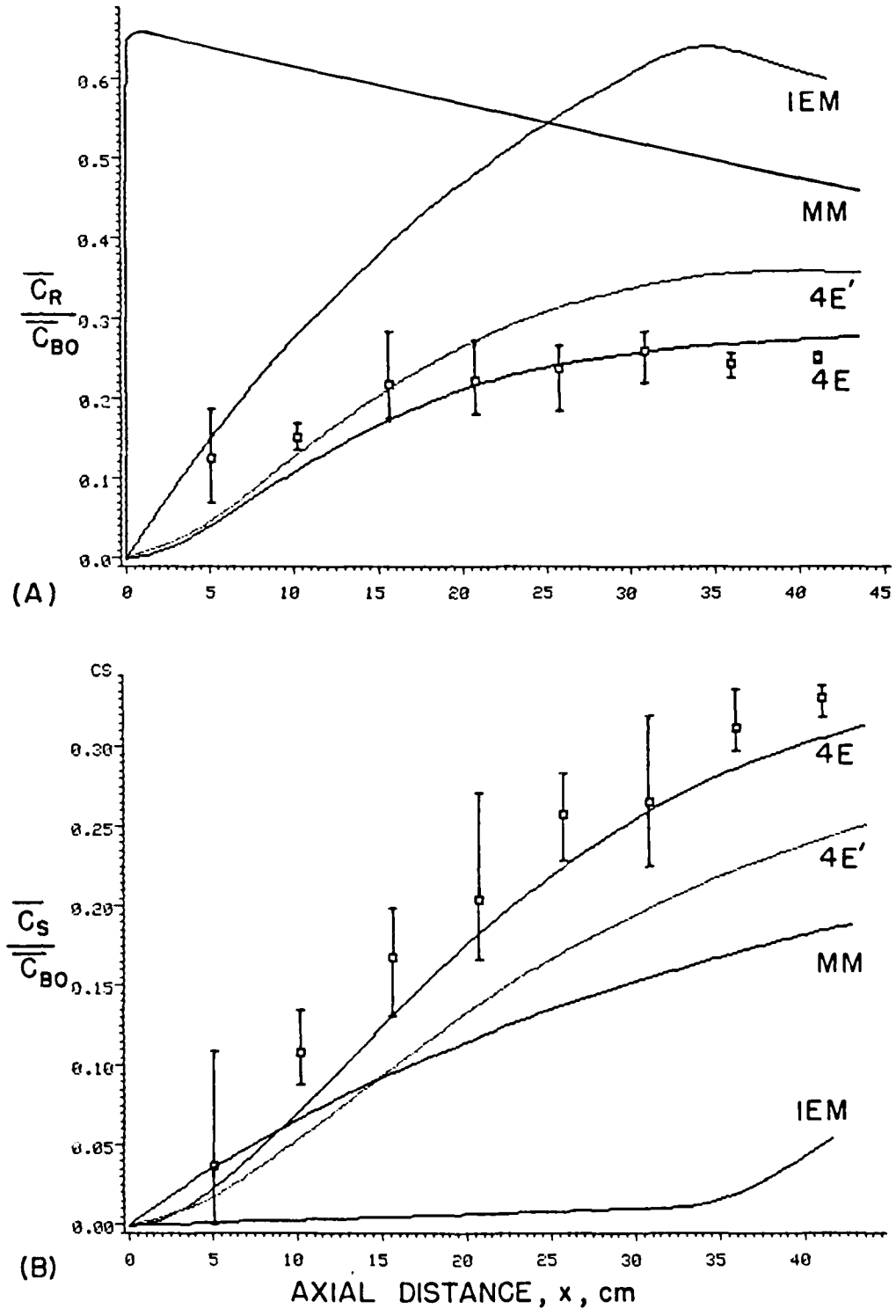

Figure 23. Mean concentration profile of products (β = 1.5, screens (M_1,M_2,M_3) upstream of injector; τ_m = 2.0 sec): (A) profile of monoazo dye, and (B) profile of diazo dye

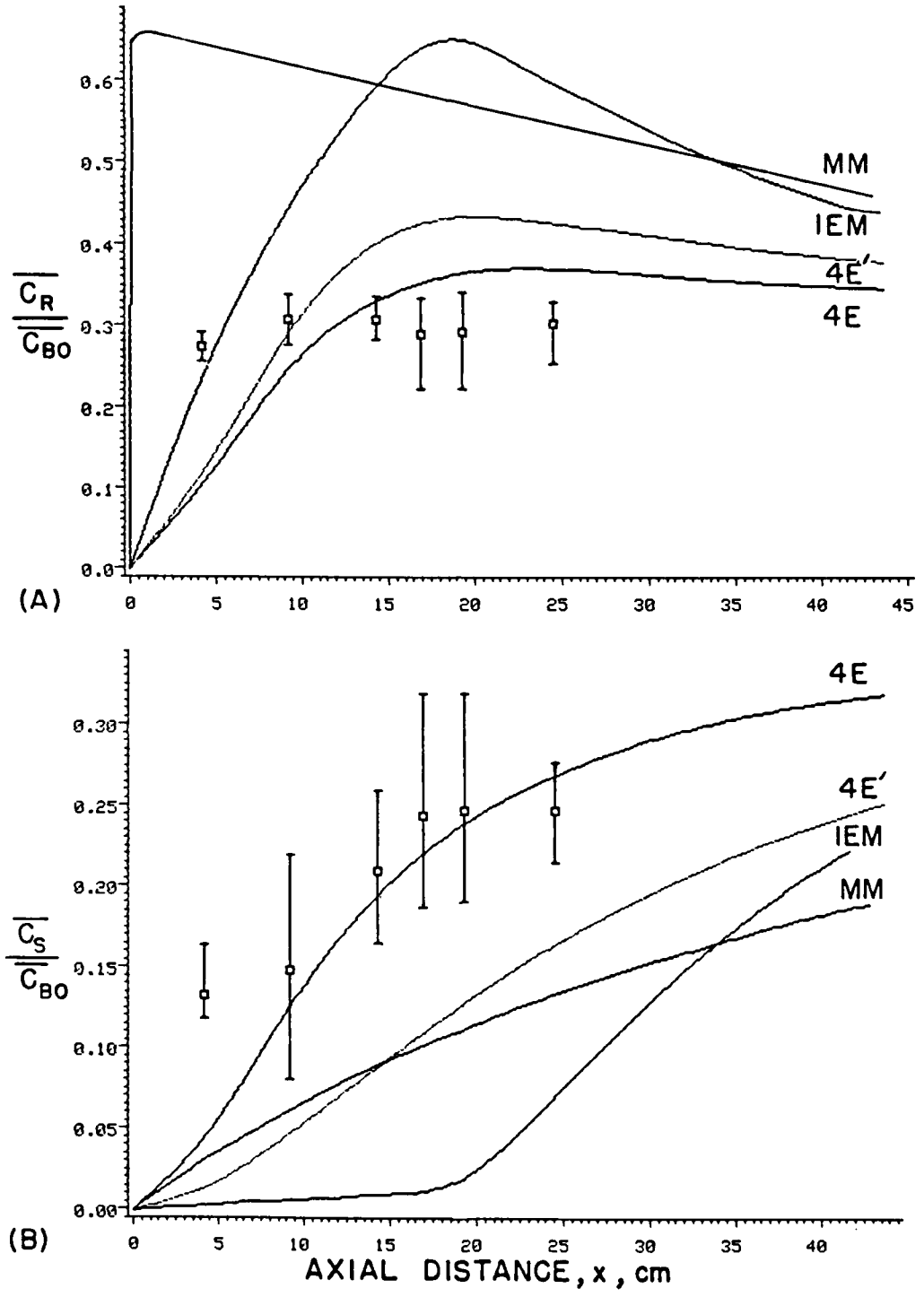

Figure 24. Mean concentration profile of products (β = 1.5; screens (M_2,M_3) downstream of injector; τ_m = 1.0 sec): (A) profile of monoazo dye, and (B) profile of diazo dye

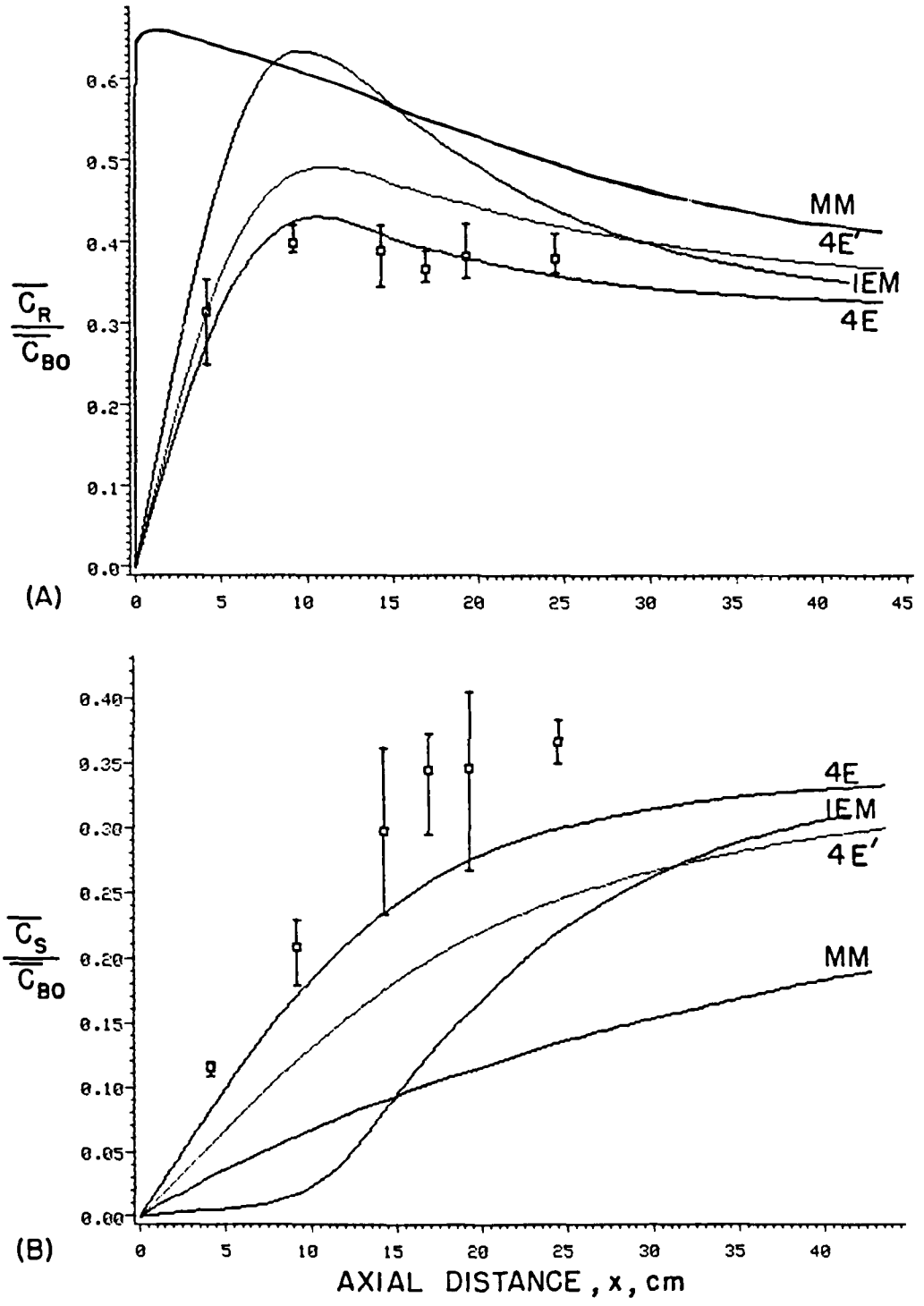

Figure 25. Mean concentration profile of products (β = 1.5; screen (M_1) downstream of injector; τ_m = 0.5 sec): (A) profile of monoazo dye, and (B) profile of diazo dye

is the axial distance from the injector needle tips. The squares represent the arithmetic mean of experimental data at each location, and the "error bars" represent the range over which the experimental results varied in successive runs (typically three runs). The "error bars" are not based on statistical measures (e.g., standard deviation) since experiments were repeated only three times. The smooth curves are the predictions of various models--maximum mixedness (classical PFR), IEM and 4E. The curves labeled as 4E' are 4E predictions for k_2 given by Equation (27).

Figures 21-25 reveal that the "error bars" are quite large, implying relatively large variations in the measured concentrations. The "error bars" merit some discussion before the model discrimination is pursued in detail. The magnitude of variations is similar for both R and S. Many sources may contribute to these variations, such as: errors involved in measuring and maintaining the feed flowrates (Q_A and Q_B) at a constant level; errors associated with preparing feed solutions of known concentrations (C_{AB}, C_{BO}); minor variations in pH from run to run; errors caused by a fairly low signal to noise ratio associated with the present measurement system; the fact that the optical fiber was exposed directly to the solutions and hence subjected to possible undesirable chemical interactions; and that the measurements could be made only at five wavelengths. Apart from Q_B, which is highly concentrated (C_{BO} ~ 10-40 mol/m^3), the feed conditions were controlled quite precisely. A maximum variation in Q_B, determined from the metering pump calibrations, is estimated to be $\pm$ 0.06 ml/sec and can cause only a 3 percent variation in $\bar{C}_{BO}$. Azo coupling is an electrophilic aromatic substitution and the

reactive species are 1-naphtholate and the diazonium ions, not the molecular 1-naphthol and diazotised sulfanilic acid. The concentrations of the reactive ions are pH dependent and so are the rate constants k_1 and k_2 (which are based on total--ionized and nonionized--concentrations). Nevertheless, the reaction medium was adequately buffered--10 mol/m^3 Na_2CO_3 and 10 mol/m^3 $NaHCO_3$ (I = 40 g ion/m^3) as compared to 0.3 mol/m^3 1-naphthol--and the pH was found to be constant (within ± 0.02 of 10.00). The effect of operating temperature also is expected to be minimal. Thus, it is concluded that the large "error bars" result principally from inherent limitations of the present absorbance measurement system. Of course, it should also be emphasized that the experimental concentration levels are very low and are intrinsically difficult to measure accurately.

The input parameters for the models were the feed flow rates (Q_A and Q_B), the unmixed feed concentrations (C_{A0} and C_{B0}), the operating temperature (T_{avg}), the mean axial velocity ($\bar{U}$) and the micromixing time (τ_m). Since each experiment was repeated at least three times, the corresponding values of the input parameters were taken as arithmetic averages of the actual input conditions for all runs at the same nominal operating conditions. A constant value of $\bar{U}$ = 7.6 cm/s was used as input for all the simulations. Although the value of k_2 given by Equation (26) is emphasized in the discussion of model comparison with experiment, predictions corresponding to a k_2 given by Equation (27) are also plotted (curves 4E') to show the sensitivity of the comparison to the value of k_2.

The only adjustable parameter of the models is τ_m. The actual model parameters--R_S for 4E and h for IEM--are related to τ_m through

the turbulence analogy (cf. Table 1). The models may be used to fit the experimental data by varying τ_m. The fluid mechanical results in conjunction with the turbulence analogy have suggested that τ_m may lie between two and nine seconds. In view of the scatter in the experimental data, an "eyeball" fit was used to determine the "best" τ_m rather than a more sophisticated statistical method.

Ordinarily, both models should be used to fit the data independently and then evaluated for their relative success. In the present study, however, the IEM model was unable to simultaneously match the experimental profiles of both R and S, regardless of the value of τ_m or k_2 used, for $\beta \geq 1$. A reasonable match of the IEM model predictions for $\bar{C}_R$ always led to very poor predictions of $\bar{C}_S$. In fact, $\bar{C}_S$ profiles could not be matched at all unless an arbitrarily higher value of k_2 was used. For $\beta = 0.4$, when virtually no S was produced, reasonably good predictions were possible with the IEM model. As a consequence of the overall inability of the IEM model to make reasonable predictions, the question of model evaluation was narrowed down to considering the ability of only the 4E model to predict the experimental data. In Figures 21-25, the predictions of the IEM and maximum mixedness models are displayed only to highlight the differences between them and the 4E model predictions. In addition, the 4E model predictions for k_2 given by Equation (27) are also displayed to show that conclusions remain unchanged for either of the k_2 values.

Figure 21 shows the results of experiments number 35-37. These experiments were conducted with screen M_1 in its upstream position. This case was studied earlier from a fluid mechanical viewpoint (Case 4) and was found to be most suited for model evaluation because the

turbulence field was most homogeneous. In the other case where screen M_1 was placed downstream from the injector, local inhomogeneity in the turbulence field very close to the screen might obscure the model comparison somewhat. The relative uniformity of turbulence in the former case is preferable for an unambiguous evaluation of the 4E model. In experiments 35-37 the stoichiometry, β, was very low (0.4). Because of the limited B present and the fact that the first coupling ($A + B \rightarrow R$) is three orders of magnitude faster than the second coupling ($R + B \rightarrow S$), the concentration of S is expected to be nearly zero. This is essentially a single reaction case and we do not expect to be able to discriminate between models here (recall Chapter III). Because the S concentration was expected to be near zero in this case, the experimentally observed absorbance was attributed entirely to R and the approximate method of concentration calculation was used (cf. Chapter V.B.3). The reaction results displayed in Figure 21 indicate that τ_m = 2 sec is a good estimate of the micromixing time. This value of τ_m is in accord with its estimate based on fluid mechanical results ($\tau_m \sim$ 2-9 sec). With τ_m = 2 sec, the IEM model also provides a reasonably good fit to the data. In fact, the fit of the IEM model could be improved if a somewhat lower value of τ_m were chosen. As mentioned above, this data set can not be used for model discrimination; however, it is quite useful in determining the value of τ_m for either. Effectively, this operating condition (β = 0.4) serves as a fast single reaction calibration case allowing us to fix a value of τ_m.

The results of experiments with an equimolar feed (β = 1.0; experiments 8-13), but with an identical screen-injector

configuration as in Figure 21 ($\beta = 0.4$), are depicted in Figure 22. Although there is scatter in the experimental data, particularly for S close to the injector (due to very low values of $\bar{C}_S$), the 4E model predictions are in satisfactory agreement with the data for a value of $\tau_m = 2$ sec. Note that the hydrodynamic conditions in this case ($\beta = 1.0$) are identical to those of the previous case ($\beta = 0.4$) and thus τ_m should be the same. The striking failure of the IEM model ($\tau_m = 2$ sec) is also evident in this figure, particularly in the prediction of S concentration.

The data for an even higher stoichiometric ratio ($\beta = 1.5$), but again for the same screen-injector arrangement is shown in Figure 23 (experiments 16-23, 34). Again, the 4E model compares quite favorably with the experimental data for a value of $\tau_m = 2$. It should be pointed out that experiments 22 and 23 involved use of two finer screens (M_2 and M_3) in the upstream position, and yet no change in the R and S concentration profiles were observed (see Appendix G). This is consistent with our findings from the fluid mechanical measurements that when a screen was placed upstream of the injector, its effect on the turbulence intensity was indistinguishable from that of the injector itself. The IEM model grossly overpredicts the concentration of R and predicts negligible concentration of S, which is in stark contrast with the experimental measurements.

In view of the three cases discussed above, it is clear that the effect of mixing on the experimental selectivity (concentrations of R and S) is very large. This is also reflected in the large difference between the experimental data and the maximum mixedness (classical PFR) predictions. Both models--4E and IEM, predict a large effect on

the concentration of R, but only the 4E model is able to fit the S concentration data well. It is concluded from these comparisons with experiments that the 4E model is able to simulate the effect of varying feed stoichiometry (β) on the selectivity ($\bar{C}_S/(\bar{C}_R + 2\bar{C}_S)$) under constant mixing conditions (constant τ_m) quite well.

The ability of the 4E model to respond to changes in mixing time at a fixed feed stoichiometry ($\beta = 1.5$) was tested by experiments 16-23, 24 (M_1 in upstream position), 31-33 (M_1 in downstream position), 25-27 (M_2 in downstream position) and 28, 30 (M_3 in downstream position). There was no observable difference between the results for the two finer screens (M_2 and M_3; see Appendix G). Consequently, those results are averaged together and displayed on the same plots (Figure 24). The 4E model predictions for $\tau_m = 1.0$ sec are in reasonable agreement with the data for this set except in the region near the injector where the model underpredicts the conversion. For the case where the coarser screen (M_1) was placed in its downstream position (Figure 25), the predictions are satisfactory for $\tau_m = 0.5$ sec. It is also clear that screens in their downstream location induce additional mixing as compared to upstream position.

It is important to recognize the effect of the initial zone of inhomogeneous turbulence (first one-eighth of the reactor) on the experimental concentrations. The first reaction ($A + B \rightarrow R$) is very fast (characteristic time of 0.5 msec) and is dominantly mixing limited. The second reaction ($R + B \rightarrow S$) is much slower (characteristic time of 1 sec) and is not as sensitive to the reduced mixing time (due to higher turbulence intensities) in the initial zone as the first reaction. This is evident in the proportionately greater variation in R concentration

in going from Figure 23 to 25 (τ_m = 2.0, 1.0 and 0.5 sec, respectively) as compared to S.

In view of the foregoing discussion, it is concluded that the 4E model is a more reliable model of mixing and chemical reaction than the 3E, SD and IEM models. The failure of the IEM model is simulating the experimental reactor is very striking and may be attributed to its structural deficiency as pointed out recently by Zwietering (1984) or earlier in this thesis (cf. Chapter III).

Additional comments on several recent suggestions which have appeared in the literature are appropriate in light of the results of this work. It has been proposed that in a competing reaction scheme similar to the present one, that the final concentrations of reaction products (i.e., $\bar{C}_R$ and $\bar{C}_S$ when $\bar{C}_B = 0$), are always the same for fixed initial conditions (feed flow rates, concentrations, temperature, pH) in a plug flow reactor, regardless of the axial concentration profiles (Brodkey and Lewalle, 1985). This suggestion implies that any reasonable mixing model should predict the same final selectivity, regardless of the value of the mixing time and also that all mixing models should yield the same final selectivity as long as the qualifying conditions of the above proposal are met. The first implication is in conflict with the 4E model, as it predicts significant differences in the final selectivity for the experimental case of $\beta = 1.0$ (case shown in Figure 22). For example, when τ_m = 2.0 sec, $\bar{C}_R/\bar{C}_{BO} = 0.57$ and $\bar{C}_S/\bar{C}_{BO} = 0.21$ and when τ_m = 0 sec, $\bar{C}_R/\bar{C}_{BO} = 1.0$ and $\bar{C}_S/\bar{C}_B = 0.00$. The second implication also is not in accord with the present study as large differences are observed between the 4E and IEM model predictions at $\beta = 1.0$. For example, when τ_m = 2 sec, at long times, 4E predicts

$\bar{C}_R/\bar{C}_{BO} = 0.57$, $\bar{C}_S/\bar{C}_{BO} = 0.21$, and IEM predicts $\bar{C}_R/\bar{C}_{BO} = 0.92$, $\bar{C}_S/\bar{C}_{BO} = 0.02$. However, no significant differences are observed between the two model predictions if a lower value of τ_m, say the one appropriate to Vassilatos's reactor (Vassilatos and Toor, 1965), i.e., 0.0082 sec, is used. In such a case, the model simulations indicate that the reactions go to completion within the first 3 cm of the reactor length. This again demonstrates the importance of having a highly segregated experimental reactor, as was the case in the present study, to discriminate among mixing models.

A surprising feature of the experimental results is that the finer screens (M_2 and M_3) seem to induce less mixing ($\tau_m = 1.0$ sec) as compared to the coarser screen (M_1; $\tau_m = 0.5$ sec) when the screens are placed downstream of the injector. Recall that they do not affect mixing when placed in the upstream location. Also, both the fine screens appear to induce the same amount of micromixing. This is contrary to one's intuition that the finer screens, due to their smaller mesh size, would shed finer eddies and hence lead to better mixing compared to the coarser screen. The explanation is based on the possibility that under the operating conditions, the finer screens may not shed any eddies at all. It should be noted that the pipe Reynolds numbers were identical for all three screens, but for flow behind screens, the mesh Reynolds number (Re_M) is more appropriate to characterize the flow regime.

Support for the above explanation comes from the work of Keeler (1964). Keeler's experimental system was similar to the present one. It was a tubular reactor with similar screens and "hairbrush" injector. Keeler carried out experiments to determine the flow rate in the reactor-screen system at which regular shedding of eddies commenced.

From his results, one can readily estimate the onset of eddy shedding in terms of a critical Reynolds number based on the wire diameter (Re_{Cr}), provided the solidity of the screen is known. The Re_{Cr} and the actual screen Reynolds numbers (Re_d) are listed in Table 9.

Table 9

Operating Characteristics of the Screens

Screen	M_1	M_2	M_3
Solidity	0.43	0.39	0.60
Re_{Cr}	50	53	35
Re_d*	96	43	30

*$Re_d = \bar{U}d/\nu$.

Clearly, the finer screens do not exceed the critical Reynolds number and thus may not shed any eddies under the operating conditions. As a result they are less effective in generating additional turbulence. Nevertheless, they do cause some extra mixing, perhaps due to physical obstruction of the flow during its passage through the screens, and hence the associated mixing time is smaller (τ_m = 1.0 sec) than the mixing time for the case where no screens were placed downstream of the injector (τ_m = 2.0 sec).

A final point in this discussion is related to the overall material balance for each experiment. As described in Chapter V, three exit samples were taken during each run and analyzed to calculate the

exit concentrations of R and S. Overall material balance demands that

$$\bar{C}_{BO} = \bar{C}_B + \bar{C}_R + 2\bar{C}_S \tag{28}$$

For all the feed stoichiometries used in this study ($\beta < 2$), we should expect $\bar{C}_B = 0$ at the exit. Thus,

$$\bar{C}_{BO} = \bar{C}_R + 2\bar{C}_S \tag{29}$$

The values of $\bar{C}_{BO}$, $\bar{C}_R$ and $\bar{C}_S$ at the reactor exit are listed in Table 10 and the percentage error in the material balance is shown in the last column of the table. The material balance is satisfied within 10 percent for $\beta \leq 1.0$. However, for $\beta \sim 1.5$, with the exception of experiment 16, the output of B ($\bar{C}_R + 2\bar{C}_S$) always exceeds the input ($\bar{C}_{BO}$) by a significant amount.

It is clear from Equation (29) that any error in measuring $\bar{C}_S$ is amplified by a factor of two in the material balance calculations. It is reasonable to expect errors in $\bar{C}_R$ and $\bar{C}_S$ values whose magnitudes are similar to those implied by the "error bars" (i.e., variation by 0.02 to 0.06 mol/m^3). For experiment number 30, if $\bar{C}_R$ and $\bar{C}_S$ values were decreased by 0.06 mol/m^3, the overall material balance would be met within 10 percent rather than 50 percent as reported. It is also interesting to note that experiment number 34 has an 80 percent error in the mass balance and experiment number 22 has only a 13 percent error, and yet both the experiments yielded very similar concentration profiles of R and S (see Appendix G). The main difference between these two experiments is only in the exit concentration of S (0.13 mol/m^3 for Run #22 and 0.28 mol/m^3 for Run #34). Thus, our inability to measure $\bar{C}_S$ very accurately, may lead to such discrepancies in the

Table 10

Material Balance at Reactor Exit

Experiment	Feed Concentration $\bar{C}_{BO}$ (mol/m^3)	Exit Concentrations $\bar{C}_R$ (mol/m^3)	$\bar{C}_S$ (mol/m^3)	ΔB[a] %
8	0.30	0.18	0.07	7
9	0.30	0.17	0.06	3
11	0.30	0.19	0.06	3
12	0.30	0.18	0.08	0
13	0.30	0.18	0.07	7
16	0.44	0.22	0.11	0
19	0.46	0.23	0.22	46
20	0.46	0.26	0.20	43
22	0.46	0.26	0.13	13
23	0.46	0.28	0.17	35
25	0.46	0.24	0.15	23
26	0.45	0.22	0.14	11
27	0.44	0.21	0.15	16
28	0.44	0.25	0.17	34
30	0.44	0.22	0.22	50
31	0.45	0.22	0.21	38
32	0.45	0.22	0.18	29
33	0.45	0.20	0.19	29
34	0.46	0.26	0.28	78
35	0.12	0.11	--	8
36	0.12	0.12	--	0
37	0.12	0.11	--	8

[a] $$\Delta B = \frac{(\bar{C}_R + 2\bar{C}_S) - \bar{C}_{BO}}{\bar{C}_{BO}} \times 100$$

material balance as are seen in experiments 19 to 34. It is felt that placing a glass seal at the probe tip to protect the fiber ends will improve the accuracy of the fiber-optic probe considerably.

VII. SUMMARY AND CONCLUSIONS

Several important points have emerged from the present work. First, it was shown in Chapter III that the five mechanistic models of mixing and chemical reaction having a turbulence analogy--namely, the CRD, SD, IEM, 3E and 4E models--are not equivalent in terms of estimating selectivity of competing reactions in a PFR. The non-equivalence of models was demonstrated via numerical simulations, although the CRD and 4E models, the SD and IEM models, and the 3E and maximum mixedness models were found to yield similar predictions.

Based on simulations, a highly segregated plug flow reactor was designed and constructed for an experimental study of the effect of mixing on selectivity of two competing azo-coupling reactions. The fluid mechanical measurements discussed in Chapter VI.A provided sufficient evidence to conclude that the constructed plug flow reactor yielded a nearly homogeneous mean axial velocity field and a turbulence level which was homogeneous over 7/8 of the reactor length. The mixing-reaction data collected in this study were fairly reproducible in spite of the low concentration levels at which the reactor was operated. The data provided a valuable test to discriminate between two representative models--4E and IEM. The 4E model was found to successfully simulate the experimental behavior at all the conditions studied while the IEM model was found unable to match the experimental data. The failure of the IEM and, as shown earlier, 3E models, and the relative success of the 4E model, point to the importance of certain structural features of mixing models, such as the existence of "rich" and "lean" reacting regions and presence of regions of total

segregation. The SD model is inapplicable to unequal flow rates and hence can not be used to simulate the present experiments. The CRD model may be able to compare favorably with the data but requires prohibitively large computer time.

It is also concluded that a discrimination among several plausible mechanistic models of mixing and chemical reaction is possible only under conditions of imperfect mixing similar to ones covered in the present study. The present experimental data provide valuable information to test many turbulence closure schemes for concentration correlations as well. The plug flow reactor of the present study is a very useful arrangement to further study the interaction of turbulence, mixing and chemical reaction in an unambiguous manner.

Finally, the 4E model, which has many attractive features, like its applicability to arbitrary feed flow rates, arbitrary feed residence time distributions, and arbitrarily complex kinetics; its mathematical simplicity (O.D.E.'s) and modest computational requirements; the fact that its model parameter can be readily estimated a priori or measured from fast single reaction experiments, is recommended as the most general mechanistic chemical reactor model for homogeneous systems now available.

VIII. FUTURE WORK

Many industrial reactors are inherently limited by imperfect micromixing. The flow field of such reactors are so complex that a mechanistic model like the 4E model might be a powerful tool in a systematic study of the reactor behavior as compared to more traditional turbulence models. Based on the encouraging results of the present study, it seems reasonable to consider analyzing reported data from a high intensity or low calorific value fuel combustor, or a precipitation reactor, or a polymerization reactor within the framework of the 4E model.

Experimentally, the present reactor is a very useful system for obtaining reliable mixing and reaction data under relatively uniform and controlled fluid mechanics. However, the fluid mechanics of the present reactor should be better characterized by more accurate methods such as hot-film or laser-doppler anemometry. Even the chemistry side of the present work shows need for more accurate kinetic information. Moreover, the present fiber-optic system has demonstrated its ability to provide meaningful mean concentration data. Attempts should be made to improve the signal to noise ratio of this system so that even fluctuating components of the concentrations may be measured. Such a data base would contribute significantly in evaluation of many available closure schemes in turbulence modeling.

From a modeling point of view, incorporating a variation in the mixing time--a critical factor in practical situations--would greatly enhance the generality of the 4E model.

REFERENCES

Angst, W., J. R. Bourne, and R. N. Sharma. "Mixing and Chemical Reaction IV, The Dimensions of the Reaction Zone." Chem. Eng. Sci., 37, 585 (1982).

Aubry, C. and J. Villermaux. "Representation du melange imparfait de deux courants de reactifs dans du reacteur agite continu." Chem. Eng. Sci., 30, 457 (1975).

Baldyga, J. and J. R. Bourne. "A Fluid Mechanical Approach to Turbulent Mixing and Chemical Reaction, Part I." Chem. Eng. Commun., 28, 231 (1984).

Baldyga, J. and J. R. Bourne. "A Fluid Mechanical Approach to Turbulent Mixing and Chemical Reaction, Part III." Chem. Eng. Commun., 28, 259 (1984).

Bourne, J. R., F. Kozicki, and P. Rys. "Mixing and Fast Chemical Reaction I; Test Reactions to Determine Segregation." Chem. Eng. Sci., 36, 1643 (1981).

Bourne, J. R. "The Characterization of Micromixing Using Fast Multiple Reactions." Chem. Eng. Commun., 16, 79 (1982).

Bourne, J. R. "Mixing on the Molecular Scale (Micromixing)." Chem. Eng. Sci., 38, 5 (1983).

Brodkey, R. S. and Lewalle, J. "Reactor Selectivity Based on First-Order Closures of the Turbulent Concentration Equations." AIChE J., 31, 111 (1985).

Burgers, J. M. Lecture Notes, California Institute of Technology, U.S.A. (1951).

Cairns, E. J. and J. M. Prausnitz. "Longitudinal Mixing in Packed Beds." Chem. Eng. Sci., 12, 20 (1960).

Chang, L-J, R. V. Mehta, and Tarbell, J. M. "Evaluation of Models of Mixing and Chemical Reaction with a Turbulence Analogy." Accepted for publication, Chem. Eng. Commun. (1985).

Corrsin, S. "Simple Theory of an Idealized Turbulent Mixer." AIChE J., 3, 329 (1957).

Corrsin, S. "The Isotropic Turbulent Mixer: Part II. Arbitrary Schmidt Number." AIChE J., 10, 870 (1964).

Costa, P. and C. Trevissoi. "Reactions with Nonlinear Kinetics in Partially Segregated Fluids." Chem. Eng. Sci., 27, 2041 (1972).

Curl, R. L. "Dispersed Phase Mixing: Part I. Theory and Effects in Simple Reactors." AIChE J., 9, 175 (1963).

Danckwerts, P. V. "Continuous Flow Systems: Distribution of Residence Times." Chem. Eng. Sci., 2, 1 (1953a).

Danckwerts, P. V. "The Definition and Measurement of Some Characteristics of Mixtures." Appl. Sci. Res., 3, 279 (1953b).

Danckwerts, P. V. "The Effect of Incomplete Mixing on Homogeneous Reactions." Chem. Eng. Sci., 8, 93 (1958).

Evangelista, J. J., S. Katz, and R. Shinnar. "Scale-Up Criteria for Stirred Tank Reactors." AIChE J., 15, 843 (1969).

Fisher, D. A. "Development and Application of a Model for Fast Reactions in Turbulently Mixed Liquids." Ph.D. Thesis, University of Minnesota, U.S.A. (1974).

Garbini, J. L., F. K. Forster, and J. E. Jorgensen. "Measurement of Fluid Turbulence Based on Pulsed Ultrasound Technique, Part 2. Experimental Investigation." J. Fluid Mech., 118, 471 (1982).

Garside, J. "Industrial Crystallization from Solution." Chem. Eng. Sci., 40, 3 (1985).

Geurden, J. M. G. and D. Thoenes. "Influence of Mixing on the Rate of Conversion of Chemical Reactions in Viscous Liquids." Proc. Fifth European/Sixth International Symp. on Chemical Reaction Engineering, Amsterdam (1972).

Harada, M., K. Arima, W. Eguchi, and S. Nagata. "Micromixing in a Continuous Flow Reactor. Mem. Fac. Eng., Kyoto University, Japan, 24, 431 (1962).

Hinze, J. O. Turbulence. 1st Edition, McGraw-Hill, NY (1959).

Jorgensen, J. E., D. N. Campau, and D. W. Baker. "Physical Characteristics and Mathematical Modelling of the Pulsed Ultrasonic Flowmeter." Med. Biol. Eng., 11, 404 (1973).

Kattan, A. and R. J. Adler. "A Conceptual Framework for Mixing in Continuous Chemical Reactors." Chem. Eng. Sci., 27, 1013 (1972).

Keeler, R. N. "Mixing and Chemical Reactions in Turbulent Flow Reactors." Ph.D. Thesis, University of California, Berkeley, U.S.A. (1964).

Keeler, R. N., E. E. Petersen, and J. M. Prausnitz. "Mixing and Chemical Reaction in Turbulent Flow Reactors." AIChE J., 11, 221 (1965).

Kozicki, F. R. "Selektivitat Mischungsmaskierter Reaktionen in Rührkesseln." Ph.D. Thesis, ETH (1980).

Lee, J. and R. S. Brodkey. "Light Probe for the Measurement of Turbulent Fluctuations." Rev. Sci. Instr., 34, 1086 (1963).

Levenspiel, O. Chemical Reaction Engineering, Wiley, NY (1962).

Li, K. T. Personal Communication, Carnegie-Mellon University, Pittsburgh, PA (1984).

Loerhke, R. I. and H. M. Nagib. "Experiments on Management of Free-Stream Turbulence." AGARD Report No. 598 (1972).

Lumley, J. L. and J. F. McMohan. "Reducing Water Tunnel Turbulence by Means of a Honeycomb." J. Basic Eng., Trans. ASME, Series D, 89, 764 (1967).

Mahalingam, S. and R. Chevray. "Concentration Fluctuation Measurements in Reacting Flows." Annal. N. Y. Acad. Sci., 404, 351 (1983).

Mao, K. W. and H. L. Toor. "A Diffusion Model for Reactions with Turbulent Mixing." AIChE J., 16, 49 (1970).

McKelvey, K. N., H. N. Yieh, S. Zakanycz, and R. S. Brodkey. "Turbulent Motion, Mixing, and Kinetics in a Chemical Reactor Configuration." AIChE J., 21, 1165 (1975).

Mehta, R. V. and J. M. Tarbell. "Four Environment Model of Mixing and Chemical Reaction, Part I." AIChE J., 29, 320 (1983a).

Mehta, R. V. and J. M. Tarbell. "Four Environment Model of Mixing and Chemical Reaction, Part II." AIChE J., 29, 329 (1983b).

Ng, D. Y. C. and D. W. T. Rippin. The Effect of Incomplete Mixing on Conversion in Homogeneous Reactions. Third European Symposium on Chemical Reaction Engineering, Amsterdam, September 1964. Pergamon Press, Oxford, 161-165 (1965).

Ottino, J. M., W. E. Ranz, and C. W. Macosko. "A Lamellar Model for Analysis of Liquid-Liquid Mixing." Chem. Eng. Sci., 34, 877 (1979).

Patterson, G. K. "Application of Turbulence Fundamentals to Reactor Modelling and Scaleup." Chem. Eng. Comm., 8, 25 (1981).

Plasari, E. Etude Fondamentale du Micromelange dans un Reacteur Agite Continu en Phase Liquide au Mogen d'une Reaction du type Michaelis-Menten. These de Doctorat es sciences, INPL, Nancy, France (1976).

Pope, A. In Wind Tunnel Testing, John Wiley and Sons, Inc., NY (1947).

Pratt, D. T. "Mixing and Chemical Reaction in Continuous Combustion." Prog. Energy Combust. Sci., 1, 73 (1976).

Ritchie, B. W. and A. H. Tobgy. "Mixing and Product Distribution with Series-Parallel Reactions in Stirred Tank and Distributed Feed Reactors." Adv. Chem. Ser., Am. Chem. Soc., 133, 376 (1974).

Ritchie B. W. and A. M. Tobgy. "General Population Balance Modelling of Unmixed Feedstream Chemical Reactors: A Review." Chem. Eng. Commun., 2, 249 (1978).

Ritchie, B. W. and A. H. Tobgy. "A Three-Environment Micromixing Model for Chemical Reactors with Arbitrary Separate Feedstreams." Chem. Eng. J., 17, 173 (1979).

Rosensweig, R. E. "Idealized Theory for Turbulent Mixing in Vessels." AIChE J., 10, 91 (1964).

Rosensweig, R. E. "Isotropic Turbulent Mixing with Boundary Sources." Can. J. Chem. Eng., 44, 255 (1966).

Spielman, L. A. and O. A. Levenspiel. "A Monte Carlo Treatment for Reacting and Coalescing Dispersed Phase Systems." Chem. Eng. Sci., 20, 247 (1965).

Steele, R. L. "The Design of a Small Water Tunnel." M.S. Thesis, The Pennsylvania State University (1951).

Tan-Atichat, J., H. M. Nagib, and R. I. Loehrke. "Interaction of Free-Stream Turbulence with Screens and Grids: A Balance Between Trubulent Scales." J. Fluid Mech., 114, 501 (1982).

Tarbell, J. M. and R. V. Mehta. "Mechanistic Models of Mixing and Chemical Reaction with a Turbulence Analogy." Physicochemical Hydrodynamics, in press (1985).

Torrest, R. S. and W. E. Ranz. "Concentration Fluctuations and Chemical Conversion Associated with Mixing in Some Turbulent Flows." AIChE J., 16, 930 (1970).

Treleaven, C. R. and A. H. Tobgy. "Residence Times, Micromixing, and Conversion in an Unpremixed Feed Reactor--I." Chem. Eng. Sci., 27, 1653 (1972a).

Treleaven, C. R., and A. H. Tobgy. "Monte Carlo Methods of Simulating Micromixing in Chemical Reactors." Chem. Eng. Sci., 27, 1497 (1972b).

Treleaven, C. R. and A. H. Tobgy. "Residence Times, Micromixing, and Conversion in an Unpremixed Feed Reactor--II. Chem. Eng. Sci., 28, 413 (1973).

Van der Molen, T. J., A. Koenen, H. H. J. Oosterwijk, and H. Th. Van der Bend. "Effect of Process Conditions on Light-Off Temperature and Consumption of Sixteen Initiators, as Determined from High Pressure Radical Polymerization of Ethylene." Ing. Chim. Ital., 18, 7 (1982).

Vassilatos, G. and H. L. Toor. "Second-Order Chemical Reactions in a Non-homogeneous Turbulent Fluid." AIChE J., 11, 666 (1965).

Villermaux, J. and J. C. Devillon. "Representation de la Coalescence et de la redisperison des domainesde segregation dans un fluide par un modele dinteraction phenomenologique." 2nd Symp. Chem. Reaction Eng. B-1-13 (1972).

Villermaux, J. "Mixing in Chemical Reactors." ACS Symp. Series No. 226, 135 (1983).

Villermaux, J. Personal Communication, December (1984).

Zwietering, Th. N. "A Backmixing Model Describing Micromixing in Single-Phase Continuous-Flow Systems." Chem. Eng. Sci., 39, 1765 (1984).

APPENDIX A

COMPUTER PROGRAMS FOR THE MODELS

The computer codes given in this appendix were used in all the model computations for competing reactions in this study. The main input parameter for the models are:

QA, QB = Feed flow rate of two streams (cm^3/s)

CA0, CB0 = Unmixed feed concentration (mol/cm^3)

U or VEL = Mean axial velocity in the reactor (cm/s)

TEMP = Mean reactor temperature (°C)

TAUM - Mixing time (s)

These values are either read as data or directly specified in the main program. The rate constants, RK1 and RK2, also are either read as data or internally specified or calculated within the program. All the governing equations are in their dimensionless forms. Other parameters are specified as needed by the respective numerical schemes for the numerical integration purposes or for obtaining printouts at appropriate time steps. The printed values are normalized values of concentrations relative to (mixed) concentration of B, $\bar{C}_{B0}$.

The model equations for the 4E and IEM models are as follows:

The 4E Model

$$\frac{dC_{ij}^*}{dt^*} = R_s^{\tau}\left[\left(\frac{V_i}{\hat{V}_1^L}\right)\left(C_{ji}^{o*} - C_{ji}^{L*}\right)\exp(-R_s^{\tau}t^*)\right.$$

$$\left. + \frac{\hat{V}_k^L}{\hat{V}_i^L}\left(C_{jk}^{L*} - C_{ji}^{L*}\right)\right] \pm \gamma_{ji}^* \qquad \begin{array}{l} j = A,B,R,S \\ i = 1,2 \\ k = 3-i \end{array} \qquad (A.1)$$

where notations are in accordance with Mehta and Tarbell (1983a). γ_{ji}^* is the local production (+) or consumption (-) term given in terms of local concentrations and rate constants (k_1 and k_2).

The IEM Model (dimensional form)

$$\frac{dC_{ij}}{dt} = h(\bar{C}_j - C_{ij}) \pm \gamma_{ij} \qquad (A.2)$$

$$\bar{C}_j = \left(\frac{Q_1}{Q_1+Q_2}\right) C_{ij} + \left(\frac{Q_2}{R_1+R_2}\right) C_{kj} \qquad \begin{array}{l} i = 1,2 \\ k = 3-i \\ j = A,D,R,S \end{array} \qquad (A.3)$$

γ_{ij} is the production (+) or consumption (-) rate of the species j. The initial values are the unmixed feed concentrations in the respective feedstreams.

APPENDIX A.1--Slab Diffusion (SD) Model

```
CC ------------------------------------------------------------------
CC  SLAB DIFFUSION MODEL FOR COMPETING REACTIONS-
CC ------------------------------------------------------------------
      IMPLICIT REAL*8(A-H,O-Z)
      COMMON/CONC/ CA(200),CB(200),CR(200),CAOLD(200)
      COMMON/TRID/ B(200),A(200),C(200),D(200),V(200)
      COMMON/PREV/ CAP(200),CBP(200),CRP(200)
      COMMON/GRID/ X(200),CC(200,3)
      PI = 3.1415926586DO
CC ------------------------------------
CC   DEFINE SYSTEM PARAMETERS
CC ------------------------------------
      TAUM= 0.630
      QA = 1.DO
      QB = 1.DO
      CBO = 0.2D-3
      CAO = 0.2D-3
      U    = 6.30
      RK1  = 7.3D6
      RK2  = 3.5D3
      PA = QA / (QA+QB)
      PB = QB / (QA+QB)
      CBOBAR = CBO*PB
      CAOBAR = CAO*PA
      BETA = CBOBAR/CAOBAR
      GAMMA= RK2/RK1
      TSCALE = 2.DO*TAUM*PI**2
      DA   = CBO*RK1*TSCALE
      WRITE(6,800) QA,QB,PA,PB
      WRITE(6,100) CAO,CBO,BETA,RK1,RK2,GAMMA
  100 FORMAT(/2X,'CAO = ',F8.3,2X,'CBO = ',F8.3,2X,'BETA = ',F8.3,2X
     * ,'RK1 =',D11.4,2X,'RK2 = ',D11.4,2X,'GAMMA = ',D11.4/)
      WRITE(6,110) TAUM, DA
  110 FORMAT(2X,'TAUM = ',D11.4,2X,'DA NUM = ',D11.4)
  800 FORMAT(2X,'QA = ',F10.4,2X,'QB = ',F10.4,2X,'PA=',D11.4,
     *  2X,' PB=',D11.4)
CC ----------------------------------------
CC  DEFINE NUMERICAL SOLUTION PARAMETERS
CC ----------------------------------------
C ---- DT = TIME STEPS , NT= # OF TIME STEPS TO BE RUN -------
      DT = 0.001
      NT = 400
      NXA  = 49
      NXB  = 49
CC ----- NXA1= # OF GRIDS IN PART A ,NAB1= # OF GRIDS IN PART B ---
      NXA1 = NXA+1
      NXB1 = NXB+1
      NX   = NXA1+NXB1
      DXA  = PA/(NXA+0.5)
      DXB  = PB/(NXB+0.5)
      DXA2 = DXA**2
      ALFA = DXA2/DT
      DXB2 = DXB**2
      ALFB = DXB2/DT
```

```
      DXL2 = ( (DXA+DXB)**2/4.D0 +DXA**2 ) /2.D0
      DXH2 = ( (DXA+DXB)**2/4.D0 +DXB**2 ) /2.D0
      ALFL = DXL2/DT
      ALFH = DXH2/DT
      DO 14 I = 1,NXA1
   14 X(I) = DXA*(I-1)
      DO 24 I = 1,NXB1
   24 X(I+NXA1) = X(NXA1)+(DXA+DXB)/2.D0+DXB*(I-1)
      X(1) = 0.D0
      X(NX)= 1.D0
      WRITE(6,180) NXA1,NXB1,DXA,DXB,DT,NT
  180 FORMAT(2X,'NXA1=',I5,2X,'NXB1=',I5,2X,'DXA=',D11.4,2X,
     * 'DXB=',D11.4,2X,'DT=',D11.4,2X,'NT=',I5/)
      MX = 150
      TOR = 1.0D-3
CC ----------------------------------------
CC  INITIAL CONDITIONS
CC ----------------------------------------
      DO 2 I=1,NX
      IF(I.LE.NXA1) CA(I)=1.D0
      IF(I.LE.NXA1) CB(I)=0.D0
      IF(I.GT.NXA1) CA(I)=0.D0
      IF(I.GT.NXA1) CB(I)=1.D0
      CR(I) = 0.D0
    2 CONTINUE
      WRITE(6,145) (CA(I),I=1,NX)
      WRITE(6,145) (CB(I),I=1,NX)
  145 FORMAT(7D11.4)
CC ==========================================================
CC  START THE NUMERICAL SOLUTION ROUTINES
CC  SEQUENCE : A --> R --> B --> CHECK CONVERGENCE OF B
CC             |                                    |
CC             |-<----------------------------------|
CC ==========================================================
      TIME = 0.D0
      DO 1 LT = 1,NT
      DO 17 I=1,NX
      CAP(I) = CA(I)
      CBP(I) = CB(I)
      CRP(I) = CR(I)
   17 CONTINUE
      NPRINT = 0
      IF(LT/10*10.EQ.LT) NPRINT=1
      TIME = TIME+DT
      DO 5 NS = 1,MX
CC ---------------------------------------
CC   SOLVE FOR CA
CC ---------------------------------------
CC      B.C. AT X=0.D0
      A(1) = -(2.D0+ALFA+DA*CB(1)*DXA2)
      C(1) = 2.D0
      D(1) = -ALFA*CAP(1)
CC ------ LOWER PART -------------------------------
      DO 15 I=2,NXA
```

```
      B(I) = 1.D0
      A(I) = -(2.D0+ALFA+DA*CB(I)*DXA2)
      C(I) = 1.D0
      D(I) = -ALFA*CAP(I)
   15 CONTINUE
CC     SPECIAL CASES NEAR THE INTERFACE LINE
      B(NXA1) = 1.D0
      A(NXA1) = -(2.D0+ALFL+DA*CB(NXA1)*DXL2)
      C(NXA1) = 1.D0
      D(NXA1) = -ALFL*CAP(NXA1)
CC ------------------------------------------------
      B(NXA1+1) = 1.D0
      A(NXA1+1) = -(2.D0+ALFH+DA*CB(NXA1+1)*DXH2)
      C(NXA1+1) = 1.D0
      D(NXA1+1) = -ALFH*CAP(NXA1+1)
CC --- UPPER PART ----------------------------------
      DO 25 I=2,NXB
      B(NXA1+I) = 1.D0
      A(NXA1+I) = -(2.D0+ALFB+DA*CB(NXA1+I)*DXB2)
      C(NXA1+I) = 1.D0
      D(NXA1+I) = -ALFB*CAP(NXA1+I)
   25 CONTINUE
CC       B.C. AT X=1.D0
      B(NX) = 2.D0
      A(NX) = -(2.D0+ALFB+DA*CB(NX)*DXB2)
      D(NX) = -ALFB*CAP(NX)
      CALL TRIDAG(1,NX,B,A,C,D,V)
      DO 3 I=1,NX
    3 CA(I) = V(I)
CC ----------------------------------------
CC   SOLVE FOR  CR
CC ----------------------------------------
CC       B.C. AT X=0.D0
      A(1) = -(2.D0+ALFA+DA*DXA2*GAMMA*CB(1))
      C(1) = 2.D0
      D(1) = -ALFA*CRP(1) -DXA2*DA*CAP(1)*CBP(1)/BETA
CC ------ LOWER PART -----------------------------
      DO 16 I=2,NXA
      B(I) = 1.D0
      A(I) = -(2.D0+ALFA+DA*DXA2*GAMMA*CB(I))
      C(I) = 1.D0
      D(I) = -ALFA*CRP(I) -DXA2*DA*CAP(I)*CBP(I)/BETA
   16 CONTINUE
CC     SPECIAL CASES NEAR THE INTERFACE LINE
      B(NXA1) = 1.D0
      A(NXA1) = -(2.D0+ALFL+DA*DXL2*GAMMA*CB(NXA1))
      C(NXA1) = 1.D0
      D(NXA1) = -ALFL*CRP(NXA1) -DXL2*DA*CAP(NXA1)*CBP(NXA1)/BETA
CC ------------------------------------------------
      B(NXA1+1) = 1.D0
      A(NXA1+1) = -(2.D0+ALFH+DA*DXH2*GAMMA*CB(NXA1+1))
      C(NXA1+1) = 1.D0
      D(NXA1+1) = -ALFH*CRP(NXA1+1)-DXH2*DA*CAP(NXA1+1)*CBP(NXA1+1)/BETA
CC --- UPPER PART ----------------------------------
```

```
      DO 35 I=2,NXB
      B(NXA1+I) = 1.D0
      A(NXA1+I) = -(2.D0+ALFB+DA*DXB2*GAMMA*CB(NXA1+I))
      C(NXA1+I) = 1.D0
      D(NXA1+I) = -ALFB*CRP(NXA1+I)-DA*DXB2*CAP(NXA1+I)*CBP(NXA1+I)/BETA
   35 CONTINUE
CC       B.C. AT X=1.D0
      B(NX) = 2.D0
      A(NX) = -(2.D0+ALFB+DA*DXB2*GAMMA*CB(NX))
      D(NX) = -ALFB*CRP(NX) -DXB2*DA*CAP(NX)*CBP(NX)/BETA
      CALL TRIDAG(1,NX,B,A,C,D,V)
      DO 36 I=1,NX
   36 CR(I) = V(I)
CC ---------------------------------------
CC   SOLVE FOR CB
CC ---------------------------------------
CC       B.C. AT X=0.D0
      A(1) = -(2.D0+ALFA+DA*DXA2*(CA(1)/BETA+CR(1)*GAMMA))
      C(1) = 2.D0
      D(1) = -ALFA*CBP(1)
CC ------ LOWER PART -----------------------------
      DO 45 I=2,NXA
      B(I) = 1.D0
      A(I) = -(2.D0+ALFA+DA*DXA2*(CA(I)/BETA+CR(I)*GAMMA))
      C(I) = 1.D0
      D(I) = -ALFA*CBP(I)
   45 CONTINUE
CC     SPECIAL CASES NEAR THE INTERFACE LINE
      B(NXA1) = 1.D0
      A(NXA1) = -(2.D0+ALFL+DA*DXL2*(CA(NXA1)/BETA+CR(NXA1)*GAMMA))
      C(NXA1) = 1.D0
      D(NXA1) = -ALFL*CBP(NXA1)
CC ------------------------------------------------
      B(NXA1+1) = 1.D0
      A(NXA1+1) = -(2.D0+ALFH+DA*DXH2*(CA(NXA1+1)/BETA
     *              +CR(NXA1+1)*GAMMA) )
      C(NXA1+1) = 1.D0
      D(NXA1+1) = -ALFH*CBP(NXA1+1)
CC --- UPPER PART ----------------------------------
      DO 46 I=2,NXB
      B(NXA1+I) = 1.D0
      A(NXA1+I) = -(2.D0+ALFB+DA*DXB2*(CA(NXA1+I)/BETA
     *             +CR(NXA1+I)*GAMMA) )
      C(NXA1+I) = 1.D0
      D(NXA1+I) = -ALFB*CBP(NXA1+I)
   46 CONTINUE
CC       B.C. AT X=1.D0
      B(NX) = 2.D0
      A(NX) = -(2.D0+ALFB+DA*DXB2*(CA(NX)/BETA+CR(NX)*GAMMA))
      D(NX) = -ALFB*CBP(NX)
      CALL TRIDAG(1,NX,B,A,C,D,V)
      DO 47 I=1,NX
   47 CB(I) = V(I)
CC ---------------------------------------------
```

```
CC    CHECK CONVERGENCE FOR THIS TIME STEP
CC ---------------------------------------------
      IF (NS.EQ.1) GO TO 9
      ERRL = 0.D0
      DO 11 I=1,NX
      ERR = DABS((CA(I)-CAOLD(I))/CA(I))
      IF(ERR.GT.ERRL) ERRL = ERR
   11 CONTINUE
  170 FORMAT(15X,'NS = ',I5,2X,'ERRL = ',D12.5)
      IF(ERRL.GT.TOR) GO TO 9
      GO TO 12
    9 DO 56 I=1,NX
      CAOLD(I) = CA(I)
   56 CONTINUE
    5 CONTINUE
CC ------------------------------------------------
CC    INTEGRATION TO FIND AVERAGE CONCENTRATIONS
CC ------------------------------------------------
   12 IF(NPRINT.NE.1) GO TO 1
      WRITE(6,160) LT
  160 FORMAT(/2X,'LT = ',I5)
      CALL ICSCCU(X,CA,NX,CC,200,IER)
      CALL DCSQDU(X,CA,NX,CC,200,0.D0,1.D0,Q,IER)
      Q1 = Q
      CAAVG = Q*CA0/CB0BAR
      CALL ICSCCU(X,CR,NX,CC,200,IER)
      CALL DCSQDU(X,CR,NX,CC,200,0.D0,1.D0,Q,IER)
      CRAVG = Q*CB0/CB0BAR
      CALL ICSCCU(X,CB,NX,CC,200,IER)
      CALL DCSQDU(X,CB,NX,CC,200,0.D0,1.D0,Q,IER)
      CBAVG = Q*CB0/CB0BAR
      FA = 1.D0-(QA+QB)/QA*Q1
      CSAVG = CA0BAR/CB0BAR -CAAVG-CRAVG
      RTIME = TIME*TSCALE
      Z     = U*RTIME
      WRITE(6,150) Z,RTIME,FA
  150 FORMAT(5X,'Z =',F9.4,2X,'REAL TIME =',D11.4,2X,'FA =',F8.5)
CC ------------------------------------------------
CC    OUTPUT RESULTS FOR THIS TIME STEP
CC ------------------------------------------------
      WRITE(6,140)CAAVG,CBAVG,CRAVG,CSAVG,NS,ERRL
  140 FORMAT(5X,'CA = ',D11.4,2X,'CB = ',D11.4,2X,'CR =',D11.4,
     *       2X,'CS =',D11.4,2X,'NS = ',I5,2X,'ERR=',D11.5)
      IF(CBAVG.LE.1.0D-6) GO TO 260
    1 CONTINUE
  260 STOP
      END
CC
CC
      SUBROUTINE TRIDAG (IF,L,B,A,C,D,V)
      IMPLICIT REAL*8(A-H,O-Z)
C
C  SUBROUTINE FOR SOLVING A SYSTEM OF LINEAR SIMULTANEOUS
C   EQUATIONS HAVING A TRIDIAGONAL COEFFICIENT MATRIX.
```

```
C   SUB-DIAGONAL, DIAGONAL, AND SUPER-DIAGONAL COEFFICIENTS
C   ARE STORED IN THE ARRAYS B,A, AND C.  THE COMPUTED
C   SOLUTION VECTOR V(IF).....V(L) IS STORED IN THE ARRAY V.
      DIMENSION BETA(201),GAMMA(201)
      DIMENSION  B(200),A(200),C(200),D(200),V(200)
C -------------------------------------------------------------
C
C       ..... COMPUTE INTERMEDIATE ARRAYS BETA AND GAMMA .....
      BETA(IF) = A(IF)
      GAMMA(IF)=D(IF)/BETA(IF)
      IFP1 = IF + 1
      DO 1 I= IFP1, L
      BETA(I)=A(I)- B(I)*C(I-1)/BETA(I-1)
    1 GAMMA(I) = (D(I) -B(I)*GAMMA(I-1))/BETA(I)
C
C       ..... COMPUTE FINAL SOLUTION VECTOR V .....
      V(L) =GAMMA(L)
      LAST =L-IF
      DO 2 K=1,LAST
      I = L-K
    2 V(I) = GAMMA(I) - C(I)*V(I+1)/BETA(I)
      RETURN
      END
```

APPENDIX A.2--Coalescence-Redispersion (CRD) Model

```
CC ------------------------------------ ----------------
CC   CRD MODEL FOR COMPETING REACTIONS
CC ---------------------------------------------------------------
      IMPLICIT REAL*8(A-H,O-Z)
      DIMENSION CA(505),CB(505),CR(505),CS(505)
      INTEGER IR(2)
CC ---------------------------------
CC  DEFINE SYSTEM PARAMETERS
CC ----------------------------
      TAUM=0.630D0
      QA   = 1.D0
      QB   = 1.D0
      CA0 = 0.200D-3
      CB0 = 0.2D-3
      RK1   = 7.3D6
      RK2   = 3.5D3
      VEL = 6.30
      CA0BAR = CA0*QA/(QA+QB)
      CB0BAR = CB0*QB/(QA+QB)
      BETA=CB0BAR/CA0BAR
      GAMMA = RK2/RK1
      GAMMA1 = 1.D0/(1.D0-GAMMA)
      WRITE(6,100) CA0,CB0,BETA,RK1,RK2,GAMMA
  100 FORMAT(2X,'CA0 = ',F9.5,2X,'CB0 = ',F9.5,2X,'BETA = ',F8.3,2X
     * ,'RK1 =',D11.4,2X,'RK2 = ',D11.4,2X,'GAMMA = ',D11.4/)
      WRITE(6,200) VEL
  200 FORMAT(2X,'VEL = ',F8.3/)
CC ---------------------------------
CC  DEFINE NUMERICAL PARAMETERS
CC ---------------------------------
      NED = 300
      NED2= 150
      NED21= NED2+1
      FREQ = NED/TAUM
      DTAU = 1.D0/FREQ
      INT  = 10
      DINT = DTAU/INT
      DINTH= DINT
      NT   = 1400
      WRITE(6,300) NED,FREQ,INT,NT
  300 FORMAT(2X,'# OF EDDIES = ',I5,2X,'FREQ = ',D11.4,2X,'INT ='
     *      ,I5,2X,'#OF TIME STEP = ',I5/)
CC ---------------------------------------
CC  DEFINE INITIAL CONDITIONS FOR EACH EDDY
CC ---------------------------------------
      DO 10 I=1,NED2
      CA(I) = CA0
      CB(I) = 0.D0
      CR(I) = 0.D0
      CS(I) = 0.D0
   10 CONTINUE
      DO 20 I=NED21,NED
      CA(I) = 0.D0
      CB(I) = CB0
```

```
      CR(I) = 0.D0
      CS(I) = 0.D0
   20 CONTINUE
CC ++++++++++++++++++++++++++++++++++++++++++++++++++++++++++++++
CC  START THE COALESENCE ,REDISPERSION AND REACTION PROCEDURE
CC ++++++++++++++++++++++++++++++++++++++++++++++++++++++++++++++
      TI = 0.D0
      DO 5 LT = 1,NT
      TI = TI+DTAU
      Z    = VEL*TI
CC ------------------------------------
CC  GENERATE RANDOM NUMBERS FROM 1 TO NED
CC ------------------------------------
    2 CALL TIME(ITI)
      DSEED = ITI*500.D0
      CALL GGUD(DSEED,NED,2,IR)
      N1 = IR(1)
      N2 = IR(2)
      IF(N1.EQ.N2) GO TO 2
  500 FORMAT(2I6)
CC ------------------------------------------------
CC  CONCENTRATION REDISTRIBUTION AFTER REDISPERSION
CC ------------------------------------------------
      CA(N1) = (CA(N1)+CA(N2)) / 2.D0
      CA(N2) = CA(N1)
      CB(N1) = (CB(N1)+CB(N2)) / 2.D0
      CB(N2) = CB(N1)
      CR(N1) = (CR(N1)+CR(N2)) / 2.D0
      CR(N2) = CR(N1)
      CS(N1) = (CS(N1)+CS(N2)) / 2.D0
      CS(N2) = CS(N1)
CC --------------------------------------
CC  BATCH REACTIONS IN THE EDDIES
CC --------------------------------------
      DO 3 I=1,NED
      CAOLD = CA(I)
      CBOLD = CB(I)
      CROLD = CR(I)
      CSOLD = CS(I)
      IF (CAOLD.EQ.0.D0.OR.CBOLD.EQ.0.D0) GO TO 3
      DO 4 J=1,INT
      DINT = DINTH
      IF(CA(I)-RK1*CA(I)*CB(I)*DINT.LE.0.D0) GO TO 101
      KK   = 1
      GO TO 103
  101 KK   = 10
      DINT = DINTH/FLOAT(KK)
  103 DO 50 JJ = 1,KK
      CAP= CA(I)
      CBP= CB(I)
      CRP= CR(I)
      CSP= CS(I)
      CA(I) = CAP -RK1*CAP*CBP*DINT
      CAR = CA(I)/CAP
```

```
      CR(I) = (GAMMA1*(CAR**GAMMA-CAR) +CRP/CAP*CAR**GAMMA)*CAP
      CS(I) = CAP+CRP+CSP -CA(I)-CR(I)
      CB(I) = CBP- (CR(I)-CRP) -2.D0*(CS(I)-CSP)
      CA(I) = (CA(I)+CAP) / 2.D0
      CB(I) = (CB(I)+CBP) / 2.D0
      CA(I) = CAP -RK1*CA(I)*CB(I)*DINT
      CAR = CA(I)/CAP
      CR(I) = (GAMMA1*(CAR**GAMMA-CAR) +CRP/CAP*CAR**GAMMA)*CAP
      CS(I) = CAOLD+CROLD+CSOLD -CA(I)-CR(I)
      CB(I) = CBOLD- (CR(I)-CROLD) -2.D0*(CS(I)-CSOLD)
   50 CONTINUE
    4 CONTINUE
    3 CONTINUE
      IF(LT/20*20.NE.LT) GO TO 55
CC ------------------------------------------------------------
CC  CALCULATE THE AVERAGE CONCENTRATIONS FOR ALL EDDIES
CC ------------------------------------------------------------
      CAAVG = 0.D0
      CBAVG = 0.D0
      CRAVG = 0.D0
      CSAVG = 0.D0
      DO 6 I=1,NED
      CAAVG = CAAVG+CA(I)
      CBAVG = CBAVG+CB(I)
      CRAVG = CRAVG+CR(I)
      CSAVG = CSAVG+CS(I)
    6 CONTINUE
      CAAVG = CAAVG /NED
      FA    = (CA0BAR-CAAVG) / CA0BAR
      CBAVG = CBAVG /NED /CB0BAR
      CRAVG = CRAVG /NED /CB0BAR
      CSAVG = CSAVG /NED /CB0BAR
      CAAVG = CAAVG / CA0
CC ---------------------------------------
      DELB = 1.D0-CBAVG-CRAVG-2.D0*CSAVG
      WRITE(6,400) Z,TI,FA
  400 FORMAT(/2X,'Z=',F9.4,2X,'REAL TIME= ',D11.4,2X,'FA =',F8.5)
      WRITE(6,600) CAAVG,CBAVG,CRAVG,CSAVG,DELA,DELB
  600 FORMAT(2X,'CA=',D11.4,2X,'CB=',D11.4,2X,'CR=',D11.4,2X,'CS=',
     * D11.4,2X,'DELA=',D11.4,2X,'DELB=',D11.4)
   55 CALL TIMREM(ITJ)
      IF(ITJ.GE.200)  GO TO 5
      WRITE(16,140) Z,TI
  140 FORMAT(2X,'Z = ',F9.4,2X,'REAL TIME=',D11.4)
      WRITE(16,145) (CA(I),I=1,NED)
      WRITE(16,145) (CB(I),I=1,NED)
      WRITE(16,145) (CR(I),I=1,NED)
      WRITE(16,145) (CS(I),I=1,NED)
  145 FORMAT(7D11.4)
    5 CONTINUE
      STOP
      END
```

APPENDIX A.3--Three-Environment (3E) Model

```
C-------------------------------------------------------------
C     THREE ENVIRONMENT MODEL FOR COMPETING REATIONS
C-------------------------------------------------------------
        IMPLICIT REAL*8 (A-H,O-Z)
        EXTERNAL DFUN
        DIMENSION  Y(8,4),YMAX(4),WK(84,1),ERROR(4) ,CEXIT(4)
        COMMON/COM 1/RST,Q1,Q2,PHI,CIN(4),DM1,DM2,TAU,VLCAP
        READ (5,10)  Q1,Q2,CA0,CB0,TEMP
        READ (5,20) TAUM
        READ (5,30) HMAX,H,HMIN,EPS,TSTOP
        READ (5,31) RK1,RK2
 31     FORMAT(4X,D9.2,5X,D9.2)
        U=7.60D0
        TAU=24.0D0*2.54D0/U
        HIN=H
        RST=TAU/TAUM
        PHI=Q2/Q1
        CB0BAR=CB0*Q2/(Q1+Q2)
        CA0BAR=CA0*Q1/(Q1+Q2)
        BETA=CB0BAR/CA0BAR
        WRITE(6,40)
        WRITE(6,50)
        WRITE(6,60) Q1,Q2,CA0BAR,CB0BAR,TEMP
        IF (BETA.GT.2.0) GO TO 200
        CA10=(1.0+Q2/Q1)/BETA
        CB20=(1.0+Q1/Q2)
        DLCA0B=1.0/BETA
        DLCB0B=1.0
        C0BAR=CB0BAR
        GO TO 210
 200    CA10=(1.0+Q2/Q1)
        CB20=BETA*(1.0+Q1/Q2)
        DLCA0B=1.0
        DLCB0B=BETA
        C0BAR=CA0BAR
 210    CONTINUE
        DM1= RK1*C0BAR*TAU
        DM2=RK2*DM1/RK1
        TRXN1=TAU/DM1
        TRXN2=1.0/RK2/CA0BAR
        Y(1,1)=CA10
        Y(1,2)=CB20
        Y(1,3)=0.0D0
        Y(1,4)=0.0D0
        CA=CA10*C0BAR
        CB=CB20*C0BAR
        WRITE(6,70) RST,BETA
        WRITE(6,75) TAU,TAUM,TRXN1,TRXN2
        WRITE(6,80) HMAX,H,HMIN,EPS
        WRITE(6,90) CA,CB
 10     FORMAT(4X,F6.1,6X,F6.1,6X,D9.2,8X,D9.2,5X,F6.2)
 20     FORMAT(7X,F9.3)
 30     FORMAT(4(5X,D10.3),6X,F7.3)
 40     FORMAT(1X,120('*')/)
```

```
50     FORMAT(40X,' SELECTIVITY IN PLUG FLOW REACTOR'/35X,
     1 'BOURNE-S KINETICS :  THREE ENVIRONMENT MODEL'/)
60     FORMAT(10X,'Q1=',F5.1,'  CC/S',5X,'Q2=',F6.2,  ' CC/S',5X,
     1  /10X,'CA0BAR= ',D10.3,'MOL/L', 5X,'CB0BAR=',D10.3,'MOL/L',
     2  ,5X,'TEMP (DEG C)=',F6.2/)
70     FORMAT(10X,'T/TAUM= ',D10.3,5X,'BETA= ',D10.3/)
75     FORMAT(15X,'TAU=',F7.3,' S',5X,'TAUM=',D10.3,' S',5X,
     * 'TRXN1=',D10.3,' S',5X,'TRXN2=',D10.3,' S'/)
80     FORMAT(10X,'HMAX=',D10.3,5X,'H=',D10.3,5X,'HMIN=',D10.3,
     1  5X,'EPS=',D10.3/)
90     FORMAT(15X,'CA= ',D9.2,' MOL/L',5X,'CB= ',D9.2,' MOL/L'/)
       WRITE(6,40)
       WRITE(6,130)
       WRITE(6,140)
       DO 100 I=1,4
       CIN(I)=Y(1,I)
       YMAX(I)=1.0D0
100    CONTINUE
       T=HIN/100.0D0
      N=4
      MTH=2
      MAXDER=6
      JSTART=0
      H=HIN
      TKEEP=0.100D-03
      TSTEP=0.002
      DIST=0.0D0
900    CALL DVOGER(DFUN,Y,T,N,MTH,MAXDER,JSTART,H,HMIN,HMAX,
     * EPS,YMAX,ERROR,WK,IER)
      IF(T.LT.TKEEP) GO TO 900
      TKEEP=TKEEP+TSTEP
      IF(TKEEP.GE.0.01) TSTEP=0.01
      IF(TKEEP.GE.0.1) TSTEP=0.1
      IF (RST*T.GT.150.) GO TO 250
      THRI=DEXP(-RST*T)
      GO TO 260
250    THRI=0.0
260    CONTINUE
      QS=Q1
      DO 110 L=1,4
      IF(L.EQ.2) QS=Q2
110    CEXIT(L)=(VLCAP*Y(1,L)+THRI*(QS*CIN(L)))/(Q1+Q2)
      DLCA=CEXIT(1)
      IF (BETA.LE.2.0D0) DLCA=DLCA*BETA
      DLCR=(1.0D0/(1.0D0-RK2/RK1))*((DLCA)**(RK2/RK1)-DLCA)
      IF (BETA.LE.2.0D0) DLCR=DLCR/BETA
      DLCA=CEXIT(1)
      DLCS=DLCA0B-DLCA-DLCR
      DLCB=DLCB0B-DLCR-2.0D0*DLCS
      CHECK1=(DLCA0B  )-CEXIT(1)-CEXIT(3)-CEXIT(4)
      CHECK2=DLCB0B-CEXIT(2)-CEXIT(3)-2.0D0*CEXIT(4)
      SELECT=2.0D0*CEXIT(4)/(CEXIT(3)+2.0*CEXIT(4))
      AT=T*TAU
      DIST=T*U* TAU
```

```
      WRITE(6,120)AT,DIST,(CEXIT(JK),JK=1,4),DLCB,DLCR,DLCS,SELECT
     * ,CHECK1,CHECK2
      IF (CEXIT(2).LT.0.1D-2) GO TO 160
      IF (T.LT.TSTOP) GO TO 900
C
C
 160  WRITE(6,120)AT,DIST,(CEXIT(JK),JK=1,4), DLCB,DLCR,DLCS,SELECT
     * ,CHECK1,CHECK2
      WRITE(6,40)
      SELECT=CEXIT(3)/CEXIT(4)
      CONVA= (DLCA0B-CEXIT(1))/DLCA0B
      CONVB= (DLCB0B-CEXIT(2))/DLCB0B
      WRITE(6,170) SELECT,CONVA,CONVB
      WRITE(6,40)
 120  FORMAT(2X,F6.3,8(4X,F6.3),3(2X,D9.2))
 130  FORMAT(32X,'SCALED CONCENTRATIONS',12X,'MAX. MIXED'/)
 140  FORMAT(3X,'TIME(S)',3X,'DIST.(CM)',2X, 'CA', 9X,'CB', 8X,
     * 'CR', 8X,'CS',7X,'CBM',7X,'CRM',7X,'CSM',7X,'SELECT',
     # 7X,'DEL1',6X,'DEL2')
 170  FORMAT(10X,'SELECTIVITY: CR/CS =',D10.3,10X,'CONVERSION  OF A
     * =',D10.3,10X,'CONVERSION OF B=',D10.3/)
      STOP
      END
      SUBROUTINE DFUN(YP,TP,M,DY,PW,IND)
      IMPLICIT REAL*8 (A-H,O-Z)
      DIMENSION  YP(8,4),PW(4,4),DY(4),RXN(4)
      COMMON/COM 1/RST,Q1,Q2,PHI,CIN(4),DM1,DM2,TAU,VLCAP
      IF (RST*TP.GT.75.) GO TO 5
      AXP =DEXP(-RST*TP)
      RAT=AXP/(1.0D0-AXP)
      GO TO 6
  5   AXP=0.0D0
      RAT=1.0D0
  6   CONTINUE
      VLCAP=(Q1+Q2)*(1.0D0-AXP)
C
      RATE1= DM1*YP(1,1)*YP(1,2)
      RATE2= DM2*YP(1,2)*YP(1,3)
C
      RXN(1)=-RATE1
      RXN(2)=-RATE2 -RATE1
      RXN(3)=RATE1-RATE2
      RXN(4)=RATE2
C
      DY(1)=RST*RAT*(CIN(1)*(1.0D0/(1.0D0+PHI))-YP(1,1))+RXN(1)
      DY(2)=RAT*RST*(CIN(2)*(PHI/(1.0D0+PHI))-YP(1,2))+RXN(2)
      DY(3)= -RAT*RST*YP(1,3)+RXN(3)
      DY(4)= -RAT*RST*YP(1,4)+ RXN(4)
      IF(TP.LE.6.0D-03) GO TO 60
      DO 50 I=1,4
      IF (YP(1,I).LE.1.0D-15) DY(I)=DY(I)/10.0D0
      IF (YP(1,I).LE.1.0D-16) DY(I)=DY(I)/100.0D0
 50   IF (YP(1,I).LE.1.0D-20) DY(I)=DY(I)/100.0D0
 60   RETURN
      END
```

APPENDIX A.4--Interaction by Exchange with Mean (IEM) Model

```
CC ------------------------------------------------------
C     IEM SIMULATION PROGRAM
CC ------------------------------------------------------
      IMPLICIT REAL*8(A-H,O-Z)
      EXTERNAL DFUN
      REAL*8 MTC
      DIMENSION WK(138),CMAX(6)
      COMMON/ CONC/ C(8,6)
      COMMON/CON2/ CAAVG,CBAVG,CRAVG,CSAVG
      COMMON/PARM/ MTC ,RK1,RK2
CC -- DEFINE SYSTEM PARAMETERS -------
      TAUM=2.00
      TEMP=27.3
      U       = 7.60
      RK1     = 7.3D+6
      RK2=1.11D09*DEXP(-3.957D03/(TEMP+273))
C     RK2=1.93D12*DEXP(-5.989D03/(TEMP+273))
      Q1=131.0
      Q2=1.31
      CA0 = 0.300D-03
      CB0 = 30.08D-03
      CA0BAR = CA0*Q1/(Q1+Q2)
      CB0BAR = CB0*Q2/(Q1+Q2)
      PHI=Q1/Q2
      SM      = PHI/(1.D0+PHI)
      GAMMA = RK1/RK2
      MTC=0.5D0/TAUM
      BETA  = CB0BAR/CA0BAR
      WRITE(6,222)
 222  FORMAT(1X,120('#')/)
      WRITE(6,223)
 223  FORMAT (20X, 'IEM SIMULATION')
      WRITE(6,500) CA0,CB0,BETA,RK1,RK2,GAMMA
 500 FORMAT(/2X,'CA0 = ',D11.4,2X,'CB0 = ',D11.4,2X,'BETA = ',D11.4,2X
     * ,'RK1 =',D11.4,2X,'RK2 = ',D11.4,2X,'GAMMA = ',D11.4/)
      WRITE (6,224) TAUM,Q1,Q2
 224  FORMAT(/2X,'TAUM= ',F7.3,3X,'Q1= ',F7.3,' CC/S',3X,'Q2= ',
     *F7.3,' CC/S'/)
      WRITE(6,222)
CC -- DEFINE NUMERICAL PARAMETERS -----
      T      = 0.D0
      N      = 6
      MTH    = 2
      MAXDER= 6
      JSTART= 0
      H      = 0.01D-3
      HMIN   = 1.0D-11
      HMAX   = 0.01D0
      EPS    = 1.0D-4
      TGOAL = 0.1
      IND    = 0
CC --- INITIAL CONDITIONS -------
      C(1,1)= CA0
      C(1,2)= 0.D0
```

```
      C(1,3)= 0.D0
      C(1,4)= 0.D0
      C(1,5)= CB0
      C(1,6)= 0.D0
CC
      DO 1 I=1,N
    1 CMAX(I) = 1.D0
CC
CC INTEGRATION BY GEAR PACKAGE
CC
      ICOUNT = 0
   20 ICOUNT = ICOUNT +1
    5 CALL DVOGER(DFUN,C,T,N,MTH,MAXDER,JSTART,H,HMIN,HMAX,EPS,CMAX,
     *              ERROR,WK,IER)
      IF(IER.GE.33.AND.IER.LE.36) GO TO 60
      CAAVG = SM*C(1,1) +(1.D0-SM)*C(1,4)
      CBAVG = SM*C(1,2) +(1.D0-SM)*C(1,5)
      CRAVG = SM*C(1,3) +(1.D0-SM)*C(1,6)
      IF(ICOUNT/50*50.EQ.ICOUNT) GO TO 10
      GO TO 20
   10 FA = 1.D0 -CAAVG/CA0BAR
      Z  = T*U
      CAAVG1 = CAAVG/CB0BAR
      CRAVG1 = CRAVG/CB0BAR
      CBAVG1 = CBAVG/CB0BAR
      CSAVG1 = CA0BAR/CB0BAR -CAAVG1-CRAVG1
      WRITE(6,100) Z,T
      WRITE(6,200) CAAVG1,CBAVG1,CRAVG1,CSAVG1
      TGOAL = TGOAL+1.0
      IF (CAAVG1.GT.1.0D-06)GO TO 59
      C(1,1)=0.0D0
      C(1,4)=0.0D0
 59   IF(CBAVG1.GT.0.1D-03) GO TO 20
      GO TO 30
   60 WRITE(6,300) IER
  300 FORMAT(5X,'IER = ',I5,'------ PROGRAM WAS TERMINATED'/)
  100 FORMAT(5X,'Z = ',F9.4,2X,'TIME=',D11.4)
  200 FORMAT(5X,'CA = ',D11.4,2X,'CB = ',D11.4,2X,'CR = ',D11.4,2X
     *       ,'CS = ',D11.4/)
   30 CONTINUE
      STOP
      END
CC
CC
      SUBROUTINE DFUN(CP,TP,N,DC,PW,IND)
      IMPLICIT REAL*8(A-H,O-Z)
      REAL*8 MTC
      DIMENSION CP(8,6),DC(6),PW(6,6)
      COMMON/ CONC/ C(8,6)
      COMMON/CON2/ CAAVG,CBAVG,CRAVG,CSAVG
      COMMON/PARM/ MTC ,RK1,RK2
C -------------------------------------------------------------
CC --- FIRST EDDY ------------
      DC(1) = MTC*(CAAVG-CP(1,1)) -RK1*CP(1,1)*CP(1,2)
```

```
      DC(2)=MTC*(CBAVG-CP(1,2))-RK1*CP(1,1)*CP(1,2) -RK2*CP(1,2)*CP(1,3)
      DC(3)=MTC*(CRAVG-CP(1,3))+RK1*CP(1,1)*CP(1,2) -RK2*CP(1,2)*CP(1,3)
CC --- SECOND EDDY  ------------
      DC(4)= MTC*(CAAVG-CP(1,4)) -RK1*CP(1,4)*CP(1,5)
      DC(5)=MTC*(CBAVG-CP(1,5))-RK1*CP(1,4)*CP(1,5) -RK2*CP(1,5)*CP(1,6)
      DC(6)=MTC*(CRAVG-CP(1,6))+RK1*CP(1,4)*CP(1,5) -RK2*CP(1,5)*CP(1,6)
      RETURN
      END
```

APPENDIX A.5--Four-Environment (4E) Model

```
C-------------------------------------------------------------
C       FOUR ENVIRONMENT MODEL
C-------------------------------------------------------------
        IMPLICIT REAL*8 (A-H,O-Z)
        EXTERNAL DFUN
        DIMENSION Y(8,8),YMAX(8),WK(200,1),ERROR(8),CEXIT(4)
        COMMON/COM1/ V1LCAP,V2LCAP,RST,Q1,Q2,DM1,DM2,CIN(8)
        READ (5,10) TEMP,CB0,CA0
        READ(5,20) TAUM
        READ(5,30) HMAX,H,HMIN,EPS,TSTOP
        READ(5,32) Q1,Q2
 32     FORMAT(4X,F9.2,5X,F9.2)
        RK1=7.30D06
        RK2=1.11D09*DEXP(-3.957D03/(TEMP+273))
C       RK2=1.93D12*DEXP(-5.989D03/(TEMP+273))
        U=7.60D0
        TAU=19.0D0*2.54D0/U
        RET=2.54D0*2.0D0*U/0.01D0
        HIN=H
        RST=TAU/TAUM
        PHI=Q2/(Q1+Q2)
        BETA= CB0*Q2/CA0/Q1
        CB0BAR=CB0*PHI
        CA0BAR=CA0*Q1/(Q1+Q2)
        WRITE(6,130)
        WRITE(6,55)
        WRITE(6,65) Q1,Q2,RET,CA0BAR,CB0BAR,TEMP
        IF (BETA.GT.2.0) GO TO 200
        CA10=(1.0+Q2/Q1)/BETA
        CB20=(1.0+Q1/Q2)
        DLCA0B=1.0/BETA
        DLCB0B=1.0
        C0BAR=CB0BAR
        GO TO 210
 200    CA10=(1.0+Q2/Q1)
        CB20=BETA*(1.0+Q1/Q2)
        DLCA0B=1.0
        DLCB0B=BETA
        C0BAR=CA0BAR
 210    CONTINUE
        DM1= RK1*C0BAR*TAU
        DM2=RK2*DM1/RK1
        TM=TAU/RST
        TRXN1=TAU/DM1
        TRXN2=1.0/RK2/CA0BAR
C
C       INITIAL CONCENTRATIONS
C
       DO 96 I=1,8
       Y(1,I)=0.0D0
 96    YMAX(I)=1.0D0
       Y(1,1)=CA10
       Y(1,6)=CB20
       DO 95 I=1,8
```

```
 95     CIN(I)=Y(1,I)
        CA=CA10*COBAR
        CB=CB20*COBAR
        WRITE (6,71) RK1,RK2
 71     FORMAT(5X,'K1= ',D9.2,' L/MOL/S', 5X,'K2= ',D9.2,' L/MOL/S')
        WRITE(6,70) TAUM,RST,BETA
        WRITE(6,75) TAU,TM,TRXN1,TRXN2
        WRITE(6,80) HMAX,H,HMIN,EPS
        WRITE(6,90) CA,CB
        WRITE(6,130)
        WRITE (6,135)
        WRITE(6,140)
C
C       DEFINE PARAMETERS FOR DVOGER
C
        T=HIN/100.0D0
        N=8
        MTH=2
        MAXDER=6
        JSTART=0
        H=HIN
        TKEEP=0.1D0
        TSTEP=0.002
        DIST=0.0D0
 100    CALL DVOGER(DFUN,Y,T,N,MTH,MAXDER,JSTART,H,HMIN,HMAX,
     * EPS,YMAX,ERROR,WK,IER)
        IF(T.LT.TKEEP) GO TO 100
        TKEEP=TKEEP+TSTEP
        IF(TKEEP.GE.0.1) TSTEP=0.1
        IF (RST*T.GT.150.) GO TO 250
        THRI=DEXP(-RST*T)
        GO TO 260
 250    THRI=0.0
 260    CONTINUE
        DO 110 L=1,4
 110    CEXIT(L)=(V1LCAP*Y(1,L)+V2LCAP*Y(1,L+4)+THRI*(Q1*
     * CIN(L)+Q2*CIN(L+4)))/(Q1+Q2)
        DLCA=CEXIT(1)
        IF (BETA.LE.2.0D0) DLCA=DLCA*BETA
        DLCR=(1.0D0/(1.0D0-RK2/RK1))*((DLCA)**(RK2/RK1)-DLCA)
        IF (BETA.LE.2.0D0) DLCR=DLCR/BETA
        DLCA=CEXIT(1)
        DLCS=DLCA0B-DLCA-DLCR
        DLCB=DLCB0B-DLCR-2.0D0*DLCS
        CHECK1=(DLCA0B  )-CEXIT(1)-CEXIT(3)-CEXIT(4)
        CHECK2=DLCB0B-CEXIT(2)-CEXIT(3)-2.0D0*CEXIT(4)
        SELECT=2.0D0*CEXIT(4)/(CEXIT(3)+2.0*CEXIT(4))
        AT=T*TAU
        DIST=T*U* TAU
        WRITE(6,120)AT,DIST,(CEXIT(JK),JK=1,4),DLCB,DLCR,DLCS,SELECT
     * ,CHECK1,CHECK2
        IF (CEXIT(2).LT.0.1D-3) GO TO 160
        GO TO 100
C
```

```
C
 160   WRITE(6,120)AT,DIST,(CEXIT(JK),JK=1,4), DLCB,DLCR,DLCS,SELECT
     * ,CHECK1,CHECK2
       WRITE(6,130)
       SELECT=CEXIT(3)/CEXIT(4)
       CONVA= (DLCA0B-CEXIT(1))/DLCA0B
       CONVB= (DLCB0B-CEXIT(2))/DLCB0B
       WRITE(6,170) SELECT,CONVA,CONVB
       WRITE(6,130)
C
C
 10     FORMAT(5X,F4.1,6X,D9.2,8X,D9.2)
 20     FORMAT(7X,F9.3)
 30     FORMAT(4(5X,D10.3),6X,F5.2)
 55     FORMAT(40X,' SELECTIVITY IN PLUG FLOW REACTOR'/35X,
     1 'BOURNE-S KINETICS :   FOUR ENVIRONMENT MODEL'/)
 65     FORMAT(10X,'Q1=',F5.1,'  CC/S',5X,'Q2=',F6.2, ' CC/S',5X,
     1  'RER=',F10.1,5X/10X,'WT.ED STREAM A=',D10.3,
     2  ' MOL/L',5X,'WT.ED STREAM B=',D10.3,' MOL/L',5X,
     3  'TEMP (DEG C)=',F6.2/)
 70     FORMAT(10X,'TAUM=',D10.3,5X,
     1  'RSTAU=',D10.3,5X,'FLOW WT.ED (CB/CA)=',D10.3/)
 75     FORMAT(15X,'TAU=',F7.3,' S',5X,'TM=',D10.3,' S',5X,
     *  'TRXN1=',D10.3,' S',5X,'TRXN2=',D10.3,' S'/)
 80     FORMAT(10X,'HMAX=',D10.3,5X,'H=',D10.3,5X,'HMIN=',D10.3,
     1  5X,'EPS=',D10.3/)
 90     FORMAT( 15X,'CA= ',D9.2, ' MOL/L',5X,'CB= ',D9.2,' MOL/L'/)
 120    FORMAT(2X,F6.3,4X,F7.2,7(4X,F6.3),3(2X,D9.2))
 130    FORMAT(1X,129('-')/)
 135    FORMAT(32X,'SCALED CONCENTRATIONS',12X,'MAX. MIXED'/)
 140    FORMAT(3X,'TIME(S)',3X,'DIST.(CM)',2X, 'CA', 9X,'CB', 8X,
     *  'CR', 8X,'CS',7X,'CBM',7X,'CRM',7X,'CSM',7X,'SELECT',
     #  7X,'DEL1',6X,'DEL2')
 170    FORMAT(10X,'SELECTIVITY: CR/CS =',D10.3,10X,'CONVERSION  OF A
     *  =',D10.3,10X,'CONVERSION OF B=',D10.3/)
       STOP
       END
C
C
       SUBROUTINE DFUN(VP,TP,M,DV,PW,IND)
       IMPLICIT REAL*8 (A-H,O-Z)
       DIMENSION  VP(8,8),PW(8,8),DV(8),RXN(8)
       COMMON/COM1/ V1LCAP,V2LCAP,RST,Q1,Q2,DM1,DM2,CIN(8)
       IF (RST*TP.GT.75.) GO TO 5
       PSI1=DEXP(-2.0*RST*TP)
       PSI2=DEXP(-RST*TP)
       GO TO 6
  5    PSI1=0.0
       PSI2=0.0
  6    CONTINUE
       V1LCAP=(Q1/2.0)*(1.0-(1.0-Q2/Q1)*PSI1+Q2/Q1*(1.0-2.0*
     * PSI2))
       V2LCAP=(Q2/2.0)*(1.0-(1.0-Q1/Q2)*PSI1+Q1/Q2*(1.0-2.0*
     * PSI2))
```

```
C
      RATE1= DM1*YP(1,1)*YP(1,2)
      RATE2= DM2*YP(1,2)*YP(1,3)
      RATE3= DM1*YP(1,5)*YP(1,6)
      RATE4= DM2*YP(1,6)*YP(1,7)
C
      RXN(1)=-RATE1
      RXN(2)=-RATE2 -RATE1
      RXN(3)=RATE1-RATE2
      RXN(4)=RATE2
      RXN(5)=-RATE3
      RXN(6)=-RATE4-RATE3
      RXN(7)=RATE3-RATE4
      RXN(8)= RATE4
C
C
      DO 10 K=1,4
 10   DY(K)=RST*((Q1/V1LCAP)*(CIN(K)-YP(1,K))*PSI2+(V2LCAP/
     * V1LCAP)*(YP(1,K+4)-YP(1,K)))+RXN(K)
      DO 20 K=5,8
 20   DY(K)=RST*((Q2/V2LCAP)*(CIN(K)-YP(1,K))*PSI2+(V1LCAP/
     * V2LCAP)*(YP(1,K-4)-YP(1,K)))+RXN(K)
       IF(TP.LE.6.0D-03) GO TO 60
       DO 50 I=1,8
       IF (YP(1,I).LE.1.0D-15) DY(I)=DY(I)/10.0D0
       IF (YP(1,I).LE.1.0D-16) DY(I)=DY(I)/100.0D0
 50    IF (YP(1,I).LE.1.0D-20) DY(I)=DY(I)/100.0D0
 60   RETURN
      END
```

APPENDIX B

SAMPLE CALCULATIONS FOR THE TURBULENCE MEASUREMENTS

The phasic output of the pulsed Doppler Ultrasound Velocimeter is sampled and processed by the microprocessor and mean and the root-mean-square (r.m.s.) value of the signal are displayed in mV on the microprocessor screen. These values are used in the equation below, which is based on Equation (8) in the text, to calculate the mean and r.m.s. velocities. Basically, it incorporates the conversion of the Doppler shift, Δf_d, by the zero-crossing frequency meter to an analog voltage:

$$u(\text{cm/s}) = \frac{(1 \text{ KHz}/0.25 \text{ volt}) \cdot (u_s \text{ cm/s}) \cdot V(\text{mV})}{(f_o \text{ KHz})\ (2 \cos\theta)\ (1000 \text{ mV/volt})} \qquad \text{(B.1)}$$

For the fully developed pipe flow experiments,

u_s = 153100 cm/s (value obtained from CRC handbook)

$\theta = 43°$

$f_o = 10^4$ KHz

Then,

$$u(\text{cm/s}) = 41.87 \times 10^{-3}\ \bar{V} \qquad \text{(B.2)}$$

can be used to calculate the mean velocities by substituting the mean output voltage (in mV) for $\bar{V}$. For example, at Re = 8029, the mean voltage $\bar{V}$ = 1315 mV and correspondingly, the experimental mean velocity, $\bar{u}_{exp}$ = 55.1 cm/s.

The calculation is a little different for the r.m.s. velocity. If the turbulence field is isotropic, the measured fluctuating velocity would be the same regardless of the angle at which the probe observes the flow. This requires that for the r.m.s. velocity computations, $\theta = 0$. Equivalently,

$$u_{rms} = 30.62 \times 10^{-3} V_{rms} \tag{B.3}$$

The above equation yields the r.m.s. velocity when V_{rms} is substituted in mV. Again, for Re = 8029 and $\bar{V}$ = 1315 mV, V_{rms} equals 96 mV. Then u_{rms} = 2.9 cm/s and the turbulence intensity, $u_{rms}/\bar{U}_{exp} \times 100$, is 5.34 percent.

APPENDIX C

ESTIMATION OF ERROR INTRODUCED BY APPROXIMATION IN ABSORBANCE MEASUREMENTS

The colorimeter circuit gives an analog output, $\overline{V^{\lambda}}$, which is proportional to $\ell n(\overline{I_o^{\lambda}/I^{\lambda}})$. I_o^{λ} is the constant internal reference intensity. According to Equation (14) (see Chapter IV), however, the time average should be taken only after a natural logarithm of the signal is taken, i.e., $\overline{\ell n(I_o^{\lambda}/I^{\lambda})}$. Since Equation (16) (i.e., $\overline{A^{\lambda}} \approx \ell n(\overline{I_o^{\lambda}/I^{\lambda}})$) has been used to analyze the experimental data, it is necessary to estimate the error introduced by such an approximation. If Equation (12) (cf. Chapter IV) is rewritten as

$$\frac{I_o^{\lambda}}{I^{\lambda}} = \exp(\varepsilon_R^{\lambda}\ell C_R + \varepsilon_S^{\lambda}\ell C_S) \tag{C.1}$$

and the concentrations as

$$C_R = \bar{C}_R + C_R' \tag{C.2}$$

and

$$C_S = \bar{C}_S + C_S' \tag{C.3}$$

(overbar denotes the time-mean value and prime denotes the fluctuating component), then the following equation is obtained:

$$\frac{I_o^{\lambda}}{I^{\lambda}} = \exp(\varepsilon_R^{\lambda}\ell\bar{C}_R + \varepsilon_S^{\lambda}\ell\bar{C}_S) \cdot \exp(\varepsilon_R^{\lambda}\ell C_R' + \varepsilon_S^{\lambda}\ell C_S') \tag{C.4}$$

Taking natural logarithm of two sides of the above equation, after they are time averaged, results in

$$\ell n(\overline{\frac{I_o^{\lambda}}{I^{\lambda}}}) = \varepsilon_R^{\lambda}\ell\bar{C}_R + \varepsilon_S^{\lambda}\ell\bar{C}_S + \ell n\overline{[\exp(\varepsilon_R^{\lambda}\ell C_R' + \varepsilon_S^{\lambda}\ell C_S')]} = \overline{A^{\lambda}} + \Delta. \tag{C.5}$$

$$\overline{A^{\lambda}} = \varepsilon_R^{\lambda}\ell\bar{C}_R + \varepsilon_S^{\lambda}\ell\bar{C}_S \qquad \text{(Equation (14))},$$

$$\Delta = \ell n[\overline{\exp(m_R C_R' + m_S C_S')}] \ , \tag{C.6}$$

and

$$m_R = \varepsilon_R^{\lambda}\ell \text{ and } m_S = \varepsilon_S^{\lambda}\ell \ . \tag{C.7}$$

A series expansion of the exponential term in Equation (C.6) leads to

$$\Delta = \ell n[1 + (m_R C_R' + m_S C_S') + (m_R C_R' + m_S C_S')^2/2$$

$$+ \text{higher order terms}]$$

$$\simeq \ell n[1 + \frac{m_R^2}{2}\overline{C_R'^2} + \frac{m_S^2}{2}\overline{C_S'^2} + m_R m_S \overline{C_R' C_S'}] \tag{C.8}$$

Estimates of r.m.s. concentration fluctuations are obtained from the work of Keeler (1964). Keeler's reactor assembly was similar to the one used in this study in terms of the injector, grids and the tubular reactor. He measured concentration fluctuation intensity for an inert tracer downstream of grid and found that for a mesh Reynolds number $Re_M = 800$ ($M = 0.64$ cm), the intensity decayed from about 10 percent at 5 cm to 4 percent at 50 cm. The intensities were based on the mean concentration, which was constant across the reactor. Based on these results,

$$C_R' \sim 0.15\ \bar{C}_R g(t) \tag{C.9}$$

and

$$C_S' \sim 0.15\ \bar{C}_S h(t) \qquad (C.10)$$

may be used as estimates of fluctuations where g(t) and h(t) are random functions of time which modulate the respective amplitudes of C_R' and C_S'. Also,

$$|g(t)| \leq 1$$

$$|h(t)| \leq 1$$

and

$$\overline{g(t)} = \overline{h(t)} = 0.$$

The largest possible value of each term in Equation (C.8) can now be estimated for the experimental concentration range, and the magnitude of Δ calculated.

For $\ell = 0.001$ m(gap of the fiber-optic probe),

$\varepsilon_R = 2438\ m^2/mol$ ($\lambda = 520$ nm)

$\varepsilon_S = 888\ m^2/mol$

and typical concentrations

$\bar{C}_R = \bar{C}_S = 0.07\ mol/m^3$,

Δ is 0.3 percent of $\overline{A^{\lambda}}$ given by Equation (14).

Similarly,

for $\varepsilon_R = 3216\ m^2/mol$ (Kozicki's value at $\lambda = 520$ nm)

$\varepsilon_S = 1998\ m^2/mol$

$\ell = 0.001$ m

and

$\bar{C}_R = \bar{C}_S = 0.15\ mol/m^3$

Δ is 0.8 percent of $\overline{A^{\lambda}}$.

Thus, it is reasonable to neglect Δ in Equation (C.5) and set

$$\ell n\left(\frac{\overline{I_o^{\lambda}}}{\overline{I_o}}\right) \approx \overline{A^{\lambda}} = \varepsilon_R^{\lambda} \ell \bar{C}_R + \varepsilon_S^{\lambda} \ell \bar{C}_S$$

as is done in Equation (16) of the main text.

APPENDIX D

MEASUREMENT OF ONE-DIMENSIONAL TURBULENCE SPECTRUM BY PULSED ULTRASOUND

The microprocessor (DATA 6000) provides the one-sided spectral-density of the PUDV signal (G(f)) as a function of frequency (f). The units of G(f) are mV^2/Hz and that of frequency are Hz. The spectral data needs to be normalized for comparison with the data of Garbini et al. (1982). These researchers have compared their ultrasonic data with their own hot-film anemometer data. The following normalization (Equation (3.11) of the above reference) was used for their spectral data, which are plotted in Figure 15:

$$\frac{E_\theta(k)}{u^2_{rms_D}} = \frac{S_D(\omega)\bar{U}}{\pi k_D^2 u^2_{rms_D}} \tag{D.1}$$

where $\bar{U}$ is the local mean velocity, k_D is the magnitude of the ultrasonic wave vector ($k_D = 4\pi f_o/u_s$), u^2_{rms} is the mean-square value of the velocity fluctuations, D is the pipe diameter, $S_D(\omega)$ is the two-sided spectral-density of the detected velocity signal, with units of $(rad/s)^2/(rad/s)$, and $E_\theta(k)$ is the one-dimensional turbulence spectrum.

By definition (refer to Equations (2.3)-(2.4) of the reference), the one- and two-sided spectral densities are related by

$$S_D(\omega) = \frac{G(\omega)}{2} \tag{D.2}$$

The conversion of G(f) to G(ω) is obtained as follows. The zero-crossing meter of the PUDV gives 0.25 volt as output voltage for every Doppler shift of 1 kHz. Also,

$$\omega(rad/s) = 2\pi(rad)\ f(Hz) \tag{D.3}$$

Therefore,

$$G(\omega)\ \frac{(\text{rad/s})^2}{(\text{rad/s})} = G(f)\left(\frac{\text{mV}^2}{\text{Hz}}\right) \times \left(\frac{1\ \text{kHz}}{0.25\ \text{volt}} \times \frac{10^3\ \text{Hz/kHz}}{10^3\ \text{mV/volt}}\right)^2$$

$$\times\ 2\pi\left(\frac{\text{rad/s}}{\text{Hz}}\right) = 32\ \pi G(f) \qquad \text{(D.4)}$$

Substituting Equation (D.4) into Equation (D.2), the following is obtained:

$$S_D(\omega) = 16\pi\ G(f) \qquad \text{(D.5)}$$

Equation (D.5) can now be used in conjunction with Equation (D.1) to get normalized spectral density data. Note that the abscissa of Figure 15 is the normalized wave number, which is related to frequency by

$$KD = \frac{2\pi f D}{\bar{U}} \qquad \text{(D.6)}$$

For the fully developed pipe flow in this study:

D = 1.82 cm (pipe diameter), f_o = 10 MHz (carrier frequency of the PUDV), and u_s = 153100 cm/s (velocity of sound in water at 11°C).

The spectral data displayed in Figure 15 (circles) correspond to the numbers listed in Table D.1, and the associated $\bar{V}$ = 1081 mV and V_{rms} = 72 mV.

Table D.1

Centerline Spectral Density at Re = 5900

f (Hz)	G(f) $((mV)^2/Hz)$	KD	$\frac{S_D(\omega)\bar{U}}{\pi K_D^2 u_{rms}^2 D}$
13	664	3	0.081
21	510	5	0.062
30	472	8	0.057
40	320	10	0.039
51	255	13	0.031
61	178	15	0.022
70	133	18	0.016
80	96	20	0.012
91	84	23	0.010
101	55	26	0.007
110	38	28	0.005
120	22	30	0.003

APPENDIX E

EXPERIMENTAL DATA: FLUID MECHANICS

Case 1: Honeycomb Turbulence

Range = 0.3487 volt (1.12 cm) Temperature = 25-26°C

$\bar{U}$ (or u_{rms}) = 29.93×10^{-3} $\bar{V}$ (or V_{rms})

Distance[+] x' (cm)	PUDV Output $\bar{V}$(mV)	PUDV Output V_{rms}(mV)	$\bar{U}^{*}$ (cm/s)	u_{rms}^{*} cm/s
1.9	30	27	0.90	0.81
	43	26	1.29	0.78
4.4	36	23	1.08	0.69
	31	26	0.93	0.78
7.0	44	23	1.32	0.69
	39	23	1.17	0.69
9.5	64	20	1.92	0.60
	58	22	1.74	0.66
12.1	92	21	2.75	0.63
	93	21	2.78	0.63
14.6	142	25	4.25	0.75
	143	24	4.28	0.72
17.1	198	26	5.93	0.78
	197	25	5.90	0.75
19.7	220	26	6.58	0.78
	222	25	6.54	0.75
22.2	228	26	6.82	0.78
	229	24	6.85	0.72
24.8	233	24	6.97	0.72
	233	23	6.97	0.69
27.3	236	21	7.06	0.63
	235	22	7.03	0.66
29.8	240	21	7.18	0.63
	237	22	7.09	0.66
32.4	243	24	7.27	0.72
	243	24	7.27	0.72
34.9	249	23	7.45	0.69
	247	23	7.39	0.69
37.5	248	23	7.42	0.69
	248	24	7.42	0.72
Rise velocity of bubbles under no flow conditions	8	17	0.24	0.51
	8	17	0.24	0.51

[+] Downstream distance from the honeycomb.

[*] Not corrected for noise; corrected value = $\bar{V} - (\bar{V})_{\text{rise velocity}}$ or $V_{rms} - (V_{rms})_{\text{rise velocity}}$.

Case 2: (Honeycomb + Injector) Turbulence

Range = 0.3487 volt (1.12 cm) Temperature = 25-26°C

$\bar{U}$ (or u_{rms}) = 29.93×10^{-3} $\bar{V}$ (or V_{rms})

Distance[+] x (cm)	PUDV Output $\bar{V}$(mV)	PUDV Output V_{rms}(mV)	$\bar{U}^{*}$ (cm/s)	u_{rms}^{*} cm/s
0.6	222	39	6.64	1.17
	227	39	6.79	1.17
1.3	227	38	6.79	1.14
	228	35	6.82	1.05
1.9	236	34	7.06	1.02
	233	41	6.97	1.23
3.2	231	30	6.91	0.90
	237	30	7.09	0.90
4.4	229	27	6.85	0.81
	227	28	6.79	0.84
7.0	237	27	7.09	0.81
	240	26	7.18	0.78
9.5	249	25	7.45	0.75
	242	25	7.24	0.75
12.1	253	25	7.57	0.75
	251	23	7.51	0.69
14.6	252	25	7.54	0.75
	248	25	7.42	0.75
17.1	257	24	7.69	0.72
	255	23	7.63	0.69
19.7	258	26	7.72	0.78
	254	25	7.60	0.75
Rise velocity of bubbles under no flow conditions	9	17	0.27	0.51
	10	17	0.30	0.51

[+]Axial distance downstream of the injector needle tips.

[*]Not corrected for noise.

Case 3: (Honeycomb + Injector + Screen (M_1)) Turbulence

Range = 0.3481 volts (1.12 cm) Temperature = 25-26°C

$\bar{U}$ (or u_{rms}) = 29.93×10^{-3} $\bar{V}$ (or V_{rms})

Distance+ x (cm)	PUDV Output $\bar{V}$(mV)	PUDV Output V_{rms}(mV)	$\bar{U}$* (cm/s)	u_{rms}* cm/s
0.6	236	53	7.00	1.59
	239	52	7.15	1.56
1.9	226	35	6.76	1.05
	247	33	7.39	0.99
3.2	225	29	6.73	0.87
	229	29	6.85	0.87
4.4	234	25	7.00	0.75
	233	27	6.97	0.81
5.7	227	29	6.79	0.87
	235	25	7.03	0.75
8.3	243	22	7.27	0.66
	245	22	7.33	0.66
10.8	245	24	7.33	0.72
	243	22	7.27	0.66
13.3	248	23	7.42	0.69
	251	22	7.51	0.66
15.9	248	27	7.42	0.81
	253	26	7.57	0.78
18.4	251	26	7.51	0.78
	257	24	7.69	0.72
Rise velocity of bubbles under no flow conditions	9	16	0.27	0.48
	11	18	0.33	0.54

+Axial distance downstream of the injector needle tips.

*Not corrected for noise.

Case 4a: (Honeycomb + Injector + Screen (M_1))
(Screen upstream of the injector)

Range = 0.3479 volts (1.12 cm) Temperature = 25-26°C
$\bar{U}$ (or u_{rms}) = 29.93×10^{-3} $\bar{V}$ (or V_{rms})

Distance+ x (cm)	PUDV Output $\bar{V}$(mV)	PUDV Output V_{rms}(mV)	$\bar{U}$* (cm/s)	u_{rms}* cm/s
0.6	239	43	7.15	1.29
	242	34	7.24	1.02
1.9	229	31	6.85	0.93
	238	33	7.12	0.99
3.2	241	28	7.21	0.84
	241	24	7.21	0.72
4.4	254	24	7.60	0.72
	255	28	7.63	0.84
5.7	245	25	7.33	0.75
	253	23	7.57	0.69
8.3	248	22	7.27	0.66
	242	24	7.24	0.72
10.8	247	22	7.39	0.66
	249	22	7.45	0.66
13.3	250	21	7.48	0.63
	245	24	7.33	0.72
15.9	255	21	7.63	0.63
	255	22	7.63	0.66
18.4	253	25	7.57	0.75
	259	23	7.75	0.69
Rise velocity of bubbles under no flow conditions	6	14	0.18	0.42
	7	15	0.21	0.45

+Axial distance downstream of the injector needle tips.

*Not corrected for noise.

Case 4b: (Honeycomb + Injector + Screen (M_1)) Turbulence
(Screen upstream of the injector)

Range = 0.4750 volts (1.52 cm) Temperature = 11°C
$\bar{U}$ (or u_{rms}) = 30.56 $\bar{V}$ (or V_{rms}) cm/s

Distance+ x (cm)	$\bar{V}$(mV)	V_{rms}(mV)	$\bar{U}$* (cm/s)	u_{rms}* (cm/s)
13.6	235	25	7.18	0.76
	233	23	7.12	0.70
	233	25	7.12	0.76
18.6	237	25	7.24	0.76
	242	26	7.40	0.79
	237	30	7.24	0.92
23.7	245	27	7.49	0.83
	245	26	7.49	0.79
	244	25	7.46	0.76
28.8	256	25	7.82	0.76
	252	27	7.70	0.83
	254	28	7.76	0.86
33.9	257	26	7.85	0.79
	256	27	7.82	0.83
	262	25	8.01	0.76
39.0	262	26	8.01	0.79
	263	26	8.04	0.79
	266	26	8.13	0.79
44.0	264	31	8.07	0.95
	268	27	8.19	0.83
	267	26	8.16	0.79

x = 39.0 cm

Radial Distance γ (cm)				
0.75	266	27	8.12	0.83
	259	28	7.92	0.86
	261	25	7.98	0.76
1.5	258	28	7.88	0.86
	263	28	8.04	0.86
	256	28	7.82	0.86

+Axial distance downstream of the injector needle tips.

*Not corrected for noise.

APPENDIX F

CALIBRATION OF 1-NAPHTHOL FEEDSTREAM (A)

1-Naphthol is a primary standard and can be directly used to prepare a standard solution of it. As shown in Figure F.1, it has a characteristic peak in its absorption spectrum at λ = 245 nm (Na_2CO_3/$NaHCO_3$ buffer, pH = 10.00 ± 0.002, T = 298 K, I = 40 g ion/m^3). A typical calibration data-set is listed below.

Calibration of 1-Naphthol Solution
(C_{AO} = 0.1998 mol/m^3)

V_1 (μℓ)	V_2 (μℓ)	$\bar{C}_A$ (mol/m^3)	Absorbance at 245 nm A
1600	100	0.0118	0.265
1600	100	0.0118	0.278
1600	200	0.0222	0.525
1600	200	0.0222	0.506
1600	300	0.0316	0.726
1600	300	0.0316	0.721
1600	400	0.0400	0.916
1600	400	0.0400	0.936

V_1 = Volume of the buffer.

V_2 = Volume of the standard solution.

C_{AO} = Concentration of the standard solution.

$\bar{C}_A = (C_{AO}V_2/(V_1+V_2)$.

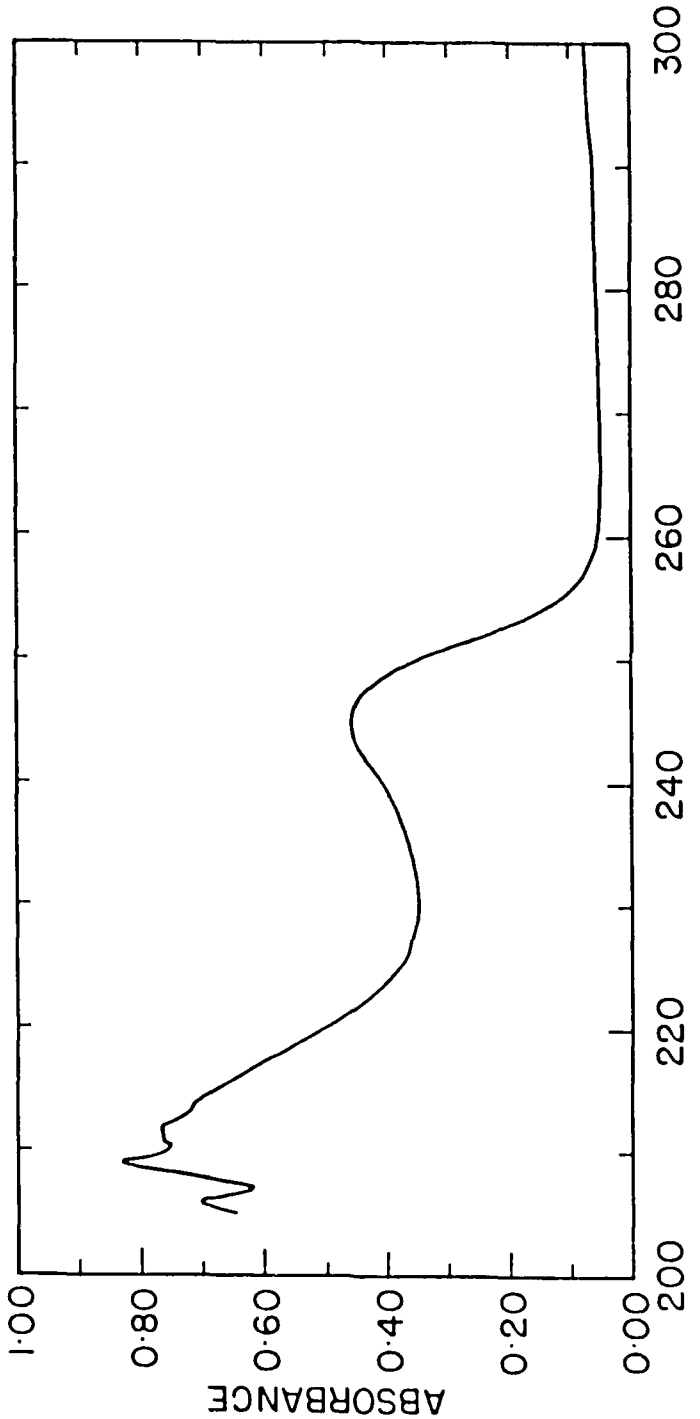

Figure F.1 UV-absorption spectrum of 1-naphthol solution
(T = 298 K, pH = 10.00, I = 40 g ion/m^3)

A linear regression results in the following equation:

$$A = 23.0918\ \bar{C}_A + 0.0009 \qquad (F.1)$$

This equation is then used to determine the concentration of a sample taken from the feed tank A for a mixing-reaction run. Typically, the absorbance of such samples, at 16:1 dilution with the buffer, was found in the range 0.40-0.42, which corresponded to C_{A0} = 0.294 - 0.309 mol/m^3.

APPENDIX G

EXPERIMENTAL DATA: MIXING-REACTION STUDIES

Experiment No. 8 | Colorimeter Output $\overline{V^{\lambda}}$ (mV) | Date: March 3, 1985

x (cm)	λ(nm) 450	470	490	520	545	$\bar{C}_R^+$ (mol/m^3)	$\bar{C}_S^+$ (mol/m^3)
Reference	943	770	819	386			
3.7	967	807*	865*	445	220	0.037	0.004
8.8	999	837	906	478*	267	0.054	0.025
14.0	1015	864	924	491	283	0.048	0.054
19.0	1027	875	942	526	293	0.070	0.047
24.0	1038	887	953*	534	319	0.077	0.054
29.0	1046	897	966	547*	319	0.077	0.065
Reference	942	774	823		178		
Exit 1	1111	982	1012	770	444		
Reference	937	775	755	476	174		
Exit 2	1122	1005	1042	815	476	0.175	0.070
Reference	931	774	758	487	172		
Exit 3	1103	985	1017	786	449		
Reference	928	774	757	488	171		
k_R^{λ} (mV/mol/m^3)	654	836	1119	1369	1224		
k_S^{λ} (mV/mol/m^3)	857	903	916	819	800		

*Injector clogged, hence purged with high flow of B.

+Obtained by regression with MINITAB.

Experiment No. 9

Colorimeter Output $\overline{V^{\lambda}}$ (mV)

Date: March 9, 1985

x (cm)	λ(nm) 450	470	490	520	545	$\bar{C}_R^+$ (mol/m^3)	$\bar{C}_S^+$ (mol/m^3)
Reference	934	769	749	485	177		
3.7	970	814	791	527*	232*	0.005	0.038
8.8	997	842	835*	570	260	0.035	0.046
14.0	1004	850*	846	586	278	0.053	0.038
19.0	1021	870	867	615	298	0.064	0.050
24.0	1029	886	876	629	311	0.069	0.058
29.0	1034	893	895	631	297	0.083	0.054
Reference	941	773	755	494	177		
Exit 1	1104	975	997	774	438		
Reference	943	779	753	498	179		
Exit 2	1100	972	991	772	433	0.165	0.058
Reference	943	777	754	497	180		
Exit 3	1095	963	979	759	422		
Reference	942	779	754	496	180		
k_R^{λ} (mV/mol/m^3)	654	836	1119	1369	1224		
k_S^{λ} (mV/mol/m^3)	857	903	916	819	800		

*Injector clogged, hence purged with high flow of B.

+Obtained by regression with MINITAB.

Experiment No. 11

Colorimeter Output $\overline{V^{\lambda}}$ (mV)

Date: March 31, 1985

x (cm)	λ(nm) 490	520	545	450	470	$\bar{C}_R^+$ (mol/m^3)	$\bar{C}_S^+$ (mol/m^3)
Reference	937	563	395	1025	856		
3.7	984	635	443	1055		0.032	0.008
8.8	1021	644*	480	1080*		0.055	0.020
14.0	1045	684	511	1096		0.075	0.023
19.0	1064	702	526*	1114	959	0.075	0.044
24.0	1069	722	531	1123*	968*	0.070	0.057
29.0	1080	735	544	1128	976	0.083	0.054
Reference	946						
Exit 1	1234	890	682	1213	1080		
Reference	959	580	402	1038	861		
Exit 2	1227	883	678	1208	1071	0.194	0.061
Reference	953	580	402	1037	862		
Exit 3	1243	906	696	1221	1089		
Reference	958	577	401	1039	862		
k_R^{λ} (mV/mol/m^3)	1119	1369	1224	654	836		
k_S^{λ} (mV/mol/m^3)	916	819	800	857	903		

*Injector clogged, hence purged with high flow of B.

+Obtained by regression with MINITAB.

Experiment No. 12

Colorimeter Output $\overline{V^{\lambda}}$ (mV)

Date: April 2, 1985

x (cm)	λ(nm) 490	520	545	450	470	$\bar{C}_R^+$	$\bar{C}_S^+$
						(mol/m^3)	
Reference	1121	982	463	1033	1039		
14.6	1264	1143*	606*	1124*	1120*	0.090	0.039
19.7	1274	1154	613	1134	1134	0.094	0.046
24.8	1284	1161	624	1144	1149	0.093	0.058
29.9	1286	1162	638	1141	1136*	0.106	0.045
34.9	1295	1176	652	1149	1146	0.115	0.046
40.0	1296	1174	647	1151*		0.108	0.055
Reference	1130	988	470	1035			
Exit 1	1207	969	747	1216	1074		
Reference	934	666	468	1035	855	0.179	0.077
Exit 2	1207	973	753	1222	1074		
Reference	933	664	471	1038	857		
k_R (mV/mol/m^3)	1119	1369	1224	654	836		
k_S (mV/mol/m^3)	916	819	800	857	903		

*Injector clogged, hence purged with high flow of B.

+Obtained by regression with MINITAB.

Experiment No. 13 | Colorimeter Output $\overline{V^{\lambda}}$ (mV) | Date: April 3, 1985

x (cm)	λ(nm) 490	520	545	450	470	$\bar{C}_R^+$ (mol/m^3)	$\bar{C}_S^+$ (mol/m^3)
Reference	781	425	230	992	981		
14.6	913	576*	382*	1085*	1083	0.089	0.038
19.7	926	598	386	1101	1099*	0.090	0.053
24.8	943	613	403*	1108	1105	0.102	0.054
29.9	946	621	411	1116*	1119	0.104	0.060
34.9	949	620	422*	1120	1133	0.103	0.065
40.0	951	631*	438	1122*		0.108	0.068
Reference	787	430	241	994			
Exit 1	1154	742	524	1176	1041		
Reference	883	435	240	992	823	0.180	0.075
Exit 2	1151	738	521	1170	1039		
Reference	879	436	240	995	821		
k_R^{λ} (mV/mol/m^3)	1119	1369	1224	654	836		
k_S^{λ} (mV/mol/m^3)	916	819	800	857	903		

*Injector clogged, hence purged with high flow of B.

+Obtained by regression with MINITAB.

Experiment No. 16

Colorimeter Output $\overline{V^{\lambda}}$ (mV)

Date: April 16, 1985

x (cm)	λ(nm) 490	520	545	450	470	$\bar{C}_R^+$ (mol/m^3)	$\bar{C}_S^+$ (mol/m^3)
Reference		476	283	1009	835		
14.6	1042	639	449	1114	969	0.088	0.061
19.7	1043	685	464	1128	978	0.102	0.062
24.8	1046	685	473	1139	983	0.115	0.062
29.9	1080	701	484	1147	1002	0.120	0.072
34.9	1083	697	498	1151		0.119	0.078
40.0	1076	710	516	1160		0.129	0.079
Reference	879	483	284	1011	840		
Exit 1	1179	859	647	1243	1116		
Reference	835	481	285	1011	840		
Exit 2	1179	865	645	1242	1120	0.216	0.107
Reference	842	481	312	1011	838		
Exit 3	1182	868	629	1243	1121		
Reference	844	479	329	1012	838		
k_R^{λ} (mV/mol/m^3)	1119	1369	1224	654	836		
k_S^{λ} (mV/mol/m^3)	916	819	800	857	903		

$^+$Obtained by regression with MINITAB.

Experiment No. 19

Colorimeter Output $\overline{V^{\lambda}}$ (mV)

Date: April 23, 1985

x (cm)	λ(nm) 490	520	545	450	470	$\bar{C}_R^+$ (mol/m^3)	$\bar{C}_S^+$ (mol/m^3)
Reference		376	215	983	815		
14.6	1025	569	377	1083	928	0.094	0.090
19.7	1039	564	399	1101	945	0.100	0.105
24.8	1044	580	418	1113	962	0.115	0.103
29.9	1055	600	423	1130	974	0.119	0.120
34.9	1075	606	429	1133	986	0.115	0.135
40.0	1072	614	452	1141	997	0.114	0.149
Reference	870	387	225	993	815		
Exit 1	1287	843	642	1270	1154		
Reference	876	391	221	990	822		
Exit 2	1266	828	631	1256	1138	0.231	0.222
Reference	875	398	222	991	821		
Exit 3	1257	817	619	1249	1131		
Reference	872	395	221	991	816		
k_R^{λ} (mV/mol/m^3)	1088	1322	1166	612	790		
k_S^{λ} (mV/mol/m^3)	605	547	543	546	602		

+Obtained by regression with MINITAB.

Experiment No. 20

Colorimeter Output $\overline{V^{\lambda}}$ (mV)

Date: April 26, 1985

x (cm)	λ(nm) 490	520	545	450	470	$\bar{C}_R^+$ (mol/m^3)	$\bar{C}_S^+$ (mol/m^3)
Reference	804	787	301	994	815		
14.6	981	969	463	1107	945	0.099	0.093
19.7	994	980	480	1121	966	0.095	0.127
24.8	1012	999	511	1126	986	0.108	0.133
29.9	1016	1014	511	1133	979	0.129	0.106
34.9	1017	1020	511	1145	999	0.106	0.158
40.0	1035	1029	526	1150	1000	0.121	0.150
Reference	816	791	309	996			
Exit 1	1302	972	695	1270	1150		
Reference	902	520	275	1002	819	0.260	0.200
Exit 2	1302	970	691	1270	1143		
Reference	904	519	273	999	820		
k_R^{λ} (mV/mol/m^3)	1088	1322	1166	612	790		
k_S^{λ} (mV/mol/m^3)	605	547	543	546	602		

+Obtained by regression with MINITAB.

Experiment No. 22 | Colorimeter Output $\overline{V^{\lambda}}$ (mV) | Date: May 4, 1985

x (cm)	λ(nm) 490	520	545	450	470	$\bar{C}_R^+$ (mol/m^3)	$\bar{C}_S^+$ (mol/m^3)
Reference	919	560	306	1042	870		
5.1	1006	663	399	1087	935	0.087	0.000
10.2	1038	688	437	1117	973	0.0773	0.041
15.6	1079	725	464	1144	994	0.093	0.061
20.7	1093	746	484	1163	1007	0.099	0.077
25.8	1110	770	503	1167	1022	0.123	0.064
30.9	1128	770	518	1183	1035	0.102	0.113
Reference	929	559	311	1044	884		
Exit 1	1357	1001	715	1305	1168		
Reference	966	569	317	1054	866		
Exit 2	1350	1002	717	1294	1170		
Reference	965	567	316	1049	869	0.257	0.125
Exit 3	1347	997	712	1289	1167		
Reference	965	567	317	1040	864		
k_R^{λ} (mV/mol/m^3)	1112	1360	1193	650	830		
k_S^{λ} (mV/mol/m^3)	744	716	704	657	723		

+Obtained by regression with MINITAB.

Experiment No. 23

Colorimeter Output $\overline{V^{\lambda}}$ (mV)

Date: May 6, 1985

x (cm)	λ(nm) 490	520	545	450	470	$\bar{C}_R^+$	$\bar{C}_S^+$ (mol/m^3)
Reference	892	602	367	1036	859		
5.1	975	682	464	1095	928	0.033	0.053
10.2	1037	749	520	1131	975	0.080	0.064
15.6	1070	802	567	1167	1007	0.106	0.082
20.7	1104	841	590	1179	1038	0.130	0.087
25.8	1132	860	616	1194	1074	0.123	0.134
30.9	1171	887	651	1219	1094	0.135	0.152
Reference	893	604	380	1044	870		
Exit 1	1318	1096	815	1324	1205		
Reference	897	617	379	1044	867		
Exit 2	1337	1113	834	1335	1217		
Reference	897	617	379	1042	867	0.277	0.166
Exit 3	1339	1120	840	1339	1222		
Reference	899	620	377	1041	869		
k_R^{λ} (mV/mol/m^3)	1112	1360	1193	650	830		
k_S^{λ} (mV/mol/m^3)	744	716	704	657	723		

$^+$Obtained by regression with MINITAB.

Experiment No. 25

Colorimeter Output $\overline{V^{\lambda}}$ (mV)

Date: May 9, 1985

x (cm)	λ(nm) 490	520	545	450	470	$\bar{C}_R^+$ (mol/m^3)	$\bar{C}_S^+$ (mol/m^3)
Reference	897	464	252	1019	848		
4.1	1083	678	453	1142	997	0.129	0.066
9.2	1122	697	469	1155	1007	0.140	0.059
14.3	1126	720	495	1184	1036	0.129	0.115
16.8	1142	721	507	1176	1041	0.127	0.112
19.3	1151	730	506	1184	1044	0.131	0.115
24.5	1156	741	511	1189	1060	0.139	0.122
Reference	894	474	255	1024	858		
Exit 1	1252	869	625	1241	1131		
Reference	875	444	232	994	823		
Exit 2	1251	867	627	1242	1127		
Reference	877	442	232	991	825	0.239	0.147
Exit 3	1255	867	627	1243	1130		
Reference	876	444	231	995	825		
k_R^{λ} (mV/mol/m^3)	1112	1360	1193	650	830		
k_S^{λ} (mV/mol/m^3)	744	716	704	657	723		

$^+$Obtained by regression with MINITAB.

Experiment No. 26

Colorimeter Output $\overline{V^{\lambda}}$ (mV)

Date: May 13, 1985

x (cm)	λ(nm) 490	520	545	450	470	$\bar{C}_R^+$ (mol/m^3)	$\bar{C}_S^+$ (mol/m^3)
Reference	823	412	238	990	827		
4.1	1007*	626	433	1112	955	0.127	0.053
9.2	1025	646	451	1135	987	0.124	0.083
14.3	1052	671	464	1149	994	0.128	0.108
16.8	1058	684**	496	1149	996	0.151	0.084
19.3	1074	682	483	1152	1016	0.146	0.094
24.5	1078	687	487	1163	1015	0.143	0.105
Reference	832	424	242	999	829		
Exit 1	1247	803	602	1217	1101		
Reference	902	417	239	987	822		
Exit 2	1255	812	609	1223	1105	0.218	0.143
Reference	897	414	241	987	820		
k_R^{λ} (mV/mol/m^3)	1112	1360	1193	650	830		
k_S^{λ} (mV/mol/m^3)	744	716	704	657	723		

+Obtained by regression with MINITAB.

*One bubble on the screen.

**Two bubbles on the screen; effectively 10 percent screen blockage.

Experiment No. 27

Colorimeter Output $\overline{V^{\lambda}}$ (mV)

Date: May 14, 1985

x (cm)	λ(nm) 490	520	545	450	470	$\bar{C}_R^+$ (mol/m^3)	$\bar{C}_S^+$ (mol/m^3)
Reference	875	389	199***	975	815		
4.1	1046*	591	397	1090	955	0.115	0.057
9.2	1075	619	416	1049	968	0.152	0.036
14.3	1087**	639	435	1120	992	0.144	0.074
16.8	1086	649	453	1131	1007	0.132	0.106
19.3	1099	649	454	1133	1012	0.127	0.115
24.5	1107	660	454	1137	1011	0.148	0.096
Reference	877	399	204	983	819		
Exit 1	1224	780	560	1212	1092		
Reference	884	399	203	979	817		
Exit 2	1230	787	565	1212	1096		
Reference	885	397	203	977	815	0.212	0.147
Exit 3	1235	793	579	1211	1104		
Reference	884	399	202	977	817		
k_R^{λ} (mV/mol/m^3)	1112	1360	1193	650	830		
k_S^{λ} (mV/mol/m^3)	744	716	704	657	723		

+Obtained by regression with MINITAB.

*Two small bubbles on the screen.

**Four small bubbles on the screen.

***Six small bubbles on the screen.

Experiment No. 28 | Colorimeter Output $\overline{V^{\lambda}}$ (mV) | Date: May 17, 1985

(cm)	λ(nm) 490	520	545	450	470	$\bar{C}_R^+$ (mol/m^3)	$\bar{C}_S^+$ (mol/m^3)
Reference	849	442	218	982	820		
4.1	1007	654	434	1115	984	0.157	0.046
9.2	1042	655	430	1119	1000	0.132	0.087
14.3	1035	651	444	1123	1005	0.148	0.075
16.8	1043	666	445	1128	1011	0.129	0.101
19.3	1059	662	450	1136	1002	0.140	0.091
24.5	1047	683	457	1137	1015	0.143	0.097
Reference	855	455	217	983	827		
Exit 1	1243	903	640	1244	1143		
Reference	847	452	219	980	816		
Exit 2	1255	914	650	1254	1151		
Reference	849	453	210	981	820	0.248	0.172
Exit 3	1262	919	657	1259	1159		
Reference	849	452	215	980	819		
k_R^{λ} (mV/mol/m^3)	1112	1360	1193	650	830		
k_S^{λ} (mV/mol/m^3)	744	716	704	657	723		

+Obtained by regression with MINITAB.

Experiment No. 30 | Colorimeter Output $\overline{V^{\lambda}}$(mV) | Date: May 21, 1985

x (cm)	λ(nm) 490	520	545	450	470	$\bar{C}_R^+$ (mol/m^3)	$\bar{C}_S^+$ (mol/m^3)
Reference	547	375	178	934	770		
4.1	761	590	357	1050	925	0.117	0.072
9.2	784	602	388	1061	931	0.141	0.054
14.3	770	610	395	1082	944	0.059	0.189
16.8	788	604	390	1083	949	0.098	0.140
19.3		613	403	1079	950	0.098	0.140
24.5		613	399	1075	942	0.112	0.112
Reference		394	184	937	777		
Exit 1	1117	828	596	1192	1085		
Reference	725	380	171	936	773		
Exit 2	1140	851	617	1214	1111	0.216	0.215
Reference	731	384	177	936	767		
k_R^{λ} (mV/mol/m^3)	1148	1384	1156	672	853		
k_S^{λ} (mV/mol/m^3)	732	733	688	570	655		

+Obtained by regression with MINITAB.

Experiment No. 31

Colorimeter Output $\overline{V^{\lambda}}$ (mV)

Date: May 23, 1985

(cm)	λ(nm) 490	520	545	450	470	$\bar{C}_R^+$ (mol/m^3)	$\bar{C}_S^+$ (mol/m^3)
Reference	839	409	149	918	769		
5.1	1045	673	397	1047	938	0.183	0.023
10.2	1090	739	435	1090	979	0.215	0.052
15.6	1116	757	466	1111	1012	0.192	0.127
20.7	1138	757	472	1115	1020	0.171	0.160
25.8	1134	776	482	1119	1034	0.195	0.146
30.9	1127	782	485	1122	1037	0.199	0.146
Reference	846	397	152	902	767		
Exit 1	1260	800	592	1185	1085		
Reference	864	349	168	922	763		
Exit 2	1266	802	597	1186	1087	0.215	0.210
Reference	864	350	167	922	763		
Exit 3	1265	802	592	1185	1087		
Reference	865	350	167	922	764		
k_R^{λ} (mV/mol/m^3)	1148	1384	1156	672	853		
k_S^{λ} (mV/mol/m^3)	732	733	688	570	655		

+Obtained by regression with MINITAB.

Experiment No. 32

Colorimeter Output $\overline{V^{\lambda}}$ (mV)

Date: May 24, 1985

x (cm)	λ(nm) 490	520	545	450	470	$\bar{C}_R^+$ (mol/m^3)	$\bar{C}_S^+$ (mol/m^3)
Reference	772	452	209	931	762		
5.1	983	707	444	1066	931	0.152	0.053
10.2	1047	763	497	1103	973	0.173	0.096
15.6	1070	792	527	1117	995	0.188	0.104
20.7	1072	745	532	1128	998	0.174	0.132
25.8	1071	806	532	1130	1003	0.189	0.119
30.9	1081	807	544	1140	1016	0.163	0.170
Reference		460	212	935	767		
Exit 1	1160	904	626	1186	1075		
Reference	777	462	216	934	764		
Exit 2	1162	906	629	1189	1077		
Reference	777	462	219	935	765	0.222	0.183
Exit 3	1161	903	627	1189	1076		
Reference	776	460	216	935	764		
k_R^{λ} (mV/mol/m^3)	1148	1384	1156	672	853		
k_S^{λ} (mV/mol/m^3)	732	733	688	570	655		

+Obtained by regression with MINITAB.

Experiment No. 33

Colorimeter Output $\overline{V^{\lambda}}$ (mV)

Date: May 26, 1985

x (cm)	λ(nm) 490	520	545	450	470	$\bar{C}_R^+$ (mol/m^3)	$\bar{C}_S^+$ (mol/m^3)
Reference	850	406	236	948	780		
5.1	1081	646	464	1090	949	0.112	0.116
10.2	1126	726	523	1125	997	0.174	0.102
15.6	1153	741	546	1145	1018	0.155	0.161
20.7	1152	746	551	1146	1024	0.158	0.163
25.8	1153	758	557	1150	1034	0.165	0.164
30.9	1161	758	571	1155	1028	0.164	0.164
Reference	858	412	240	950	782		
Exit 1	1244	913	620	1191	1070		
Reference	872	497	236	950	774		
Exit 2	1246	914	624	1193	1073		
Reference	872	497	235	950	775	0.200	0.193
Exit 3	1244	913	633	1194	1072		
Reference	872	495	234	950	775		
k_R^{λ} (mV/mol/m^3)	1148	1384	1156	672	853		
k_S^{λ} (mV/mol/m^3)	732	733	688	570	655		

+Obtained by regression with MINITAB.

Experiment No. 34 | Colorimeter Output $\overline{V^{\lambda}}$ (mV) | Date: June 14, 1985

x (cm)	λ(nm) 490	520	545	450	470	$\bar{C}_R^+$ (mol/m^3)	$\bar{C}_S^+$ (mol/m^3)
Reference	848	531	244	955	790		
4.0	911	607	318	997	839	0.057	0.000
9.1	957	650	345	1024	875	0.063	0.047
14.1	982	687	383	1046	905	0.082	0.064
16.7		697	392	1054	910	0.087	0.072
19.2		699	406	1061	918	0.084	0.090
24.3		720	422	1076	937	0.086	0.116
Reference	855	540	243	966	797		
Exit 1	1329	972	749	1284	1182		
Reference	859	450	257	970	802		
Exit 2	1332	973	752	1288	1184		
Reference	858	453	264	967	802	0.258	0.276
Exit 3	1332	977	755	1285	1186		
Reference	858	449	263	971	799		
k_R^{λ} (mV/mol/m^3)	1117	1342	1186	645	818		
k_S^{λ} (mV/mol/m^3)	670	641	608	543	622		

+Obtained by regression with MINITAB.

Experiment No. 35 | Colorimeter Output $\overline{V^{\lambda}}$ (mV) | Date: June 17, 1985

x (cm)	λ(nm) 490	520	545	450	470	$\bar{C}_R$ + (mol/m^3)
Reference	740	645	248	927	752	
16.1	806	708	320	965	800	0.058
21.2	815	735	323	978	809	0.065
26.3	819	738	332	982	815	0.071
32.4	816	741	335	983	822	0.073
37.5	827	739	343	991	821	0.077
41.5	835	746	341	982	823	0.080
Reference	742	646	249	930	755	
Exit 1	890	802	383	1012	854	
Reference	767	659	252	933	755	
Exit 2	892	804	387	1014	855	0.113
Reference	766	658	252	933	757	
Exit 3	891	805	387	1014	856	
Rererence	766	657	252	934	757	
k_R^{λ} (mV/mol/m^3)	1117	1342	1186	645	818	

+Obtained through approximate analysis.

Experiment No. 36

Colorimeter Output $\overline{V^{\lambda}}$ (mV)

Date: June 18, 1985

(cm)	λ(nm) 490	520	545	450	470	$\bar{C}_R^+$ (mol/m^3)
Reference	738	587	151	910	743	
16.1	821	668	235	961	798	0.071
21.2	828	667	238	962	804	0.075
26.3	829	677	245	968	810	0.080
32.4	832	681	251	972	820	0.086
37.5	837	688	252	970	812	0.086
41.5	837	687	254	979	819	0.089
Reference	742	582	153	915	745	
Exit	872	745	297	996	853	
Reference	745	595	157	913	748	
Exit 2	875	747	299	995	855	
Reference	745	593	159	912	750	0.118
Exit 3	876	745	300	999	855	
Reference	746	593	158	914	751	
k_R (mV/mol/m^3)	1117	1342	1186	645	818	

+Obtained through approximate analysis.

Experiment No. 37

Colorimeter Output $\overline{V^{\lambda}}$ (mV)

Date: June 19, 1985

x (cm)	λ(nm) 490	520	545	450	470	$\bar{C}_R^+$ (mol/m^3)
Reference	787	534	159	913	742	
16.1	859	615	224	956	797	0.061
21.2	862	608	240	962	803	0.070
26.3	869	627	249	967	810	0.077
32.4	872	632	259	973	817	0.082
37.5	878	645	256	973	815	0.084
41.5	883	635	262	981	819	0.088
Reference	788	537	158	915	744	
Exit 1	1102	534	303	1002	858	
Reference	971	382	162	919	754	
Exit 2	1100	535	305	1003	857	0.119
Reference	969	381	162	919	754	
Exit 3	1100	534	304	1004	859	
Reference	971	381	162	919	754	
k_R^{λ} (mV/mol/m^3)	1117	1342	1186	645	818	

+Obtained through approximate analysis.